REPORT DOCUMENTATION PAGE

READ INSTRUCTIONS BEFORE COMPLETING FORM

1. REPORT NUMBER AFIT/CI/NR 86- 189D	2. GOVT ACCESSION NO.	3. RECIPIENT'S CATALOG NUMBER
4. TITLE (and Subtitle) Surface Wind Fields In The Vicinity Of Meso-Convective Storms As Derived From Radar Observations: Non-Tornadic Storms		5. TYPE OF REPORT & PERIOD COVERED THESIS/DISSERTATION
		6. PERFORMING ORG. REPORT NUMBER
7. AUTHOR(s) Joel David Bonewitz		8. CONTRACT OR GRANT NUMBER(s)
9. PERFORMING ORGANIZATION NAME AND ADDRESS AFIT STUDENT AT: Texas A&M		10. PROGRAM ELEMENT, PROJECT, TASK AREA & WORK UNIT NUMBERS
11. CONTROLLING OFFICE NAME AND ADDRESS		12. REPORT DATE 1986
		13. NUMBER OF PAGES 157
14. MONITORING AGENCY NAME & ADDRESS(if different from Controlling Office)		15. SECURITY CLASS. (of this report) UNCLASS
		15a. DECLASSIFICATION/DOWNGRADING SCHEDULE

16. DISTRIBUTION STATEMENT (of this Report)

APPROVED FOR PUBLIC RELEASE; DISTRIBUTION UNLIMITED

DTIC ELECTE NOV 0 4 1986 D
E

17. DISTRIBUTION STATEMENT (of the abstract entered in Block 20, if different from Report)

18. SUPPLEMENTARY NOTES
APPROVED FOR PUBLIC RELEASE: IAW AFR 190-1

LYNN E. WOLAVER   3 oct 86
Dean for Research and
Professional Development
AFIT/NR

19. KEY WORDS (Continue on reverse side if necessary and identify by block number)

20. ABSTRACT (Continue on reverse side if necessary and identify by block number)

ATTACHED ...

DD FORM 1 JAN 73 1473   EDITION OF 1 NOV 65 IS OBSOLETE

SURFACE WIND FIELDS IN THE VICINITY OF MESO-CONVECTIVE STORMS

AS DERIVED FROM RADAR OBSERVATIONS: NON-TORNADIC STORMS

A Dissertation

by

JOEL DAVID BONEWITZ

Submitted to the Graduate College of
Texas A&M University
in partial fulfillment of the requirement for the degree of

DOCTOR OF PHILOSOPHY

December 1986

Major Subject: Meteorology

SURFACE WIND FIELDS IN THE VICINITY OF MESO-CONVECTIVE STORMS

AS DERIVED FROM RADAR OBSERVATIONS: NON-TORNADIC STORMS

A Dissertation

by

JOEL DAVID BONEWITZ

Approved as to style and content by:

George L. Huebner, Jr.
(Chairman of Committee)

Phanindramohan Das
(Member)

James P. McGuirk
(Member)

Rudolf J. Freund
(Member)

Glen N. Williams
(Member)

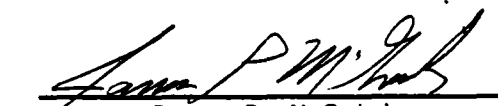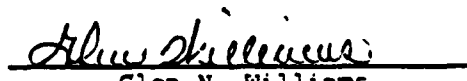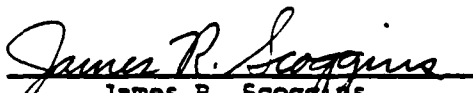
James R. Scoggins
(Head of Department)

December 1986

ABSTRACT

Surface Wind Fields in the Vicinity of Meso-Convective Storms

as Derived from Radar Observations: Non-Tornadic Storms.

(December 1986)

Joel David Bonewitz, B.A.E., Georgia Institute of Technology

M.S., University of Oklahoma

M.S., Johns Hopkins University

Chairman of Advisory Committee: Dr. George L. Huebner, Jr.

→ This thesis sought

The objective of this investigation was to test the hypothesis that there is a determinable relationship between the true surface wind field and radar derived wind data. Data used were composed of National Severe Storms Laboratory single-Doppler radar data, surface automated mesonet (SAM) data, and tall-tower data from the Next Generation Weather Radar (NEXRAD) Interim Operational Test Facility (IOTF) Spring 1983 Demonstration. Analyses used data from storms that occurred in the data collection area on 22 April, 27 June, and 28 June 1983. The radial wind data provided by the single-Doppler radar were complemented by data derived from application of the NEXRAD Transverse Wind algorithm. This pattern translation algorithm derives a wind field through a statistical correlation technique using temporally separated scans of radar reflectivity.

Data derived through the NEXRAD Transverse Wind algorithm were examined to assess the algorithm's general usability and to select operational parameters. The relationship of the derived data to other sources of surface wind data was examined in some detail.

An important result of this investigation is the validation of the use of the Transverse Wind algorithm with data obtained at low elevation angles and short time spans between reflectivity scans. The use of maximum correlation coefficient and reflectivity thresholds are shown to improve the derived wind field. Single-Doppler radial velocity data, winds derived from the NEXRAD Transverse Wind algorithm, and SAM data are compared. The dissimiliar natures of the Doppler radial velocity data and the derived wind data are demonstrated. The derived wind field is shown to be closely related to the surface wind field as represented by the surface meso-analyses for three cases. A feature ("marching vectors"), which appears in areas of relatively weak uniform reflectivity, is identified in the derived wind data. The NEXRAD Transverse Wind algorithm is used for the first time in an area (gust front) where there is confidence that the vectors are derived from motions at their own level and not from some generator level.

ACKNOWLEDGMENTS

It is with great pleasure that I acknowledge those individuals who have contributed to the successful completion of this research effort. First and foremost, I wish to express graditude to my graduate committee. I appreciate their support and interest. I wish to especially thank them for so generously giving me their time in my efforts to complete this work. Special thanks must go to my chairman, Dr. George Huebner. I could not have asked for a nicer or more supportive mentor; without his unfailing confidence, I might have never finished.

This work was accomplished while the author was assigned to Texas A&M University under the auspices of the Air Force Institute of Technology. This research was funded in part by NOAA Grant Number NA83AA-D-00060 and supported the Next Generation Weather Radar (NEXRAD) program. Grateful acknowledgment is made of the support of the NEXRAD Joint System Program Office (JSPO), the NEXRAD JSPO's Operational Test Facility (Mr. Ken Wilk and his staff), and personnel at the National Severe Storms Laboratory.

I am pleased to recognize four fellow students and one staff member whose assistance was essential to me. Capt. Rich Bensinger implemented the NEXRAD Transverse Wind algorithm and saved me countless hours of programming effort. Mr. David Wolff provided able assistance in accomplishing many tasks, particularly in developing graphics programs to display surface and tower data. Capt. Dan Pophin contributed to many helpful discussions, and his suggestions were always useful. Capt. Rob Cox helped me over a number of rough spots by serving as a sounding

board for my ideas and providing valuable suggestions, taking the time to read and comment on my many drafts, and always providing an optimistic viewpoint. Mr. Charles Brenton, Practical Meteorologist, took my original meso-analyses and applied his 35+ years of practical experience to correct, improve, and polish them to a level of "correctness" I would have never attained alone.

Special recognition is due fellow student Major Gary Sickler for his work in support of our NOAA grant and his contributions to this research.

Acknowledgment and thanks is gratefully given to Mr. Jack Grant, Texas A&M University Copy Center, for his willing assistance in getting sharp reductions and clear copies for this document.

I would like to recognize two individuals who were instrumental in my involvement in Doppler weather radar and in this research effort. The first is Lt. Col. Ray Bonesteele, who introduced me to the Doppler technology and with whom I had the pleasure of working for a number of years. The second is Lt. Col. Cam Tidwell, with whom I enjoyed working during our time in the NEXRAD JSPO and who encouraged me to return to school one more time. Both of these individuals provided me with a level of motivation, confidence, and enthusiasm, which has done much to carry me to this point.

To all of these people and many others, thank you very much for your help, support, and friendship.

DEDICATION

To my parents, Emmett B. and Martha L. Bonewitz. Through the years they have provided me with inspiration, motivation, and love; who could have asked for more.

TABLE OF CONTENTS

LIST OF TABLES

LIST OF FIGURES

CHAPTER I

INTRODUCTION

Overview

For many years the conventional weather radar has served as a powerful tool in the observing and warning of potentially hazardous weather. While it is generally accepted that a well-calibrated weather radar can diagnose the relative strength of thunderstorms from the reflectivity data, only subjective interpretation can be made about turbulence and other hazardous phenomena such as wind gusts and shear. Accurate identification and assessment of these phenomena, their location and movement, is of great importance to the success of the weather radar as an operational tool.

The potential of Doppler weather radar in the identification of storm kinematics has been recognized for some time (Smith and Holmes, 1961; Atlas, 1963; Lhermitte, 1964). Doppler techniques have been developed for improved storm warnings (Donaldson, 1970; Burgess, 1976; Brown and Lemon, 1976). Lemon et al. (1978) provide a good overview of the application of Doppler radar to severe storm detection and warning. These developments have stimulated activities leading to a joint use Doppler weather radar system.

This paper follows the style of the _Journal of the Atmospheric Sciences_.

The Joint Doppler Operational Project (JDOP*), conducted in the Spring of 1977, 1978, and 1979 in Norman, Oklahoma, showed the advantage of a Doppler radar over the conventional weather radar in early and accurate real-time identification of thunderstorm hazards (Burgess, et al., 1978; JDOP Staff, 1979). JDOP not only provided significant meteorological results, but also brought together in a coordinated effort the principal Government agencies involved in the operational use of weather radar. The Departments of Commerce (National Weather Service), Defense (Air Force Air Weather Service), and Transportation (Federal Aviation Administration) are working together to jointly design, acquire, and operate the Next Generation Weather Radar (NEXRAD) (Bonewitz, 1981).

The future implementation of NEXRAD has placed increasing emphasis on the development of techniques to use the data available through single-Doppler radar. The NEXRAD Joint System Program Office (JSPO) established a series of "technical needs" to direct advanced developments necessary for NEXRAD to succeed in meeting the operational requirements of the users. These "technical needs" include automated analysis techniques for precipitation, thunderstorms, turbulence, and winds (NEXRAD JSPO Staff, 1983a).

Statement of Problem

Doppler weather radar provides the ability to measure the radial velocity of targets as well as their intensity (reflectivity). A

---

*A summary of acronyms and abbreviations as used in this paper is provided in Appendix A.

discussion of the basic principles of Doppler weather radar is provided in Appendix B. Doppler weather radar has these inherent limitations: range ambiguity, velocity ambiguity, and the ability to measure only radial velocities. While the first two of these limitations can be circumvented to an acceptable level through a combination of hardware and software, the restriction to measure only radial velocities remains a serious problem.

As stated by the National Severe Storms Laboratory (NSSL) Staff (1971), the "forecasting of hazardous wind gusts is a four-fold problem of detection, interpretation, pattern extrapolation of the smoothed field, and prediction of maximum gusts." The ultimate goal of this research is to determine the surface wind field in the vicinity of thunderstorms by the use of radar data. However, except at the very short ranges (< 40 km), the measurements being made by the radar are above the boundary layer*, and the region being sampled may or may not be coupled to the surface. Due to the Earth's curvature and atmospheric refraction, the beam will usually be above the ground at normal operational antenna elevations. The height of the beam center (H) is shown mathematically (Burgess, 1977) as

$$H = r \sin \phi + (0.375\ r^2 \cos^2 \phi) / R \qquad\qquad (1)$$

where: r = slant range in km,
       R = radius of Earth (6371.23 km), and
      ϕ = elevation angle in degrees.

---

*The term "boundary layer" can take on more than one vertical dimension as the surface layer, which is measured in 10's of meters, and as the mixed layer, which extends up to 1 - 2 km.

It follows that a major step in meeting the ultimate goal of this line of research is to develop relationships between the low-level radar data and the actual surface winds. Therefore, the objective of this investigation is to test the hypothesis that there is a determinable relationship between the true surface wind field and radar derived wind data.

Present Status of the Problem

While there has been much research on thunderstorms since the time of the Thunderstorm Project (Byers and Braham, 1949), most of the Doppler radar studies of thunderstorms (e.g., Armstrong and Donaldson, 1969; Burgess, 1976; and Brown et al., 1978) and thunderstorm outflow (e.g., Brandes, 1975, 1976, 1977) have been associated with well-developed mesocyclones. Bonewitz (1978), in conjunction with JDOP, first examined the single-Doppler detection of cold air outflow from non-tornadic storms. With the reality of NEXRAD in view, more attention has been focused on extracting the full potential of single-Doppler data in the non-tornadic as well as the tornadic storms. In the meantime, as observed by Zrnic (1985), great volumes of data have been collected, while only cursory examinations have been made of any but the most exciting cases: work in the area of non-tornadic storms and non-severe storms is almost non-existent.

One reason for the lack of work in the area of non-tornadic storms may be the complexity of the problem. Two somewhat distinct scales of motion are involved: (1) the environmental winds in the region outside the convective area, which may represent a major component of storm motion, and (2) the internal wind field as it responds to the dynamics

of the convection. The winds in the region of interaction between the storm and the environment (outflow, entrainment, etc.) belong to this second scale. Various approaches (e.g., flow line construction, velocity-azimuth display, velocity volume processing, correlation tracking, simulated dual-Doppler, and echo tracking) have been taken to measure the motion on these scales with a single Doppler radar. Of these, only correlation tracking, commonly referred to as the transverse wind technique, can be used in and around convective activity.

Lhermitte (1969) constructed flow lines within the storm. The zero radial velocity contour is assumed to be motion perpendicular to the beam as calm winds are unlikely. Changes along a radial are due to turning of the flow. Kraus (1973) and Lemon et al. (1978) are two examples of the successful use of this approach. The velocity-azimuth display (VAD) was first proposed by Lhermitte and Atlas (1961) as a technique to obtain the true wind field from a single-Doppler radar's radial velocity data. This approach is limited to operating in a region with a uniform wind field. Rabin and Zrnic (1980) extended this technique to its use in clear air (i.e., precipitation free environment). Velocity Volume Processing (VVP) was developed by Waldteufel and Corbin (1979) as a statistical regression technique similar to VAD, but one that uses a full volume of data. VVP is similarly limited in that it must also be used in a uniform wind field. Echo tracking as proposed for NEXRAD by Bjerkaas and Forsyth (1980) computes storm motion, which may provide the steering winds (i.e., environmental winds), but may also be biased by echo growth and decay. Peace et al. (1969) proposed simulating dual-Doppler analysis by using two scans of the radial velocity data from the same radar separated by 5

to 10 minutes. The two viewing aspects (different times) of steady-state flow should provide the same perspective on the storm as two radars at two locations observing the storm at the same time. Bonesteele and Lin (1978) used a modification of this technique to derive synthetic dual-Doppler data to model storm flow. While this technique may work well in many cases, particularly supercell storms, this approach requires the analyst to assume that the velocity field within the convective storm under study remains constant for a longer period of time than may be reasonable (Battan, 1973).

Rinehart and Garvey (1978) presented the technique of "tracking of radar echo with correlations" as a method for determining internal storm motions, which could be implemented on a conventional or a single-Doppler radar. This technique determines the horizontal wind speed and direction through a "correlation analysis pattern recognition" approach applied to temporally separated fields of radar reflectivity. Smythe (1981) developed independently a similar technique for application to the radial velocity field to retrieve the transverse wind. Hamidi et al. (1983) in his work for the NEXRAD Interim Operational Test Facility (IOTF) provided further testing and validation of the correlation technique proposed by Rinehart. This correlation technique was adopted for potential use in NEXRAD (NEXRAD JSPO, 1983a) and was referred to as the transverse wind technique. Smythe and Harris (1984), in work performed for the Air Force Geophysics Laboratory, tested the correlation technique in acquiring subcloud motions and concluded that "the technique does not detect air motions, but instead it appears to track precipitation generators that are at heights above the analysis levels." In the work by Rinehart (1979), Smythe (1981), and Smythe and

Harris (1984), the basic verification test has been a comparison with the wind field derived from dual-Doppler data. Only Hamidi et al. have attempted a comparison with surface observations or instrumented tower data. In spite of the concerns expressed about limitations of the transverse wind approach, this algorithm is given a high priority for the NEXRAD system (Snell, 1985) and remains included in the NEXRAD Algorithm Report. However, its implementation (or the implementation of an improved technique) awaits further research (NEXRAD JSPO Staff, 1984).

The transverse wind technique determines the horizontal wind speed and direction by seeking similar patterns in two fields of radar reflectivity separated in time. As shown in Fig. 1.1, a sector is selected to have outer boundaries, which enclose an area of interest. This region is then divided into boxes (called BOX1's) with a given number of radials and range gates (i.e., pulse volumes) in each. A radius of search is identified around the first BOX1, based on storm speed and the time lapse between radar scans (i.e., ΔT). Using multiple correlation formula, the BOX1 from the first scan is compared with all the boxes in the 2nd scan (BOX2's) whose centers fall within the radius of search. The correlation coefficients (CC) are computed by

$$CC = \frac{\sum_n dBZ(1)_n dBZ(2)_n - \frac{1}{n} \sum_n dBZ(1)_n \sum_n dBZ(2)_n}{\left[\sum_n \left| dBZ(1)_n^2 - n\left(\sum_n \frac{dBZ(1)_n}{n}\right)^2 \right| \sum_n \left| dBZ(2)_n^2 - n\left(\sum_n \frac{dBZ(2)_n}{n}\right)^2 \right| \right]^{\frac{1}{2}}} \quad , (2)$$

where dBZ(1) and dBZ(2) are the reflectivity values in BOX1 and BOX2, respectively, and the summation is over all (n) of the pulse volumes making up BOX1 and BOX2. Velocity vectors are formed between the center

of the BOX1 and the location derived from a second order curve fit

across the center of the BOX2 with the highest correlation coefficient.

The magnitude of the velocity vector is computed as

$$\vec{V} = \frac{\text{Distance from center BOX1 to optimum corr. point}}{\text{Time between SCAN1 and SCAN2}} \quad . \quad (3)$$

This process is repeated for each BOX1 in the area of interest.

With one exception (Hamidi et al., 1983), previous researchers have

validated the winds derived from the transverse wind technique by

comparing the derived wind field with that indicated by dual-Doppler
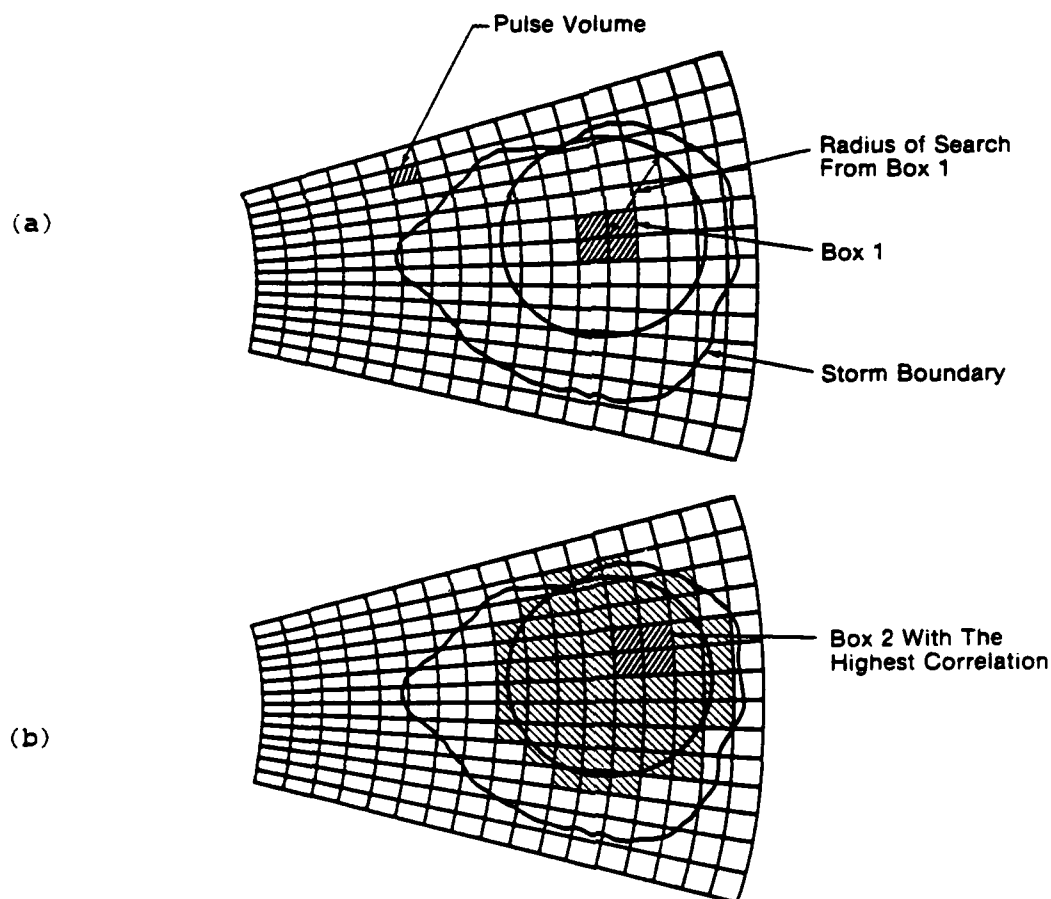
Fig. 1.1. Transverse wind algorithm grid at (a) time 1 and (b) time 2.

radars. This use of vector matching to validate the transverse wind technique must contend with the objection, as noted by Hamidi et al. (1983), of trying to "compare apples and oranges." The transverse wind technique provides a wind which is effectively a temporal and spatial average, while the Doppler velocity (whether the single-Doppler radial component or multiple Doppler derived wind field) is an instantaneous, high-resolution "snapshot" wind. Although they may be different, both of these winds may be "correct" in terms of their relevance to different scales of atmospheric motion. Even if a comparison of the transverse wind data with Doppler velocity data fails due to the "apples and oranges" nature of the data, two other comparisons would be valuable. The first is a comparison of the transverse wind derived data with actual surface observations. However, this also suffers from the problem of a scale difference. A surface observation is a snapshot in time and a single point in space. As observed by Gal-Chen and Kropfli (1983), this may not compare well with a data field which is a temporal and spatial average. The final comparison is one between the transverse wind derived data and the features of observed mesoscale meteorological phenomena with special attention placed on features identified by researchers from theoretical models of these phenomena. This approach allows us to bridge the problem of differing temporal and spatial scales by examining the data in grosser detail, allowing real features to stand out from the noise. At the same time, if a good comparison is obtained, the radar observations will have provided a derived surface wind field.

CHAPTER II

PROCEDURE

Introduction

This research involves the study of weather radar data at low levels
in and around non-mesocyclone convective storms, along with surface data
in the same location and time frame as the radar data. Data used were
composed of single-Doppler radar data, surface automated mesonet (SAM)
data, and NSSL tall-tower data from the NEXRAD IOTF Spring 1983
Demonstration. Data acquisition is discussed in Chapter III. Analysis
uses data from storms that occurred in the data collection area on
22 April, 27 June, and 28 June. These were non-supercell storms, which
produced non-tornadic severe wind events, and data were captured by both
the single-Doppler radar and individual SAM sites. The mesoscale
features of these cases are discussed in Chapter IV. The general
procedure in this project was to acquire appropriate data sets,
structure them as necessary in computer data files, analyze the data
through a set of computer programs, and evaluate and interpret the
meteorological ramifications of the analysis products.

Data were acquired during the NEXRAD IOTF Spring 1983 Demonstration
by staff of the NSSL and the NEXRAD IOTF under the direct supervision of
Mr. Ken Wilk, Chief, NEXRAD IOTF. During the planning for and conduct
of this data acquisition, the author functioned as reviewer and approval
authority in his role as Chief, Research and Development Branch, NEXRAD
JSPO. Data sets for analysis were selected following review of the NSSL
radar (reflectivity) and SAM data. Initial review was done by Sickler

(1984). This chapter discusses the data processing, transverse wind parameter selection, methods of data comparison, and procedure for assessing meteorological ramifications.

Processing

The early stages of this research effort were directed toward developing the tools (i.e., computer programs) essential for the needed analysis. None of the computer programs discussed herein were available at Texas A&M University when this research began. Due to their different computers, no programs were available in a transportable form from another weather radar research facility. All programs were developed locally to support the analysis efforts. All computer programs were written in VS-FORTRAN and implemented on the Texas A&M University Amdahl computer system. In order to facilitate possible transfer of these programs to other computer facilities, such as the Texas A&M University meteorology department's Harris 500, care was taken to avoid using IBM extensions to the language. In fact, this transfer is being accomplished (Cox, 1986).

Disk Write

Disk Write (DISKW) is a complex computer program developed to transfer specified Doppler radar data from universal format tapes (UFT) (Barnes, 1980) to sequential access disk files. Format of the UFT is given in Appendix C. DISKW was designed to find a specified volume sector defined by beginning and ending elevation angles, azimuth angles, and ranges. While the program does the necessary conversions to the data (e.g., application of the radar constant and system time constant

to convert reflectivity data from dBm to dBZ), no data suppression to weak signals or velocity unfolding was applied at this time. Data are stored on disk by range bin, radar field, azimuth, and elevation angle for a full volume. Two files (housekeeping and data) were created for each volume. The housekeeping file serves the same general purpose as the header blocks in the UFT, i.e., to provide necessary pointers to the data in the data file. In addition, the housekeeping sheet (Fig. 2.1) serves as a hard-copy index to the data stored in that disk file. This is the only IBM based UFT system known to be in use in the research community (Bumgardner, 1985).

The basic approach used in this program was suggested by the transverse wind program implemented at the NEXRAD IOTF by Hamidi. DISKW evolved from the attempt to implement the program obtained from Hamidi (1984) within the local computer facility. While DISKW was initially validated when all the housekeeping data matched known values, final validation rested on testing output data sets.

B-Scan and Vertical Cross-Section

In order to test the validity of the approach taken in DISKW, a program was needed to provide detailed output of the Doppler radar data fields in a form that could be compared with known data sets. The program implemented was a B-scan routine (BSCAN), as B-scans are routinely used in the Doppler radar research community to examine data

UNIVERSAL FORMAT TAPE TO DISK TRANSFER

```
INPUT DATA FROM TAPE S/N. 007670     FILE NUMBER  13
DATA OUTPUT TO DISK FILE   J520.DB.DA22APR.VOL13
HOUSEKEEPING TO DISK FILE: J520.DB.HK22APR.VOL13

DATA SELECTION SPECIFIED FROM:    0.5 TO   18.5 DEGREES ELEVATION
                                  280  TO  350. DEGREES AZIMUTH
                                  30   TO   80  KILOMETERS IN RANGE
```

```
DATE  22 APR 1983

RADAR NAME:  NSSL
SITE  NAME:  NORMAN, OK

LATITUDE:   35 / 14 / 11    (DEG/MIN/SEC  NORTH)
LONGITUDE:  97 / 27 / 47    (DEG/MIN/SEC  WEST)
HEIGHT OF ANTENNA ABOVE SEA LEVEL:  370 (M)

SWEEP-RATE (INSTANTANEOUS) =  6.00 (DEG/SEC)
BEAM WIDTH (DEG):  HORIZONTAL= 0.81     VERTICAL= 0.81
RECEIVER BANDWIDTH =    85 (MHZ)
POLARIZATION TRANSMITTED:  VERTICAL
WAVELENGTH =   10.52 (CM)
THRESHOLD FIELD: SIGNAL-TO-NOISE    THRESHOLD VALUE =  -999
PULSE REPETITION TIME =  1075 (MICROSEC)
```

```
FIELDS IN THIS VOLUME  3

FIELD NAME: REFLECTIVITY (DBM CONVERTED TO DBZ)
RADAR CONSTANT = 70.42
NOISE POWER = -108.00 (DBM)     RECEIVER GAIN = ******** (DB)
PEAK POWER =    88.75 (DBM)     ANTENNA GAIN =   46.80 (DB)
PULSE DURATION = 1.00 (MICROSEC)
RANGE TO FIRST GATE =   O (KM)
ADJUSTMENT TO CENTER OF FIRST GATE =   81 (M)
SAMPLE VOL SPACING = 840 (M)   # SAMPLE VOLS =  761    FIELD DEPTH = 639.2 (KM)
NUMBER OF SAMPLES USED IN FIELD ESTIMATE =  8

FIELD NAME: RADIAL VELOCITY
NYQUIST VELOCITY =   24.45 (M/S)
RANGE TO FIRST GATE =   O (KM)
ADJUSTMENT TO CENTER OF FIRST GATE =   81 (M)
SAMPLE VOL SPACING = 210 (M)   # SAMPLE VOLS =  761    FIELD DEPTH = 159.8 (KM)
NUMBER OF SAMPLES USED IN FIELD ESTIMATE =  64

FIELD NAME: SPECTRUM WIDTH
RANGE TO FIRST GATE =   O (KM)
ADJUSTMENT TO CENTER OF FIRST GATE =   81 (M)
SAMPLE VOL SPACING = 210 (M)   # SAMPLE VOLS =  761    FIELD DEPTH = 159.8 (KM)
NUMBER OF SAMPLES USED IN FIELD ESTIMATE =  64
```

```
TAPE INFORMATION
ELEVATION 0.6: SECTOR CONTAINS  70 RADIALS / BEGINS AT TIME = 195708 / ENDS AT TIME = 195719
        AZIMUTHS:  280.6 281.6 282.5 283.6 284.5 285.5 286.4 287.4 288.4 289.5
                   290.6 291.6 292.6 293.6 294.6 295.5 296.6 297.6 298.6 299.6
                   300.7 301.6 302.6 303.7 304.7 305.6 306.6 307.6 308.7 309.6
                   310.6 311.6 312.6 313.6 314.6 315.6 316.7 317.7 318.7 319.7
                   320.7 321.7 322.7 323.7 324.7 325.7 326.7 327.8 328.8 329.8
                   330.8 331.8 332.8 333.8 334.8 335.7 336.7 337.7 338.7 339.8
                   340.9 341.9 342.9 343.9 344.9 345.9 346.9 348.0 349.0 350.0
ELEVATION 0.6: SECTOR CONTAINS  70 RADIALS / BEGINS AT TIME = 195806 / ENDS AT TIME = 195817
        AZIMUTHS:  280.6 281.6 282.6 283.6 284.6 285.6 286.6 287.6 288.6 289.6
                   290.6 291.6 292.6 293.6 294.6 295.5 296.6 297.6 298.6 299.6
                   300.6 301.5 302.5 303.6 304.7 305.7 306.6 307.6 308.7 309.7
                   310.8 311.7 312.7 313.7 314.7 315.6 316.7 317.7 318.7 319.7
                   320.7 321.7 322.6 323.6 324.6 325.6 326.6 327.6 328.6 329.7
                   330.8 331.8 332.8 333.8 334.9 335.8 336.9 337.9 338.9 340.0
                   341.0 342.0 342.9 343.9 344.9 345.9 346.9 347.9 349.0 350.0

A TOTAL OF  2 ELEVATION ANGLES WERE CONVERTED IN VOLUME  1 OF  1 VOLUMES REQUESTED
DATA COVERS  29.48 TO  79.88 KILOMETERS IN SLANT RANGE
```

Fig. 2.1. Example of DISKW housekeeping sheet.

sets in detail. DISKW and BSCAN were validated when the output data were compared to B-scans produced at NSSL from the same data. These matches were sufficient to conclude that the data transfer (DISKW) and output (BSCAN) were both correctly implemented. In addition to validating DISKW, BSCAN also provides a format to interpret horizontal data fields. Vertical Cross-Section (VCS) serves as a vertical B-scan program, providing a cross-section along user selected azimuths. These two programs give access to the actual quantitative values of the full resolution of the Doppler radar data. However, while these programs provide fine detail by printing values in every range bin, they do not present the data in their proper perspective (i.e., in BSCAN the diverging nature of radial data is lost, and in VCS the actual vertical spacing of the data is lost). Since the actual orientation of the data is essential to the analysis, additional routines were required.

Radar Plot and Vertical Cross-Section Plot

Graphic plotting routines were written to provide properly oriented horizontal and vertical contoured cross-sections of the selected data sets. These programs, radar plot (RADPLOT) and vertical cross-section plot (VCSPLOT), make use of the National Center for Atmospheric Research (NCAR) graphic package as implemented on the Amdahl computer system at Texas A&M University (Reid, 1981). RADPLOT and VCSPLOT employ the contouring subroutine (CONREC), with user supplied functions to convert from rho-theta to x-y data, to plot Doppler radar data in a dynamically specified window. The CONREC subroutine performs the contouring by linearly interpolating between gridpoints through the grid domain.

Fig. 2.2 is an example of RADPLOT output for reflectivity. The
finer resolution and noisy nature of the velocity data resulted in a
RADPLOT of limited value. In addition, a profiling program was
available to highlight features in the examined storms (Sickler et al.,
1985a).

A   B   C   D   E
NORMAN DOPPLER   22 APR83   18:38:29   0.5   REFLECTIVITY
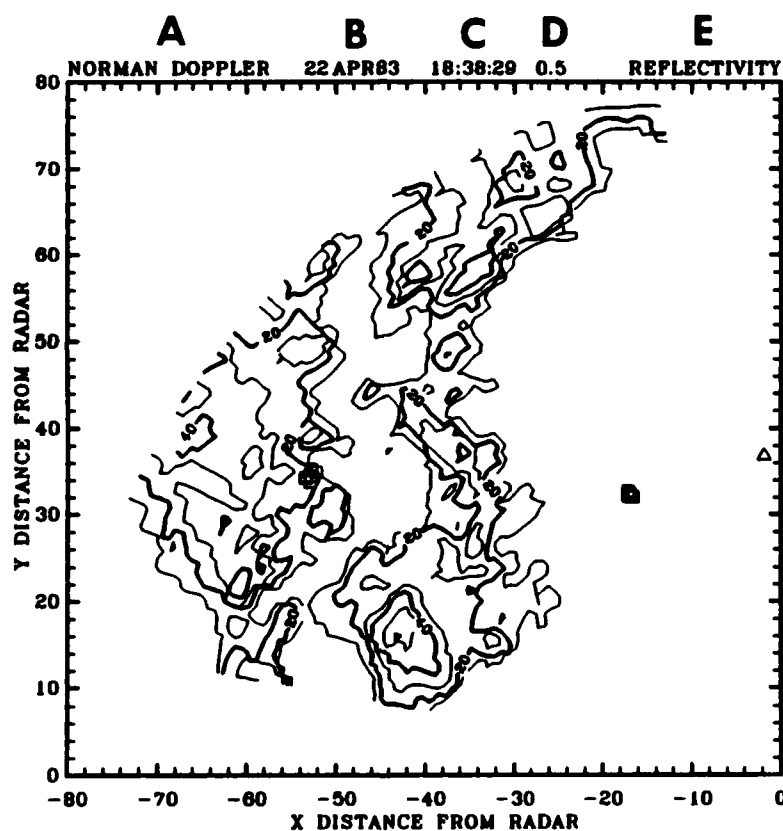
Fig. 2.2. Example of contoured Doppler radar reflectivity data.
Distances are in kilometers. Data are contoured from 10 to 60 dBZ in 10
dBZ steps. The square symbols near the (x,y) locations of (-16,32) and
(-52,34) are the 40- and 60-series SAM sites, respectively. The
triangle symbol plotted near (-2,37) is the NSSL tall tower. Heading
information includes: (A) radar data source, (B) storm date, (C) data
scan start time, (D) radar elevation angle, and (E) the Doppler radar
data field contoured.

Transverse Wind

The transverse wind program (TWIND) used in this research was written by Bensinger (1986). This program was an independent implementation of the technique from the NEXRAD algorithm description as presented in the NEXRAD Algorithm Report (NEXRAD JSPO Staff, 1984). The technique of wind acquisition through tracking reflectivity pattern correlations, as discussed in Chapter I, was developed by Rinehart (1979) and refined and tested by Hamidi et al. (1983).

The user specifies which two data sets are to be used, the data field (reflectivity, radial velocity, or spectrum width), box size, estimated storm speed, box overlap, azimuth separation in the data set, and the azimuth/range boundaries of the analysis field. The program provides printed copy output and writes its results to a disk file for later analysis. This file contains each of the x-y coordinates for BOX1, the x-y coordinates of the optimum correlation point (BOX2), the computed speed of the horizontal wind, the wind direction, the east-west and north-south components of the wind, the value of the largest correlation coefficient, and the radial velocity derived from the algorithm produced wind and the effective radar azimuth. The file also contains the time (hours, minutes, seconds) at the beginning of each of the two scans used in the analysis.

Wind Plot

The wind plot program (WPLOT) uses the data files produced by TWIND
to plot wind flags for the vector winds derived from each of the
BOX1/BOX2 maximum correlations. Fig. 2.3 is an example of the WPLOT
product. The wind flags can be plotted at one of three locations: BOX1
center, optimum correlation point, or halfway between. The time
difference between (D) and (E) is the ΔT used for classifying the data
sets. The scale of the data grid matches the grid used in RADPLOT.
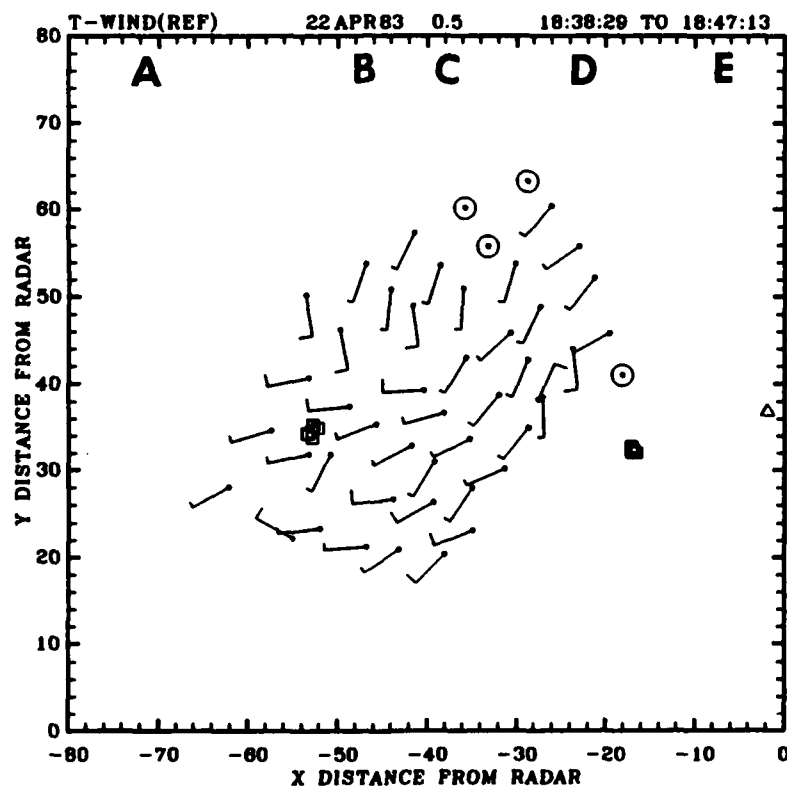
Fig. 2.3. Example of wind plot. Distances are in kilometers. Wind
flags, plotted halfway between BOX1 center and optimum correlation
point, are identified with a full flag = 10 m s⁻¹, half flag = 5 m s⁻¹,
and circle < 2.5 m s⁻¹. The header provides the (A) type of plot, (B)
date of the storm, (C) radar elevation angle, (D) start time of
transverse wind pass 1, and (E) start time of the transverse wind pass
2. SAM and TWR sites are identified as before.

Surface Automated Mesonet Plot

Surface verification data from the SAM sites were also available on tape. SAM data were selected by date and time (beginning and ending) and transferred from the NSSL data tapes to a disk file by the program SAMWRITE. This program also provides written copy to serve as a record of the exact value of each parameter at each observation. The computer program, surface automated mesonet plot (SAMPLOT), uses the data from this disk file to plot a two-hour analog chart of the variables measured by specified SAM sites. Fig. 2.4 is an example of the SAM analog plot.
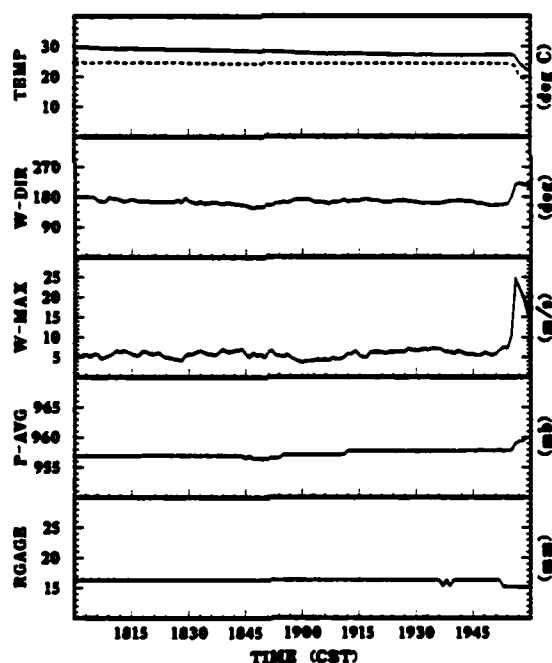
STATION NUMBER : 62

Fig. 2.4. Example of SAM analog plot. The first panel is temperature (TEMP), with the solid line being dry-bulb temperature and the dashed line being wet-bulb temperature. The second panel is wind direction (W-DIR), and the third is maximum wind speed (W-MAX). The fourth panel is the 1-minute average surface pressure (P-AVG), and the fifth is rainfall. Time is in Central Standard Time. Plot is for 1800-2000 CST.

Tower Plot

Low-level vertical cross-section verification data are provided by the NSSL tall-tower (KTVY). Tower data were selected by date and time (beginning and ending) and transferred from the NSSL data tape to disk file by the program tower write (TWRITE). This program also provides a written copy to serve as a record of the exact value of each parameter at each observation. The program, tower plot (TWRPLOT), uses the data stored on disk to produce an analog plot of the NSSL tall-tower data in a fashion similar to that of SAMPLOT. However, in this case the data are presented in the form of vertical time-sections. The data are presented in four plots (meteorological parameters), each composed of seven panels (vertical levels). An example of TWRPLOT output is given in Fig. 2.5.

Selection of Transverse Wind Parameters

Four user specified input parameters are required to run the TWIND program. These parameters are (1) storm speed, (2) box overlap, (3) azimuth/range boundaries of the analysis field, and (4) initial box size.

Storm speed was estimated from reflectivity pattern movement measured on the RADPLOT figures. Speed of movement was overestimated to ensure that a sufficient search radius was established to find the best possible match. While the additional processing that might result in this non-real-time application was not a concern, an overestimate of storm speed, resulting in too large a search radius, would cause a reduction in the number of BOX1's around the border.

20
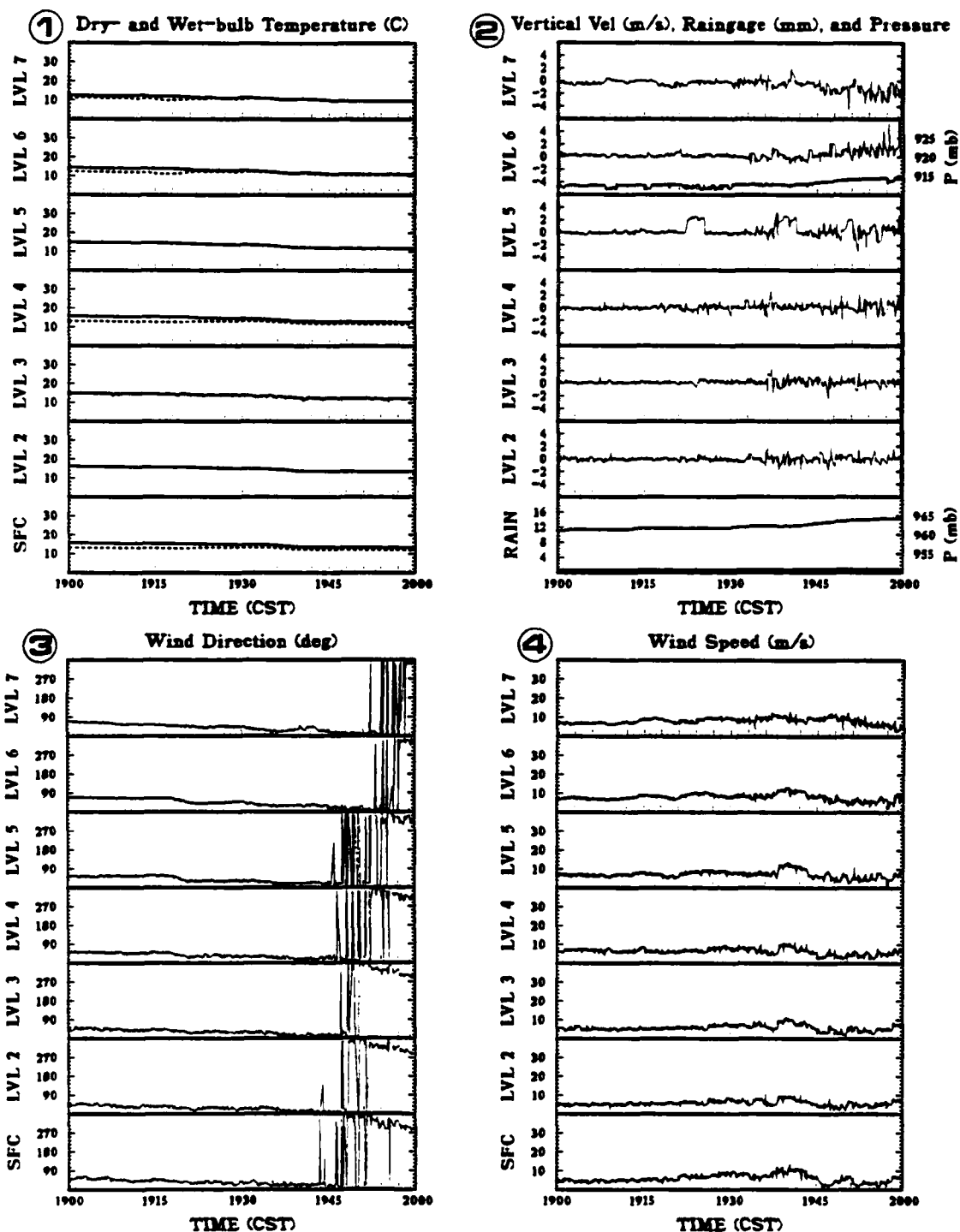
Fig. 2.5. Example of tower plot. Data from 22APR83. Plot 1 provides temperature data where the solid line is dry-bulb temperature and the dashed line is wet-bulb temperature. Plot 2 provides vertical velocity at levels 2 - 7, pressure (surface and level 6) in heavy line, and raingage (surface). Plots 3 and 4 are wind direction and wind speed, respectively.

Box overlap was set at 50% based on the work of Hamidi et al. (1983) and Bensinger (1986). Azimuth/range boundaries were selected to fix a window over the 40- and 60-series SAM clusters. This established a Eulerian view with a fixed observation window across which the storms passed. This approach, rather than setting the boundaries immediately adjacent to the storm under observation, was taken because the concern was for comparing winds from a ground relative, not storm relative, perspective.

Selection of the initial box size was perhaps the most difficult parameter decision. As had been observed by previous researchers, too small an initial array might result in random pattern matches yielding erroneous vectors. However, too large an initial array might result in excessive averaging, which would yield only the overall motion of the entire storm. Hamidi et al. (1983) empirically developed a pair of equations to derive a "reasonable compromise" between too small and too large array sizes. These equations determine the box size based on the available spatial resolution,

$$A_s \text{ (km)} = [14\Delta R + 7 \text{ R Sin}(\Delta\Theta)] / 2, \qquad (3)$$

and on the time lag between data sets,

$$A_t \text{ (km)} = 0.06 \text{ } \Delta T, \qquad (4)$$

where ΔR is the radar range gate spacing (km),
    R is the range to the center of the analysis area (km),
    $\Delta\Theta$ is the azimuth ray spacing (degrees), and
    ΔT is the actual temporal resolution available between subsequent
    radar scans (seconds).

"In the case of a large discrepancy between the available spatial and temporal resolution, it may be desirable to get the resolutions back into better agreement." The solution proposed by Hamidi et al. (1983) to discrepancies between spatial and temporal resolution was to either skip range gates/azimuth rays (when $A_t > A_s$) or skip time lags (when $A_s > A_t$). In this research it was not feasible to "skip a time lag" when $A_s > A_t$, as this moves the data into a longer ΔT classification. A compromise was established by taking a box size between those determined by (3) and (4).

Based on the radar elevation tilt sequence used, four separate time lags could be examined as shown in Table 2.1. For the longer ΔT periods ($A_t > A_s$), the decision was made to skew the box size toward A_s to account for the available spatial resolution. In this case, the box size (10 km) was selected slightly larger than that derived from (3). The use of the very large box sizes dictated by (4) would have reduced significantly the number of vectors derived and available for comparison in this study. To maintain consistency, the 10 km box size was used with the short ΔT data when comparing the data grouped by elevation angle. When conducting comparisons with just the short ΔT data, the box size (8 km) was fixed between those determined by (3) and (4), but skewed toward A_s to avoid increasing the expected "noise" by using too small a BOX1 with the resultant "random pattern matches."

Table 2.1. TWIND data processing combinations. A and B represent consecutive volumes of radar data collected in elevation tilt sequence. The numbers (1 to 4) represent the sequence number for elevation angle of 0.6°, 0.6°, 1.4°, and 2.5°. 'x' indicates no association, and '-' indicates data recorded in opposite direction.

Time (ΔT seconds) Between Associated Elevation Angles						
Pass 1	Pass 2					
	A-1	A-2	B-1	B-2	A-3	A-4
A-1	x	57	525	582	x	x
A-2	-	x	467	524	x	x
B-1	-	-	x	57	x	x
B-2	-	-	-	x	x	x
B-3	x	x	x	x	525	x
B-4	x	x	x	x	x	524

A total of seven thunderstorm cases have been examined with the transverse wind technique prior to this research and that of Bensinger (1986). All the researchers (Rinehart and Garvey, 1978; Rinehart, 1979; Smythe, 1981; Hamidi et al., 1983; Smythe, 1983; Smythe and Harris, 1984) who have worked with the transverse wind technique have observed that the elements being tracked may actually be from the generator level (Marshall, 1953; Gunn and Marshall, 1955; Langleben, 1956; Wexler and Atlas, 1959). In these previous cases, the shortest times between scans (ΔT) for transverse wind processing appear to be 62 seconds (Hamidi et al., 1983) and 66 seconds (Smythe, 1981; Smythe and Harris, 1984). Rinehart (1979) showed a strong case for improved data for shorter ΔT's. Considering these two factors (ΔT length and possible generator level

tracking), features may be observable in this data, which would provide evidence to support or dismiss the transverse wind technique as an approach to provide an improved representation of the true wind field.

If what is being tracked is a result of movement at the generator level, then the wind vectors at the low-level (0.6°) and those above (1.5° and 2.4°) should all look very much alike. If not tracking generator level motion, the low-level data should differ from the data from the higher elevation angles.

First, when comparing data with different ΔT's at an elevation angle of 0.5° (Fig. 2.6), considerable similarity in the pattern of wind flags in both directions and speeds are apparent. While some minor differences exist, they are far out-weighed by the similarities. Comparing data from 1.5° and 2.4° (Fig. 2.7), patterns again are observed, which, while not identical, are very similar. Note that the centers of these grids are at approximately 1.67 km and 2.56 km above the surface for these two elevation angles. When Fig. 2.6 (0.5° data) is compared with Fig. 2.7 (1.5° and 2.4° data), the close similarity of the wind patterns again becomes quite noticeable. At this point the conclusion is either that the winds at 0.6°, 1.5°, and 2.4° in this storm are very similar or that the transverse wind technique is indeed tracking motion originating at the generator level for data acquired at these relatively long ΔT's.

Finally, data with a very short ΔT (57 seconds) are shown in Fig. 2.8. Although there are some similarities, these data differ more from both the higher level data (Fig. 2.7) and the longer ΔT data (Fig. 2.6).
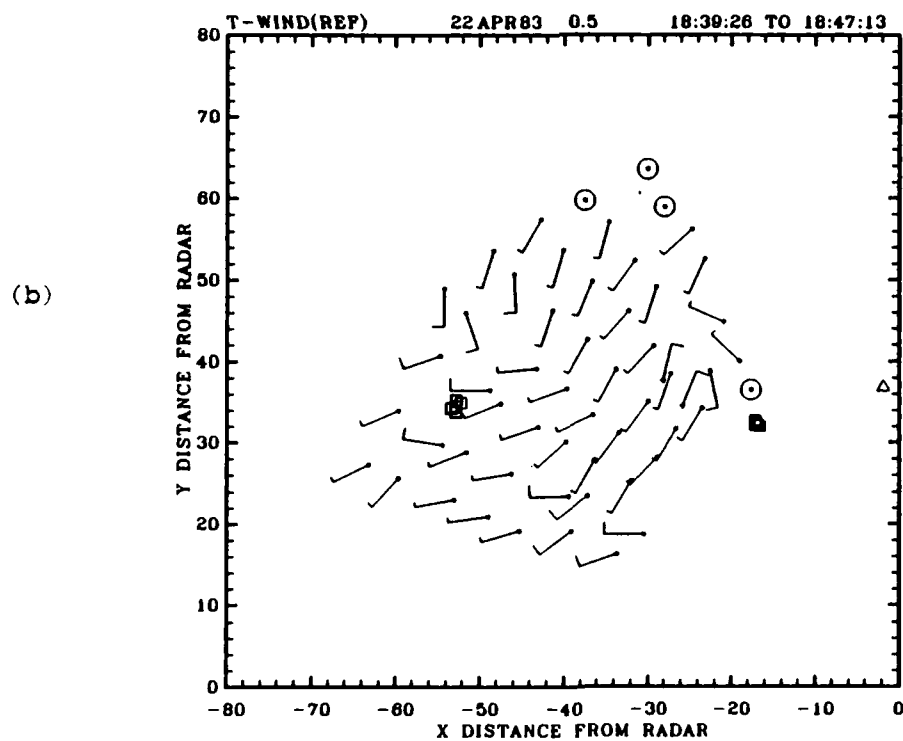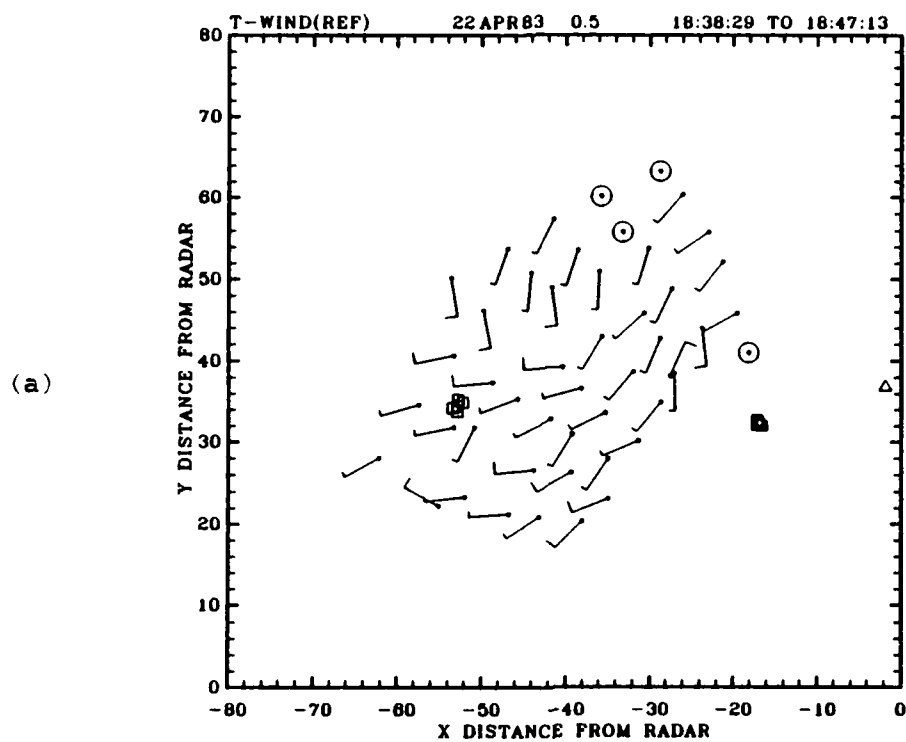
Fig. 2.6. TWIND plots for 22APR83 case at 0.5° elevation angle and ΔT of (a) 524 and (b) 467 seconds.
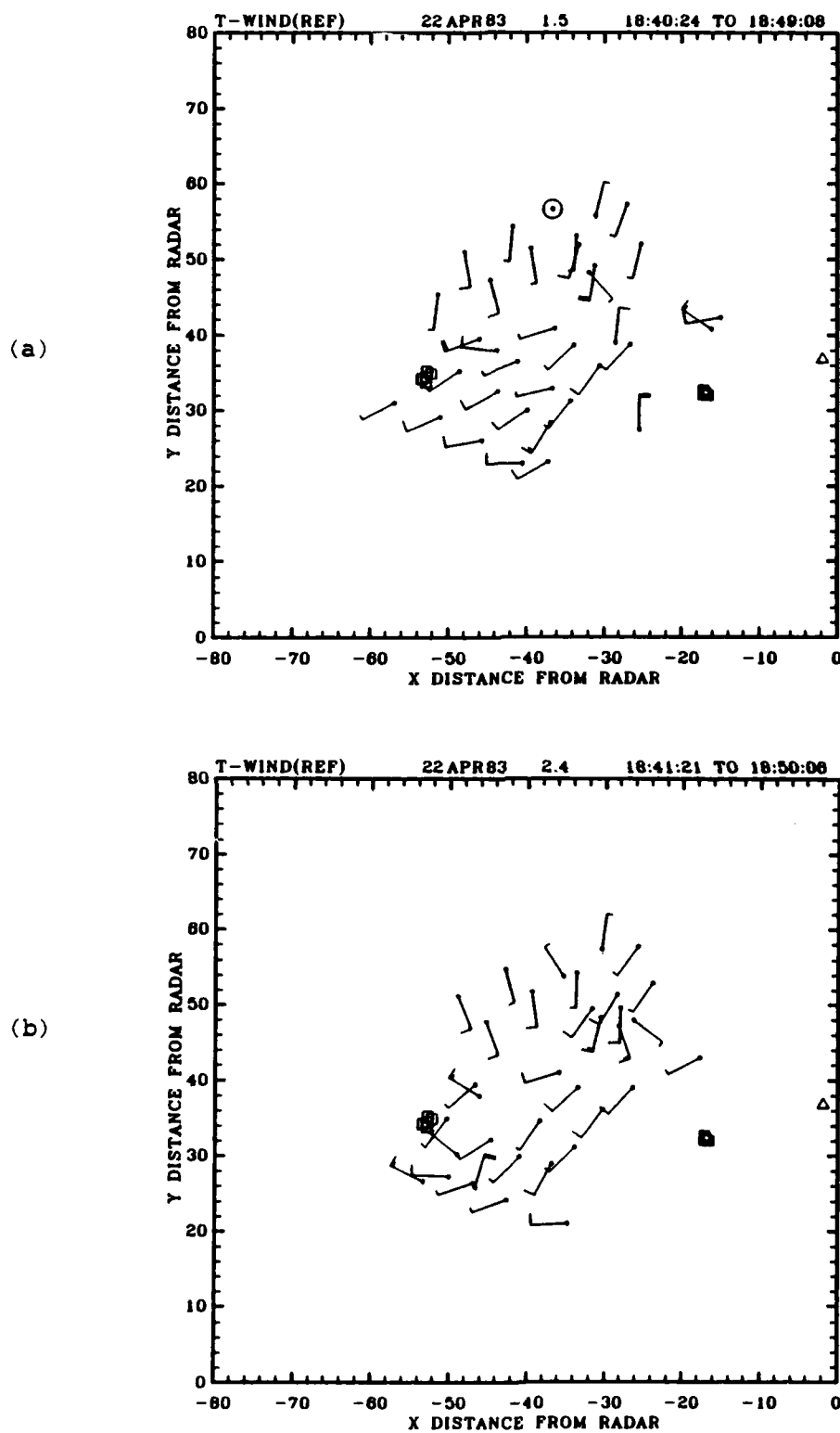
Fig. 2.7. TWIND plots for 22APR83 case at (a) 1.5° elevation angle and 524 seconds ΔT and (b) 2.4° and 525 seconds ΔT.
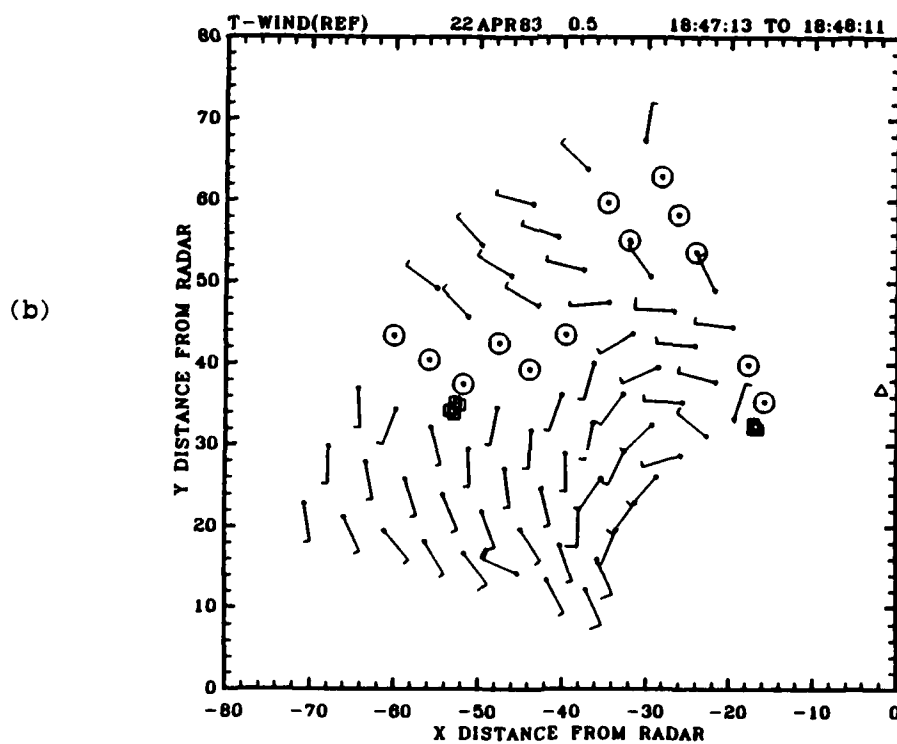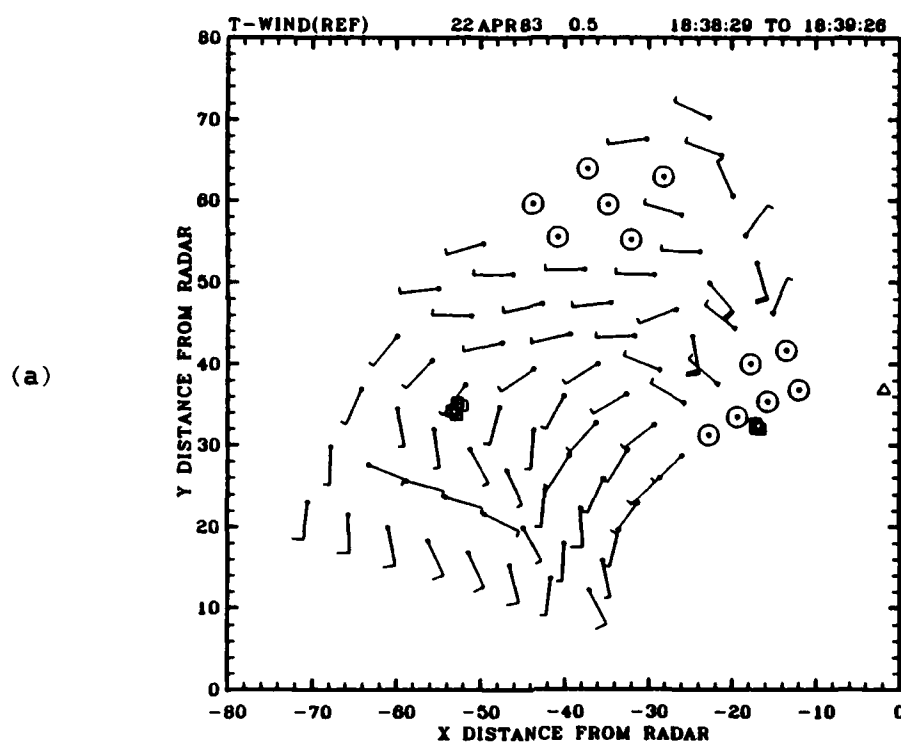
Fig. 2.8. TWIND plots for 22APR83 case at 0.5° elevation angle and ΔT of (a) 57 and (b) 58 seconds.

Albeit subjective, the interpretation here is that the shorter ΔT allows the transverse wind approach to more closely reflect the local winds. As the ΔT increases, the movement at the generator level has a greater influence on the transverse wind product.

This analysis was initially conducted on the 22APR83 data set, using a box size of 10 km (based on the long ΔT's). For the sake of completeness, this comparison was repeated with the 27JUN83 and 28JUN83 data using an 8 km box size (based on the spatial resolution and short ΔT's). The results and conclusions were the same.

One possible indication as to the degree of confidence in the winds produced by the transverse wind approach is the value of the maximum correlation coefficient used to determine the wind vector. The correlation coefficient is a measure of the strength of the relationship between a BOX1 and the associated BOX2's. Thus, more reliable wind estimates are expected with higher correlation coefficients. Rinehart (1979) observed "that the error rate is poor for low correlation" values. In line with this, the maximum correlation coefficients were tabulated and grouped by ΔT categories (Table 2.2). Over 99% of the vectors from the 57 second ΔT grouping had maximum correlation coefficients of 0.70 or greater. The other three groups (467,525, and 582 seconds ΔT) fell well short of this level (74%, 67%, and 68%, respectively). Over all three cases the maximum correlation coefficients appeared considerably higher than those found by Rinehart (1979), Smythe (1981), Hamidi et al. (1983), Smythe (1983), and Smythe and Harris (1984). Several factors may have played a role in this, including nature of the storms, range to the center of the observation window, or others.

Table 2.2. Transverse wind correlation data vs. ΔT groups for 22APR case.

Vectors		Maximum Correlation Coefficients				
ΔT(sec)	Total	1.0-0.9	.89-.80	.79-.70	.69-.60	< .60
57	704	650	45	5	1	3
467	293	17	110	91	48	27
525	823	37	269	250	167	100
582	235	0	82	78	40	35

The findings with regard to the pattern comparisons and the maximum correlation coefficient are in line with previous work indicating that the shorter ΔT's produce a more reliable vector. However, another measure of "goodness" used by previous researchers is the internal consistency of the vectors. Internally inconsistent vectors are those vectors which seem to be at odds in magnitude or direction with the general trend of those vectors in close proximity. Although variations in the wind field of a thunderstorm are to be expected, there still should be an element of consistency within groups of vectors that should be observable.

In preparation for making a count of consistent and inconsistent vectors, the examination of the TWIND plots with superimposed reflectivity contours resulted in an interesting observation. Recall that this study used an observation window which remained fixed while the storms passed through the area. At times this resulted in an

observation window containing very little of the storm. As seen in Fig.
2.9, the pre-storm environment (i.e., the region outside the 10 dBZ
contour) contains a very noisy wind field. This is not unexpected as
the transverse wind technique uses correlation of patterns in the
reflectivity field to develop the wind vectors. It is well established
that the low reflectivity values outside the storm are highly variable.
This "weak reflectivity variability" should lead to random pattern
matching, as is in fact observed. With this in mind, the decision was
made to look for internally consistent (or inconsistent) vectors only
within the 10 dBZ contour of the storms.
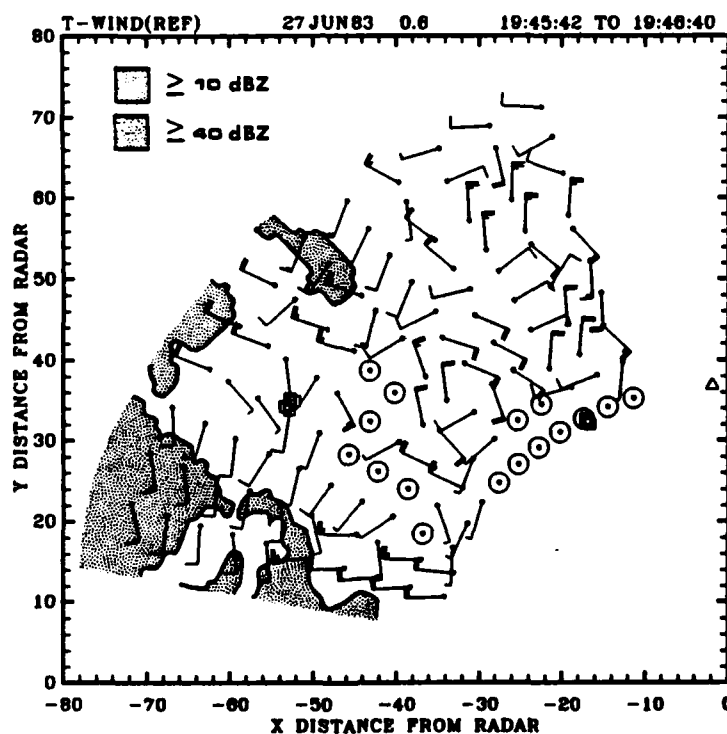
Fig. 2.9. TWIND plot for 27JUN83 case (19:45:42 to 19:46:40) without
maximum correlation coefficient thresholding. Stippling indicates area
of echo with reflectivity values of 10 dBZ or greater.

A total of 15 time periods (TWIND plots at 0.6° elevation angle, 57 seconds ΔT, and 8 km box size) from the 27JUN and 28JUN cases were examined for internally consistent and inconsistent vectors. The maximum correlation coefficients were grouped and tabulated (Table 2.3).

The results from these data (Table 2.3) were quite useful. Approximately 98% of the vectors within the 10 dBZ contour in these cases were internally consistent. Rinehart and Garvey (1978) observed that "erroneous vectors might be eliminated ... by requiring that the correlation coefficients exceed some value." Following this line of reasoning, note that 97% of the consistent vectors in this group have correlation coefficients greater than or equal to 0.85. Unfortunately, 94% of the inconsistent vectors also fall into this group. This is not

Table 2.3. Transverse wind correlation data vs. consistent/ inconsistent vectors.

Correlation	Number of Vectors	
Coefficients	Consistent	Inconsistent
1.0 - .95	363	7
.94 - .90	225	7
.89 - .85	71	1
.84 - .80	8	0
.79 - .75	7	1
< .75	2	0

out of line with the observation by Smythe (1981) that "low maximum correlation coefficients are not always associated with inconsistent arrows, nor are high maximum correlations always indicative of consistent arrows." However, having culled the vectors outside the 10 dBZ contour and with correlation coefficients below 0.85, the remaining inconsistent vectors are only 2% of the total number of accepted derived wind vectors. In addition, it was also observed that in this total group of inconsistent vectors, when plotted only one was greater than 5 m s^{-1}.

Thus, based on this entire assessment (pattern comparisons, maximum correlation coefficients, and internal consistency) the decision was made to conduct all further analyses using data obtained at an elevation angle of approximately 0.5° and a ΔT of approximately 57 seconds. In general, assessments were based only on wind vectors within the 10 dBZ contour and with a maximum correlation coeficient of 0.85 or greater.

Comparisons

As discussed in Chapter I, three types of comparisons can be done with the transverse wind derived data. The first is a comparison between the transverse wind derived data and single Doppler data. The second is a comparison of the transverse wind derived data with SAM data (i.e., actual surface point observations). The third is a comparison of transverse wind derived data with actual observed mesoscale features.

The objective of this research is to test the hypothesis that there is a determinable relationship between the true surface wind field and radar derived wind data. This objective can be divided into two parts. The first part is composed of those comparisons wherein a temporal or

spatial scale difference in the data sets may create interpretation difficulties. While these comparisons may be rejected in time due to these scale differences, the process of conducting the analysis may itself provide insight into the makeup of the data sets. The second part is composed of those comparisons where the data are viewed in a larger context (temporally and/or spatially), which allows for interpretive assessment. While interpretation may be more subjective than the comparisons in the first part, the results may be no less meaningful in terms of meteorological assessment.

Part One

The method used to accomplish the first part of this research objective was to compare at a common time the wind field as derived through two approaches. The study focused on the relationship between the true wind field obtained from the surface automated mesonet (SAM) data and (1) the wind field derived from the Transverse Wind algorithm and (2) the wind field derived from the Doppler radial wind field (DRWF) and the wind direction from the Transverse Wind algorithm. Additional analyses sought to show the relationship of the DRWF with (1) the radial component of the surface wind field derived from the SAM data and (2) the radial component of the wind field derived from the Transverse Wind algorithm. The distribution of the surface wind field was inferred from the available SAM data with time-to-space conversions to increase the coverage area.

Direct objective comparisons were not feasible due to the differences in the spatial density and temporal nature of the Doppler radial velocity data, the transverse wind derived data, and the SAM

data. These temporal and spatial differences in the surface and radar
measurements present a significant complication for any comparisons.
Due to the inherent difficulty in a point-to-point correlation of the
radar data, data derived from the TWIND program, and surface data, a
direct statistical comparison appears unlikely to be meaningful. The
next best approach is that of a subjective comparison of the data
through graphical means. The chosen approach was to plot the TWIND
derived winds, the Doppler radial velocity contours (10 m s^{-1}
increments), and the SAM winds (using time to space conversion to
increase the area coverage) in an area within 10 km of the SAM cluster.
Table 2.4 lists the data comparisons (Field 2 compared with Field 1) and
the procedure (i.e., computer program) used for each comparison. These
data comparisons are discussed in Appendix D.

Table 2.4. Exploratory data comparisons.

FIELD 1	FIELD 2	PROCEDURE
SAM Winds	Winds from TWIND	COMPLOT
SAM Winds	Modified DRWF (DW from TWIND)	MODPLOT
DRWF	SAM Radial Winds	COMPLOT
DRWF	Radial Winds from TWIND	COMPLOT

Part Two

 The method used to accomplish the second part of this research objective was to compare the wind data developed from the TWIND program within the observation window with the observed mesoscale environment. This portion of the research is discussed in Chapter IV (Meso-scale Features: Case Studies) and Chapter V (Radar-Surface Relationships).

CHAPTER III

DATA

Introduction

Data for this research were composed of NEXRAD IOTF Spring 1983
Demonstration Doppler weather radar data in universal tape format,
NEXRAD IOTF Spring 1983 Demonstration surface automated mesonet (SAM)
data, and NSSL instrumented tall-tower data. Analyses focused on storms
that occurred in the data collection area on 22 April, 27 June, and 28
June 1983. These storms produced non-tornadic severe wind events from
non-supercell storms, and data were captured by both the single-Doppler
radar and individual SAM sites. These cases are discussed in detail in
Chapter IV.

Radar Data

Radar data were collected using the NSSL Norman Doppler radar (NRO)
in Norman, Oklahoma. This radar is a modified FPS-18 with 10 cm
wavelength. Data for this research were gathered exclusively in the
"storm mode." Radar parameters for the storm mode of operation during
Spring 1983 data collection for this research project are shown in Table
3.1 (NEXRAD JSPO Staff, 1983b). The data were recorded in real-time and
transferred by staff at the NEXRAD IOTF to universal format tape (UFT)
in post-processing. As discussed in Chapter II, specific data sets were
selected for analysis by examining reflectivity plan position indicator
(PPI) displays for those cases which moved over the SAM sites.

The NSSL system employs a narrow beamwidth (0.81°) and uses a dual pulse repetition frequency (PRF) processing system, which allows the reflectivity data to be taken during a long pulse repetition period with the velocity data interspersed in a short period. This provides a longer unambiguous range for reflectivity and a shorter unambiguous range for velocity, but with a resulting higher Nyquist interval. The velocity estimates are correctly positioned in space by electronically

Table 3.1. NSSL Norman Doppler radar operational parameters for 1983 Spring NEXRAD IOTF demonstration.

PARAMETER	STORM MODE
Scan Rate	1.67 rpm
Volume Update Rate	6 minutes
Elevation Angles (10)	0.5,0.5,1.4,2.3, 3.4,4.6,6.2,8.4, 11.8,18.0 degrees
PRT	768 or 1075 μs
Pulse Length	1 μs
Number of Pulses Averaged	32
Gain	Normal
Velocity Range Gate Spacing	150 or 210 m
Intensity Range Gate Spacing	600 or 840 m
Velocity Range	115 or 161 km
Intensity Range	460 or 644 km
Unambiguous Velocity	± 34.2 or ± 24.5 m s^{-1}

comparing the reflectivity and velocity samples, thus filtering out multiple trip echoes (Burgess et al., 1978). Specific information on the NSSL Norman Doppler radar as recorded in the UFT "header" is printed on the DISKW housekeeping sheet as shown in Fig. 2.1.

Detailed discussion of the production of the three Doppler moments at each gate (pulse volume) is available from Battan (1973) and in a more engineering oriented form from Doviak and Zrnic (1984). It is sufficient for this study to observe that NSSL uses an autocovariance processor, known as a pulse-pair processor, which converts a pair of power spectral density functions for each gate into the reflectivity and radial velocity. The spectrum width is obtained from the standard deviation of the samples of radial velocity in a pulse volume.

Fig. 3.1 was produced by modifying the radar plotting program (RADPLOT) to plot the actual radar pulse volumes at their physical locations in the observation window. As shown in this figure, there are four velocity gates (pulse volumes) for each reflectivity gate. Since the gate number (the reference point to that gate) is fixed at the center of the gate, there is a half-gate overlap at the beginning of each reflectivity/velocity gate set. This figure also highlights the spatial and temporal differences between the velocity data derived from TWIND (correlation procedure using multiple reflectivity pulse volumes, Fig. 3.1a), Doppler radial velocity (individual velocity pulse volumes, Fig. 3.1b), and the SAM sites (individual points, Fig. 3.1a and b).
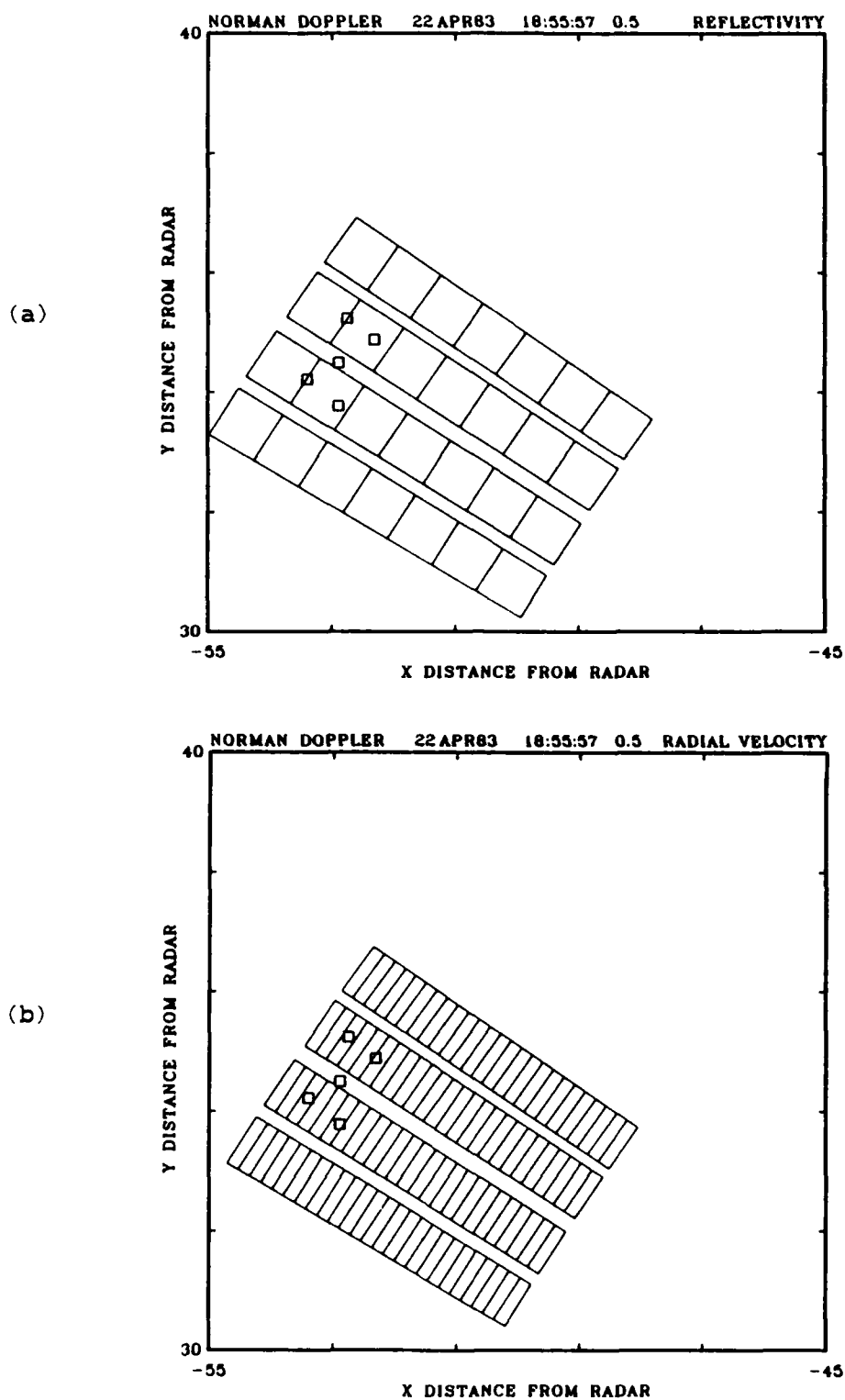
Fig. 3.1. Radar field relationships and gate spacing for (a)
reflectivity and (b) radial velocity data. Distances are in kilometers.
Small squares are the physical locations of the 60-series SAM sites.

Surface Data

The NEXRAD SAM site locations were selected to provide surface
verification for this research. The staff at NSSL installed and
calibrated the sensors, serviced the sites during the spring program,
conducted an assessment of the data quality as tapes were returned to
Norman, performed an instrument calibration check at the end of the
spring program, and archived the data set. The sites were located to
maximize the opportunity to capture surface wind events in the near-,
mid-, and far-fields of the radar. For 40- and 60-series site locations
refer to Figs. 3.2 and 3.3 and Table 3.2. The equipment spacing within
each cluster was designed to compare optimally with the radar pulse
volume at the respective ranges (See Table 3.3 and Fig. 3.3).
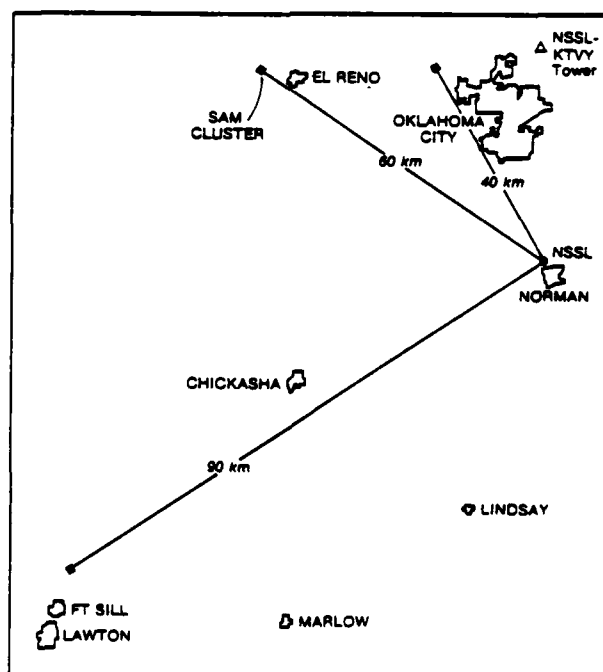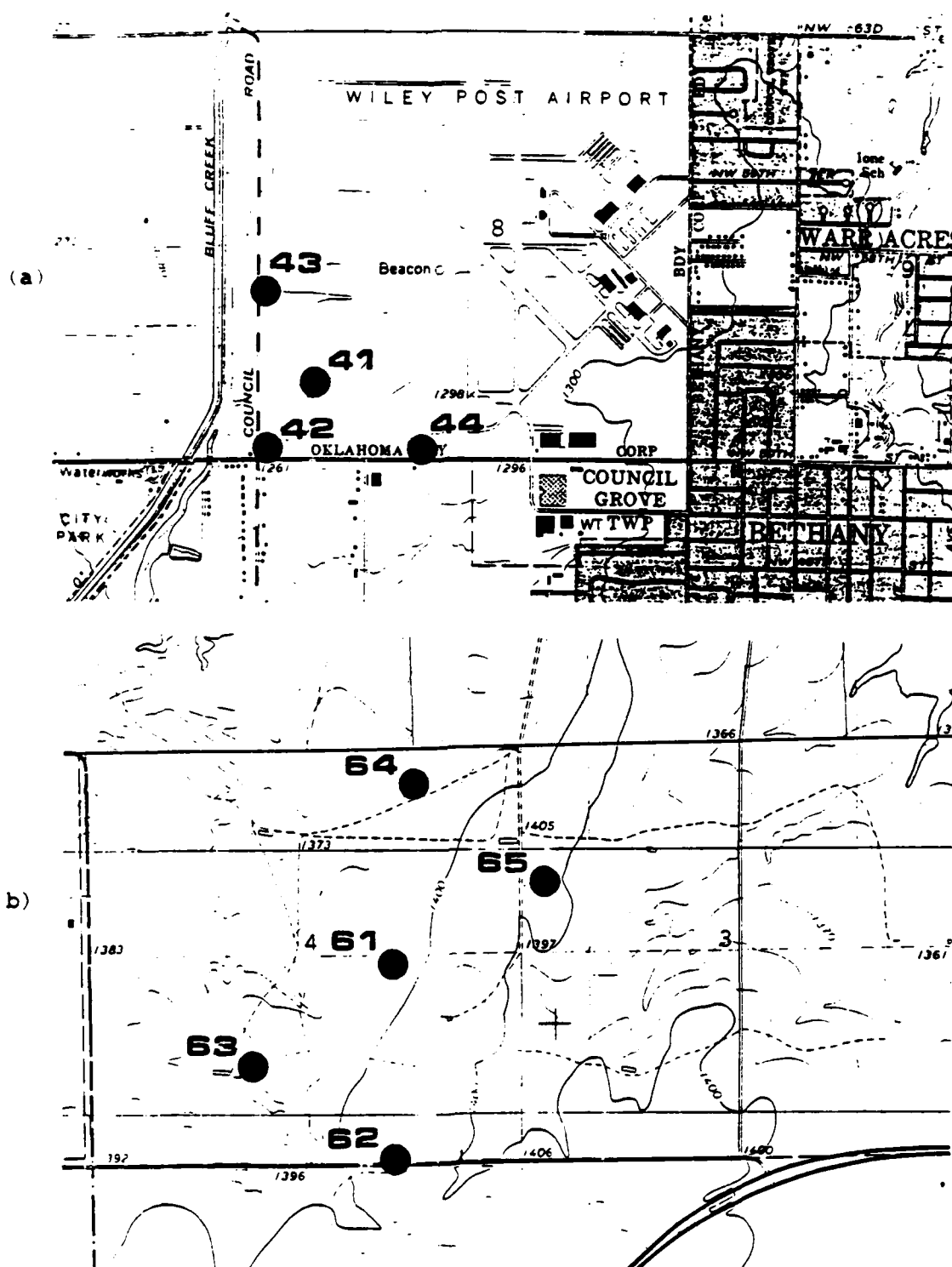

Fig. 3.2.   SAM site locations with respect to NSSL.

Fig. 3.3. USGS quadrangle maps of locale for the (a) 40-series SAM complex (Wiley Post) and (b) 60-series SAM complex (Ft. Reno).

Table 3.2. NEXRAD IOTF Spring 1983 demonstration SAM site locations.

ID	Number	MSL Elev.* (ft)	Azimuth (deg)	Range (km)
N01	8341	1270	332.28	36.52
N02	8342	1262	331.77	36.39
N03	8343	1267	332.21	36.91
N04	8344	1294	332.55	36.12
N05	8361	1395	303.10	63.14
N06	8362	1414	302.55	62.75
N07	8363	1380	302.64	63.41
N08	8364	1380	303.73	63.44
N09	8365	1402	303.68	62.87
N10	8391	1298	235.45	91.93
N11	8392	1278	235.76	93.00
N12	8393	1290	235.84	92.40
N13	8394	1275	235.05	91.30
N14	8395	1268	234.79	91.59

Table 3.3. NEXRAD IOTF Spring 1983 demonstration SAM sites/radar beam relationship.

SERIES	NAME	DIMENSIONS (m)	BEAM WIDTH (m)	BEAM HEIGHT (m)
40	Wiley Post	600 X 600	523.1	403.5
60	Fort Reno	600 X 1250	890.6	783.4
90	Fort Sill	600 X 1750	1300.6	1301.0

*plus four feet to instrument shelter

Data were sampled at a rate of one sample per parameter per second. Signal averaging formed 1-minute means from the 60 1-second samples per parameter. In addition, the maximum measured by the wind speed sensor and the minimum measured by the pressure sensor for each minute were also recorded. Temperature and pressure sensors were housed in a standard weather service Stevenson screen, which provided shielding from solar radiation.

Brief description of the sensors is included in Table 3.4, and the range of operation and meteorological resolution is given in Table 3.5. The raingage was reset to zero when the equipment was serviced (every week or two). The small variations (blips) in the raingage data are due to a problem with quantization. Large variations in wind direction can routinely occur with wind speeds below 5 m s^{-1}. This is due in part to the natural variability of the wind direction at these speeds and to the 8-bit recording scheme used for wind direction. (Wardius, 1986)

Table 3.4. NEXRAD IOTF Spring 1983 demonstration SAM sensors.

Parameter	Sensor Equipment
Wind Speed	Weather Service F-420-C rotating cup DC generator (specially calibrated)
Wind Direction	Weather Service F-420-C splayed tail wind vane (modified direction transmitter providing direction dependent DC output)
Dry/Wet Bulb Temperature	Linearized Yellow Spring Model 44202 Thermistors (self-wetting bulb with aspiration by vertical axis fan at not less than 2.5 m s^{-1})
Station Pressure	Texas Electronics Aneroid/Linear Variable Differential Transformer Unit (precision aneroid cell with electrical, but no direct mechanical, connection to motion sensing transducer)
Rainfall	Belfort Model 5-780 weighing bucket raingage (weight sensing load cell replaces spring and balance mechanism)
Corona Probe	N/A

Table 3.5. NEXRAD IOTF Spring 1983 demonstration SAM sensors (range and resolution).

PARAMETER	RANGE	METEOROLOGICAL RESOLUTION
Pressure(Avg,Min)	850 - 1000 mb	0.6 mb
Rainfall	0 - 230 mm	1 mm
Winds (u,v)	0 - ±56 m s^{-1}	0.4 m s^{-1}
Winds (speed max)	0 - 56 m s^{-1}	0.4 m s^{-1}
Temperature (Td,Tw)	0 - 50 °C	0.2 °C
Corona Current	0 - +1.25 μA	0.1 μA

Tower Data

Since 1966, NSSL has maintained and operated a meteorologically instrumented tall-tower (KTVY television tower, formerly WKY). The location of this tower (357°/37 km from the NSSL Norman Doppler radar) is shown in Fig. 3.2. Specifications for the instrumentation of the tower are given in Table 3.6. Sanders and Weber (1970), Carter (1970), and Goff and Zittel (1974) provide details about this tower. Data during the 1983 demonstration were gathered routinely, quality controlled, and made available as a data set on standard 9-track tape.

Table 3.6. NSSL-KTVY instrumented tower specifications.

VARIABLE	UNITS	TOWER LEVEL (m)
Data	MMDDYY	-
Time	HHMMSS	-
Wind Speed	m s^{-1}	sfc,26,45,89,177,266,444
Wind Direction	degrees	sfc,26,45,89,177,266,444
Temperature (Td)	°C	sfc,26,45,89,177,266,444
(Tw)	°C	sfc,89,266,444
Vertical Velocity	m s^{-1}	26,45,89,177,266,444
Pressure	MV	sfc,444
Pyranometer	ly min^{-1}	sfc
Raingage	millimeter	sfc

CHAPTER IV

MESO-SCALE FEATURES: CASE STUDIES

Introduction

This chapter is designed to provide a general discussion of three
case studies, which provide the meteorological foundation to this
research. The storms selected were non-tornadic meso-convective storms,
which occurred during the data gathering period at the NSSL Norman
Doppler radar and passed over one or both of the two surface automated
mesonet (SAM) clusters closest to the radar. Events meeting this
criteria occurred on April 22, June 27, and June 28, 1983.

The approach is to discuss each case study from a general
meteorological standpoint, incorporating a meso-analysis developed from
the routine synoptic observations in the area of interest, and point
data from the SAM sites. The goal is to obtain a general level of
understanding of the meteorological events which occurred during each of
these cases. Cases will be discussed in the following order: June 27,
June 28, and April 22. Selected hourly surface observations for each
case are provided in Appendix E.

Case 1: June 27, 1983

This case occurred in the evening of June 27, 1983. The case was
first examined by Sickler, et al. (1985a) and later by Pophin (1986).
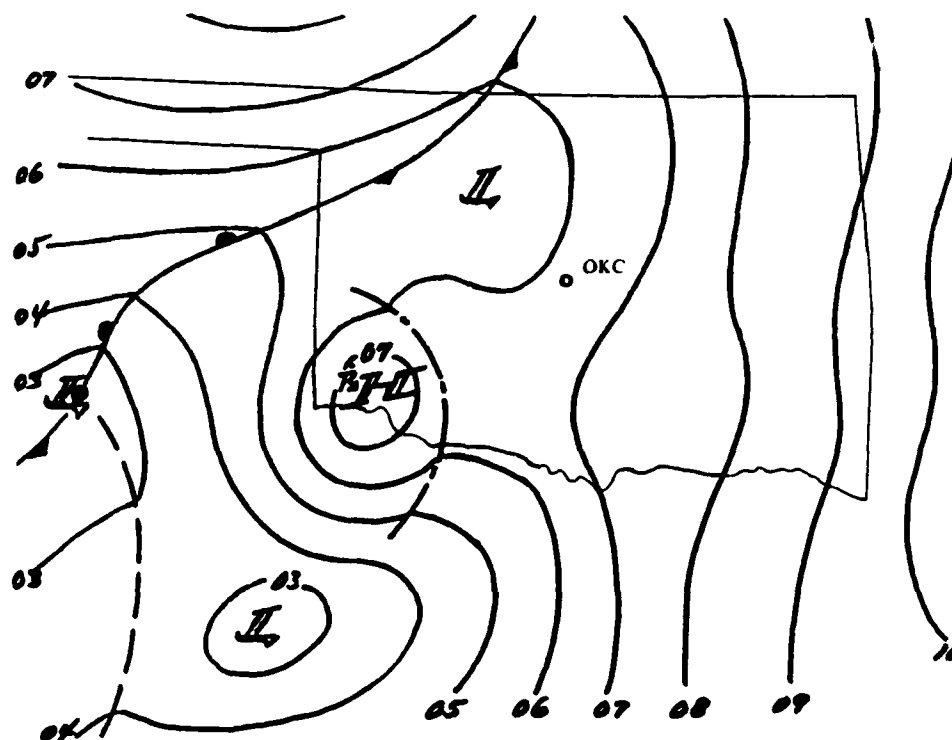The 1800 CST surface meso-analysis (Fig. 4.1) set the stage for this

Fig. 4.1. Surface meso-analysis for 1800 CST on 27JUN83.

case. A low was located in the south-central portion of the Texas

panhandle. A frontal system extended northeast through Amarillo (AMA),

Texas, passed between Gage (GAG) and Enid (END), Oklahoma, and continued

into Kansas. A meso-high had developed in the vicinity of Altus (LTS),

Oklahoma. An instability line had formed in conjunction with this meso-

high and began to propagate to the east. A line of severe thunderstorms

developed along this instability line, as in the classical model

proposed by Fujita (1955). This squall line moved toward the east at

approximately 25 m s^{-1}.

Surface conditions showed that the area around Oklahoma City was under the influence of a warm moist tropical air mass. The two northern SAM clusters (60-series and 40-series) reflected these conditions. From 1600 to 1800 CST the dry- and wet-bulb temperatures were constant (low thirties and mid-twenties, respectively). Generally, winds were from the south with speeds below 5 m s^{-1}.

At 1900 CST the local area analysis (Fig. 4.2) showed the low to be moving slowly to the east as were the warm and cold frontal systems. The meso-high continued to build in the vicinity of Wichita Falls (SPS), Texas. The instability line continued to move to the east. No changes occurred at the SAM complexes (Figs. 4.3* and 4.4), except for the usual diurnal cooling and pressure rises. When the convection at the leading edge of the instability line had approached to within 20 km of the 60-series SAM complex, the only observed change in the surface conditions was a slight increase in the wind speeds (4-5 m s^{-1} before this time to 6-7 m s^{-1} just before the thunderstorms passed over the SAM complexes). The wind direction also changed slightly from the south to the south-southwest.

---

*SAM site number 65 was not operational through the period of June 27-28, 1983.
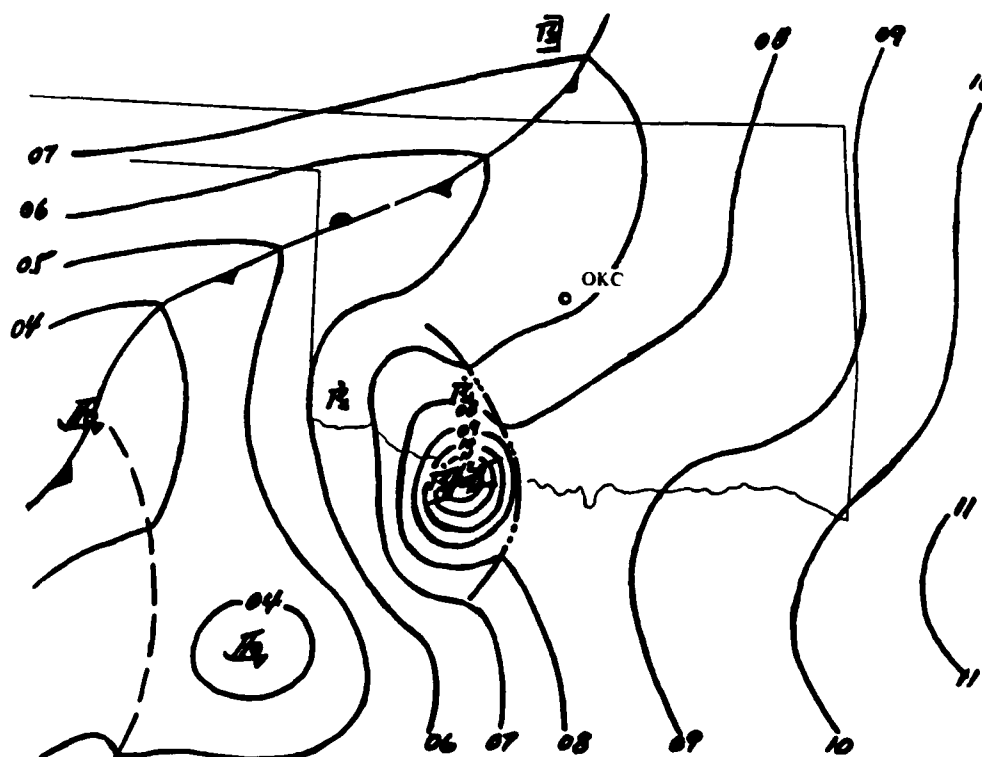
Fig. 4.2. Surface meso-analysis for 1900 CST on 27JUN83.

At 1955 CST, radar reflectivity data indicated the leading edge of the 10 dBZ area over the 60-series SAM complex (Fig. 4.5). The surface observations at the 60-series SAM complex showed that a gust front was associated with this return (Fig. 4.3). As the gust front passed the 60's complex, there was a pressure jump followed by a quick change in wind direction, a temperature fall, and drastic increase in wind speeds. The pressure rose 1 mb in the first minute and 3 mb in the first nine minutes after the gust front passed over the complex. The movement of
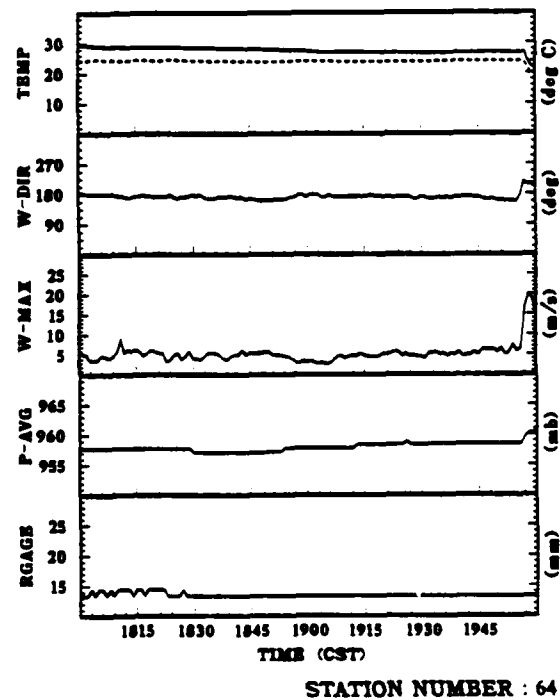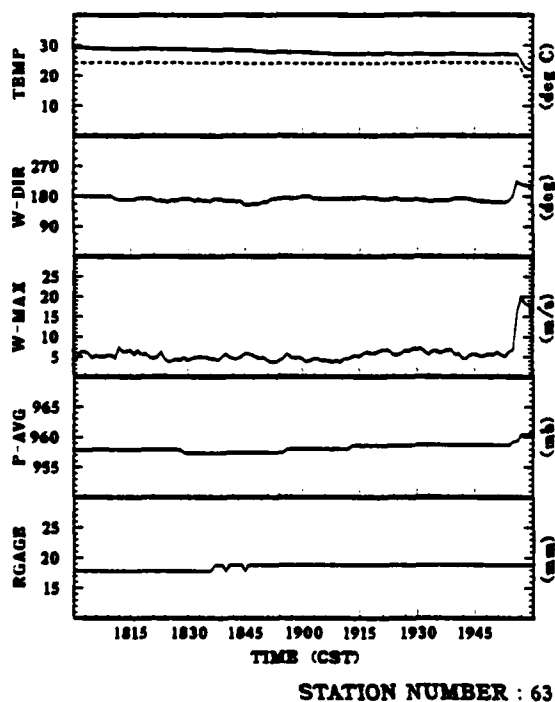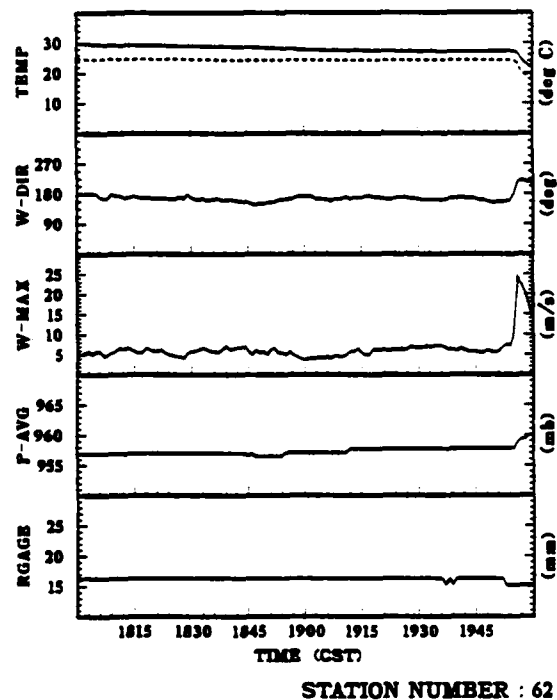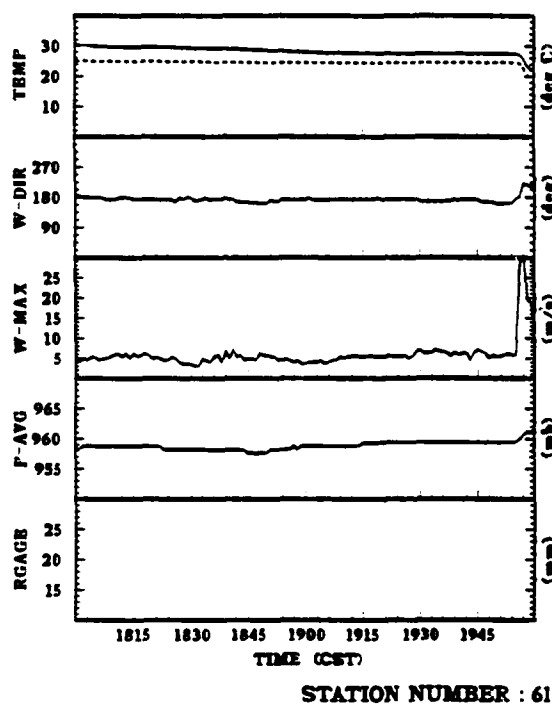
Fig. 4.3. SAM data (60-series) for 27JUN83 case (1800 - 2000 CST).
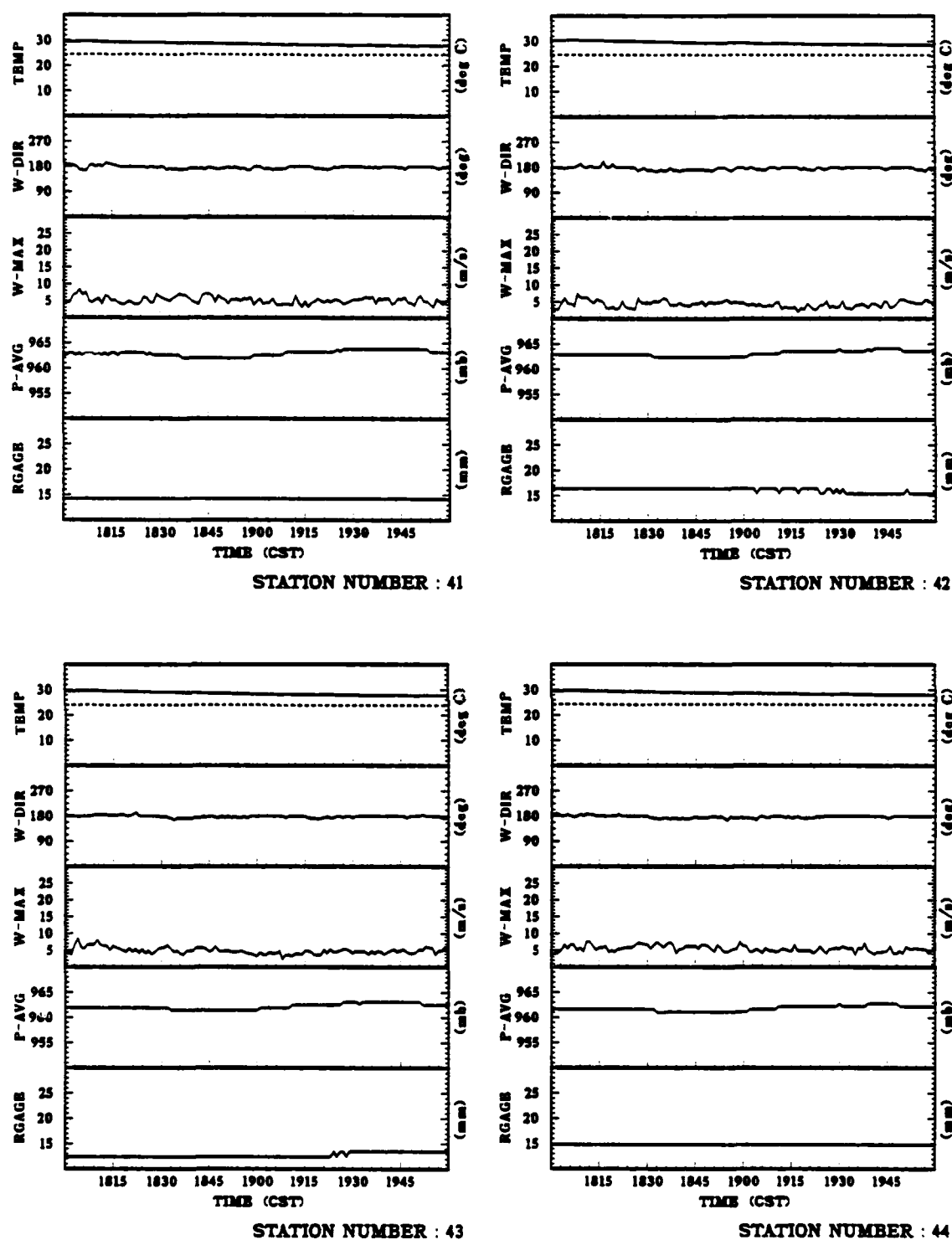
Fig. 4.4. SAM data (40-series) for 27JUN83 case (1800 - 2000 CST).

the front was estimated at about 20 m s⁻¹ which gives a pressure

gradient of about 3 mb per 10 km across the gust front. At the same

time, winds veered from the south to the southwest, perpendicular to the

gust front. Wind speeds along the front gusted to as high as 31 m s⁻¹.

The temperature fell drastically with the passage of the gust front with

a decrease in temperature of 5°C within the first 3 minutes after

frontal passage. This description fits very well with the detailed

description made by Tepper (1950) of the weather changes that typified

the passage of a squall line system at the ground. Although Tepper

noted that these changes occurred in an ordered fashion over a period of

a few minutes, in this case the observations from the complex showed

that all of the changes occurred simultaneously.
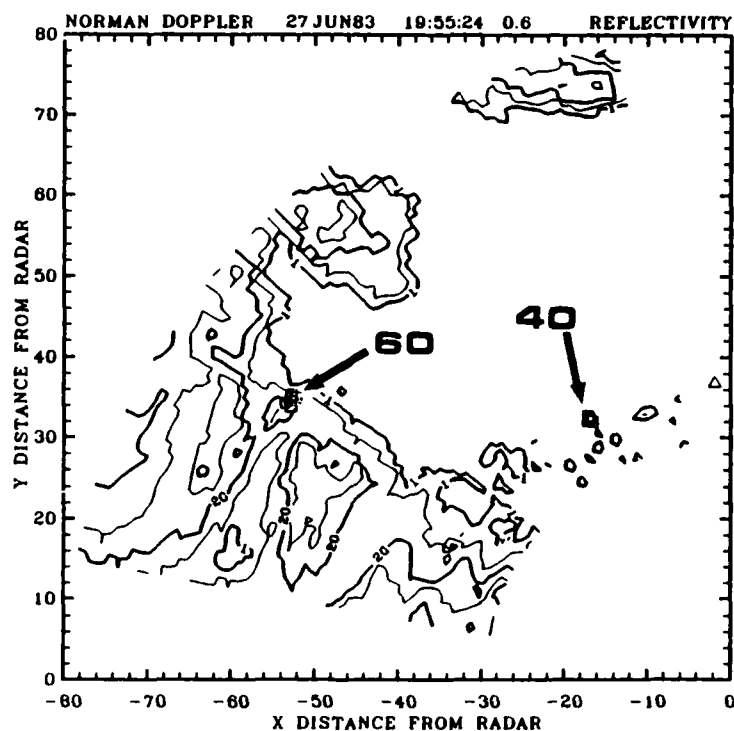
Fig. 4.5. Norman Doppler radar contoured reflectivity plot for
19:55:24 CST on 27JUN83. Arrows denote locations of SAM complexes.

By 2000 CST, the northern portion of the instability line was located southwest of OKC, and moving northeast (Fig. 4.6). The low continued to move slowly to the east, and the frontal system began to pivot about the low due to the faster movement of the northern portion of this system.
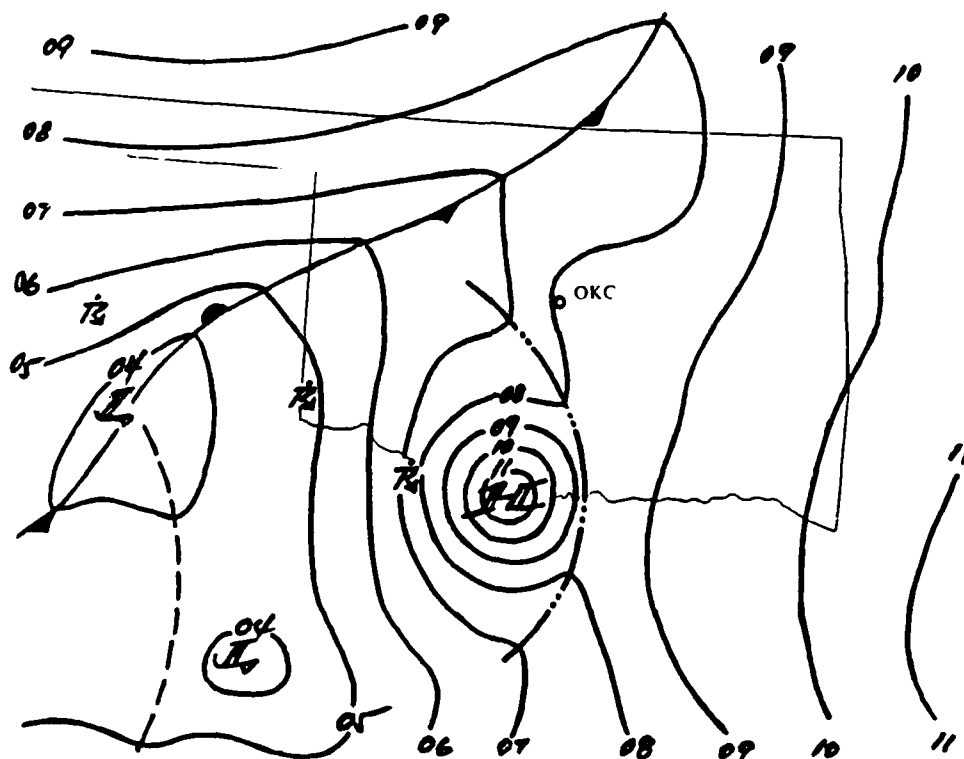
Fig. 4.6. Surface meso-analysis for 2000 CST on 27JUN83.

The arrival of a 40 dBZ core in the storm (Fig. 4.7) corresponded to the beginning of rainfall at the 60-series SAM sites (Fig. 4.8) at approximately 2005 CST. Winds peaked (21 - 30 m s^{-1}) at approximately 2005 CST, then began a gradual decline reaching a local minimum at 2047 CST. Wind direction, which had reached 248°, began backing to a southerly direction at 2048 CST. Over this same time frame, the average pressure gradually fell. This corresponds in the meso-analysis to the formation of a meso-high behind the instability line and its movement over the SAM cluster (see Fig. 4.6 and the figure on page 60).

Fig. 4.7. Norman Doppler radar contoured reflectivity plot for 20:05:06 CST on 27JUN83.

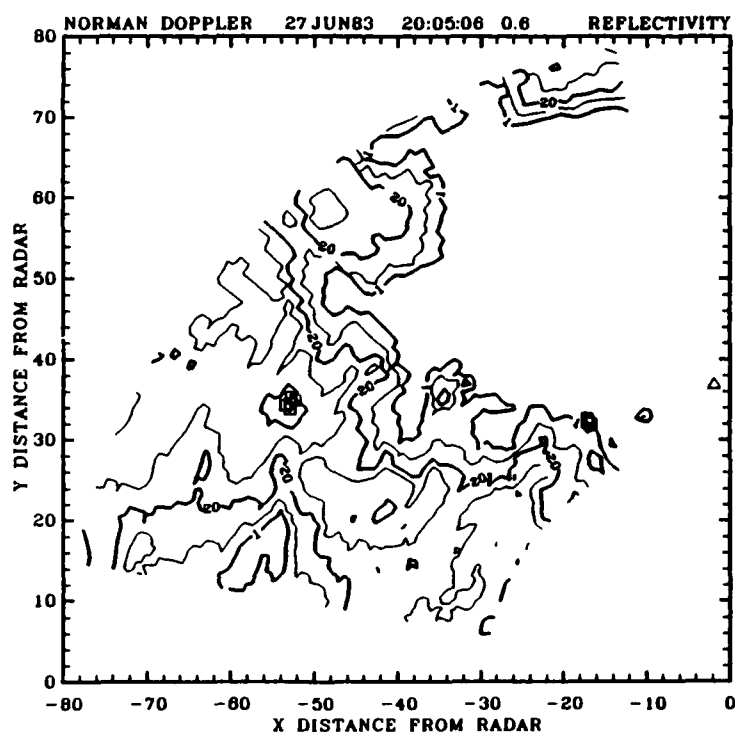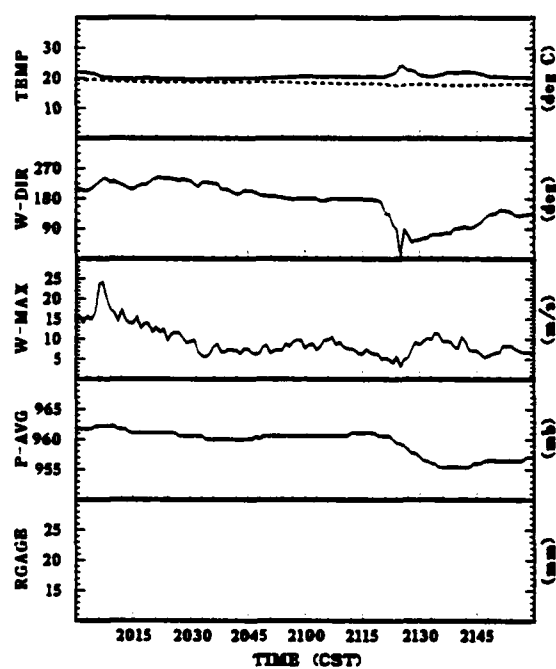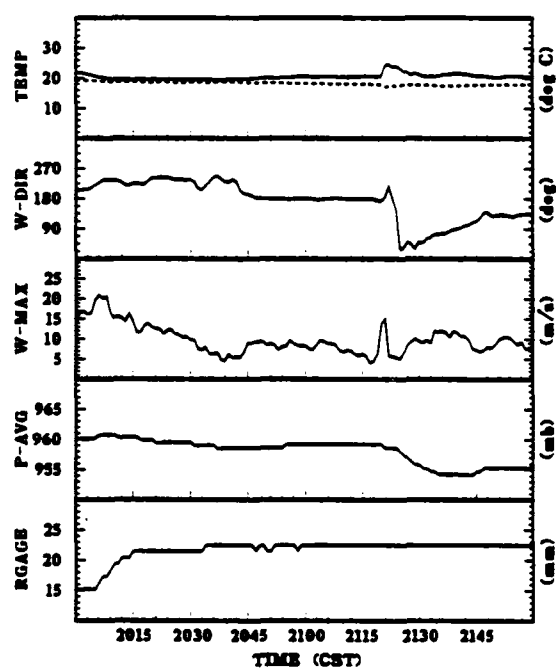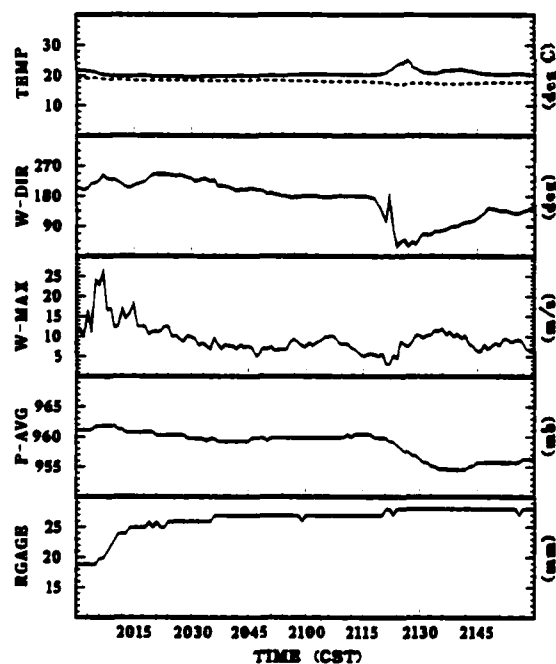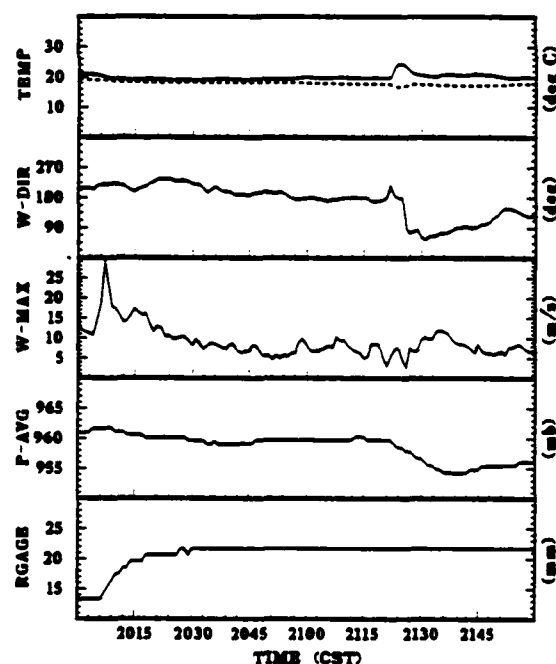Fig. 4.8. SAM data (60-series) for 27JUN83 case (2000 - 2200 CST).

At approximately 2007 CST, the instability line, convection, and gust front passed over the 40-series SAM complex. The same characteristics of the gust front were noted except all the features tended to be weaker (Fig. 4.9). At the 40-series cluster, winds rapidly increased beginning at 2006 CST reaching a peak at approximately 2015 CST. Winds were 180° and veered to 230° at approximately 2008 CST, at which time the dry- and wet-bulb temperatures decreased, and the relative humidity increased. Concurrently, the average pressure began a slow increase. The pressure rise was 1 mb in the first minute, but only 2.5 mb in the first fourteen minutes. The pressure gradient along this portion of the front was 1.5 mb per 10 km, about half as strong as when the front passed the 60's complex. The temperature fall was about the same as with the 60's complex, 5.6°C.

The tower data (Fig. 4.10) show the gust front passage with a rapid decrease in dry- and wet-bulb temperatures at 2018 CST at all levels. Humidity increased to saturation at level 7 at 2026 CST and at the surface at 2033 CST. First indication of rainfall was at 2035 CST. At the upper levels there was a "dry warming" pulse at 2047 CST at level 6 and 2050 CST at level 7. The wind direction trace showed decreasing variability from the surface to the upper levels. Wind direction was
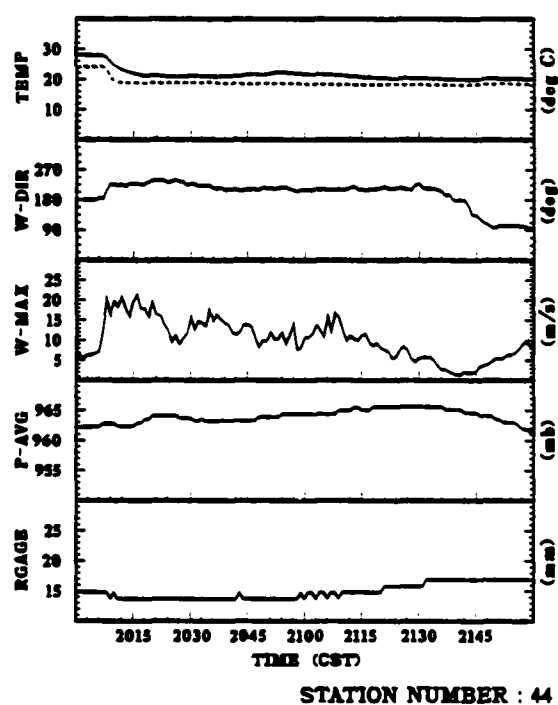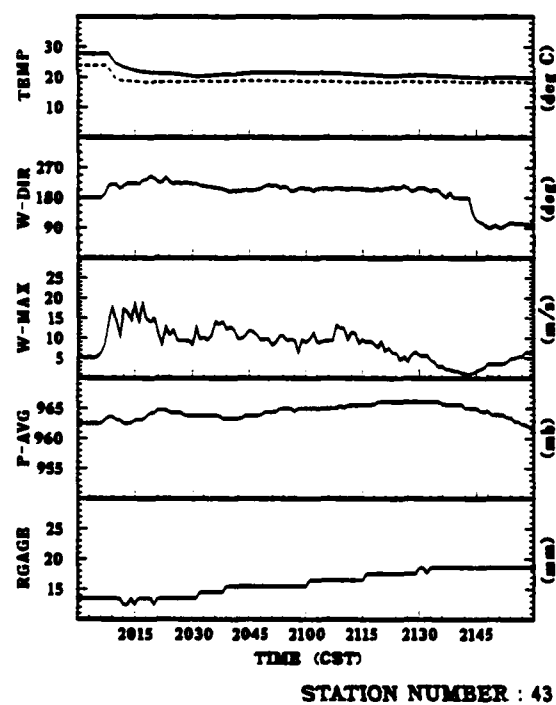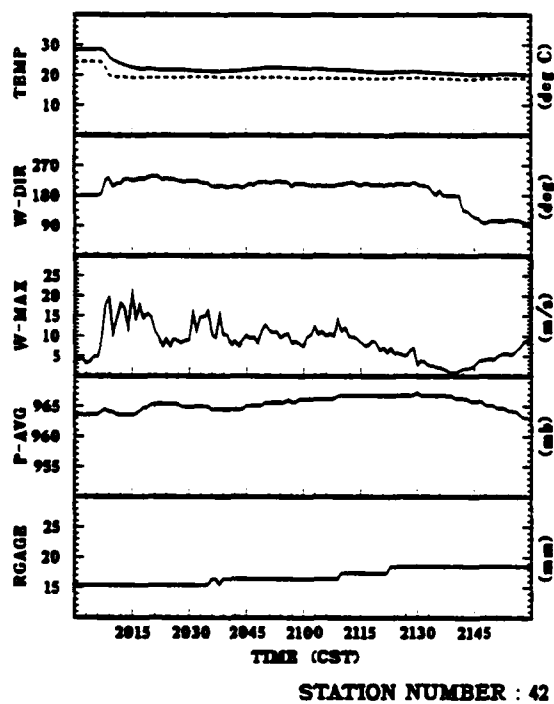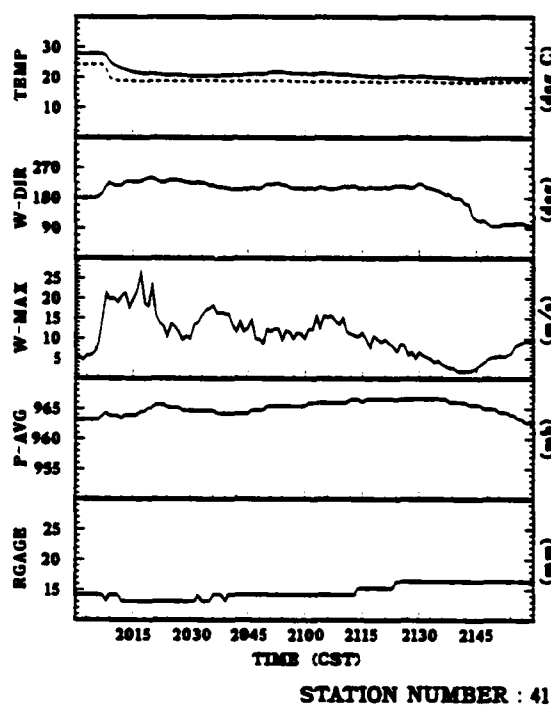
Fig. 4.9. SAM data (40-series) for 27JUN83 case (2000 - 2200 CST).

from the south and at about 2017 CST rapidly veered to the west-southwest. Upper level winds remained from the west-southwest, while the lower levels showed the winds begin to back and return to southerly about 2049 CST. Wind speeds showed a very interesting profile. Speeds began at around 5 m s^{-1} for the low levels, and at 12 m s^{-1} for the upper level. All levels showed a sudden increase in speeds at about 2017 CST. At the surface, winds peaked at 22 m s^{-1}. Above the surface, winds peaked at 28 m s^{-1}. Then the speeds dropped back below 10 m s^{-1} at the surface by 2030 CST, whereas the upper levels remained noticeably stronger (10 to 20 m s^{-1}). In fact, at the upper level, the wind speed remained above 20 m s^{-1}. Pressure at the surface began a slow increase at about 2018 CST following a sudden small increase. At level 6, the pressure showed a small drop at 2012 CST and then a gradual increase beginning at about 2018 CST. Rainfall began at about 2035 CST. In general, vertical velocity showed a net of zero, except at the upper two levels during the period from 2016 to 2027 CST. During this period there was a strong net upward component at these two levels.
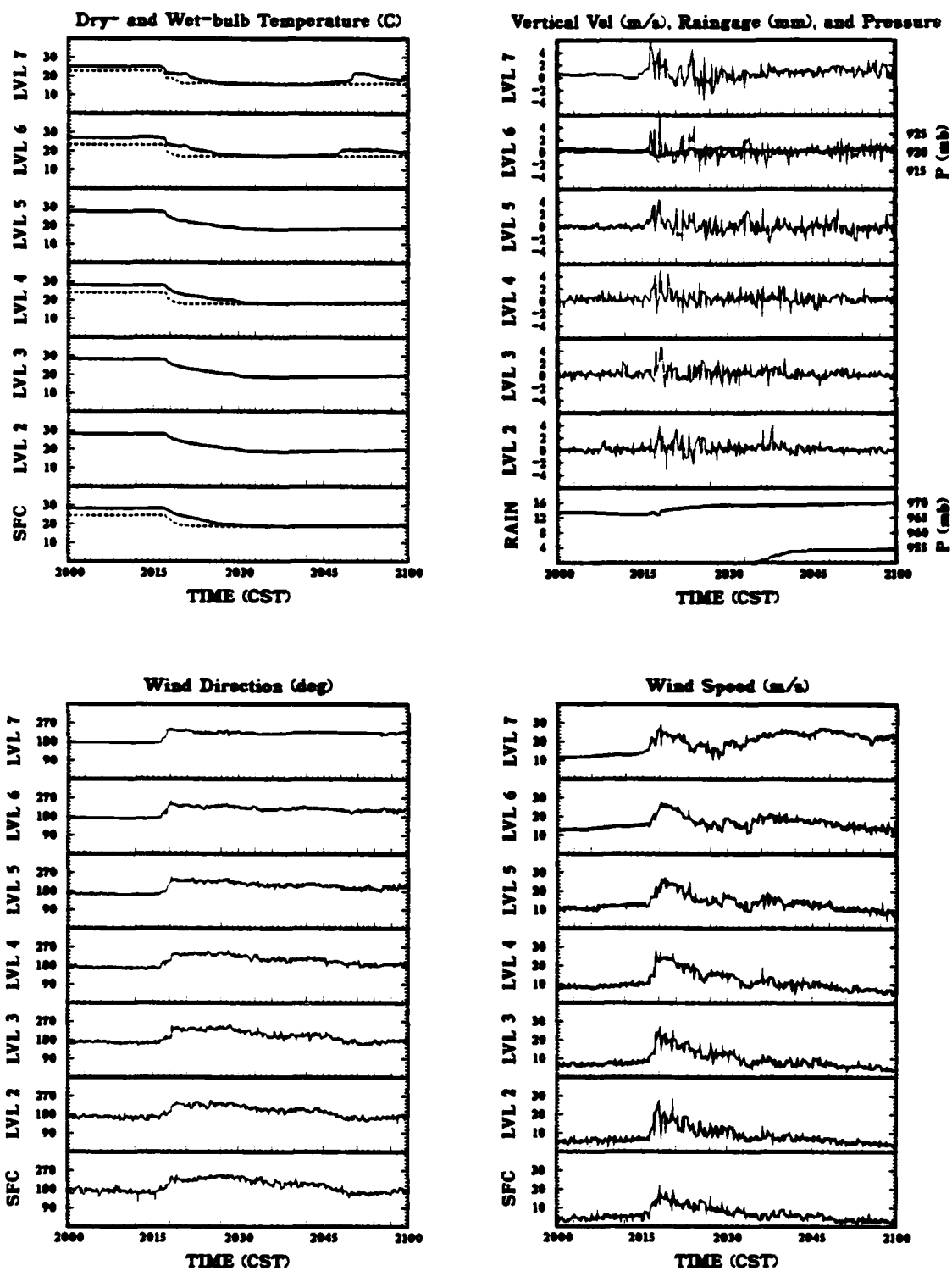
Fig. 4.10. NSSL-KTVY tower data for 27JUN83 case (2000-2100 CST).

From the 2100 CST meso-analysis (Fig. 4.11), the low and the frontal system continued to move slowly to the east. The instability line had passed through OKC, and as discussed previously, a pair of meso-highs had formed behind this line. After the initial precipitation fell, no other measurable precipitation was observed during the study period.

As the instability line moved off to the east, an interesting feature appeared in the 60's complex data. At about 2122 CST, a quick rise in temperature, fall in pressure, backing in wind direction, and increase in wind speed was observed. This event looked like the "wake low" described by Fujita (1963). With the drastic shift in wind from the south to the north-northeast, all indications were that the core of the downdraft had passed over a c plex at about 2122 CST.
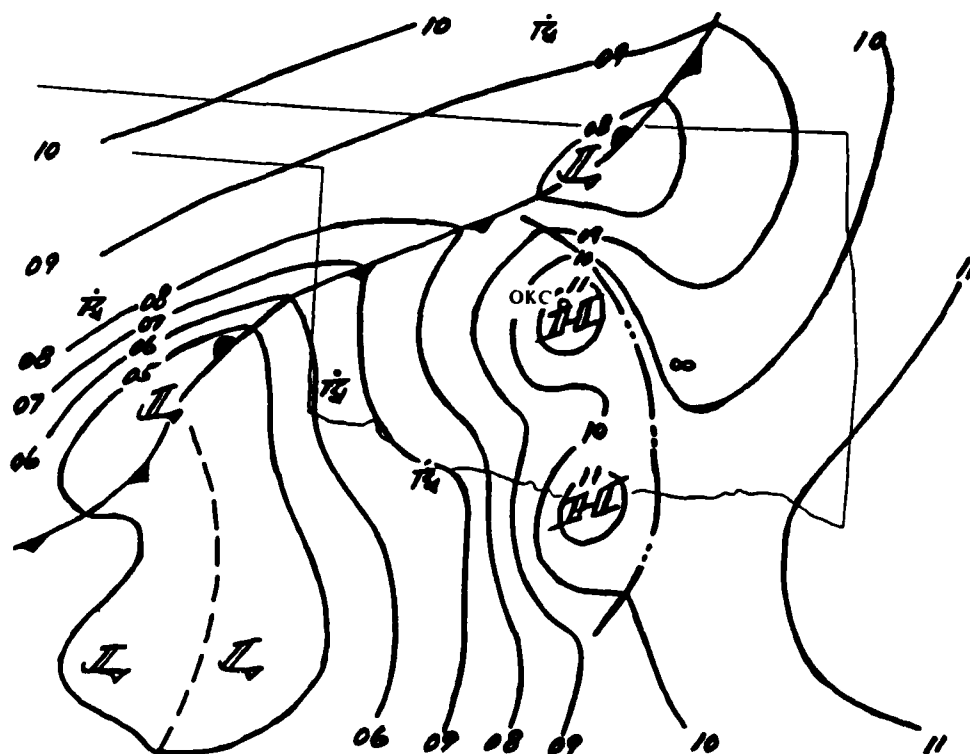
Fig. 4.11. Surface meso-analysis for 2100 CST on 27JUN83.

The tower (Fig. 4.12) also recorded the "dry warming pulse" at levels above the surface. Initial appearance of this pulse was at the top level at 2110 CST, followed at level 6, 12 minutes later. This pulse was identifiable down to level 3 at 2154 CST. Wind direction showed some veering from the surface (southerly) to the tower top (southwesterly) at 2100 CST. Winds slowly veered with time at all levels until approximately 2146 CST, when the surface winds began to rapidly back, becoming southeasterly by 2200 CST. This backing was evident in the lowest four levels with level four beginning to back at 2159 CST. One result of this "tilt" in the system was that at 2200 CST the surface winds were from 126° and the winds at the tower top (444 m) were from 306°. At the surface during the period 2100 CST to 2200 CST wind speed never exceeded 10 m s^{-1}. At the upper level, wind speed was about 25 m s^{-1} and gradually declined to about 6 m s^{-1} along a rather uniform slope. At the mid-levels, however, the speeds began at 4 m s^{-1} to 12 m s^{-1} and peaked at about 20 m s^{-1} (levels 5 and 6) and 16 m s^{-1} (level 4) around 2126 CST. At the top level, the vertical velocity was upward from 2100 to 2136 CST.

As the storm moved away from the complexes, all variables returned to ambient conditions until the next instability line approached. This second line of thunderstorms developed on the frontal system from just west of Wichita (ICT), Kansas, to just south of Dalhart (DHT), Texas. The line began moving slowly to the southeast at 2000 CST. These storms are discussed as case 2, based on the time of observation over central Oklahoma (2330 CST, June 27, to 0200 CST, June 28, 1983).
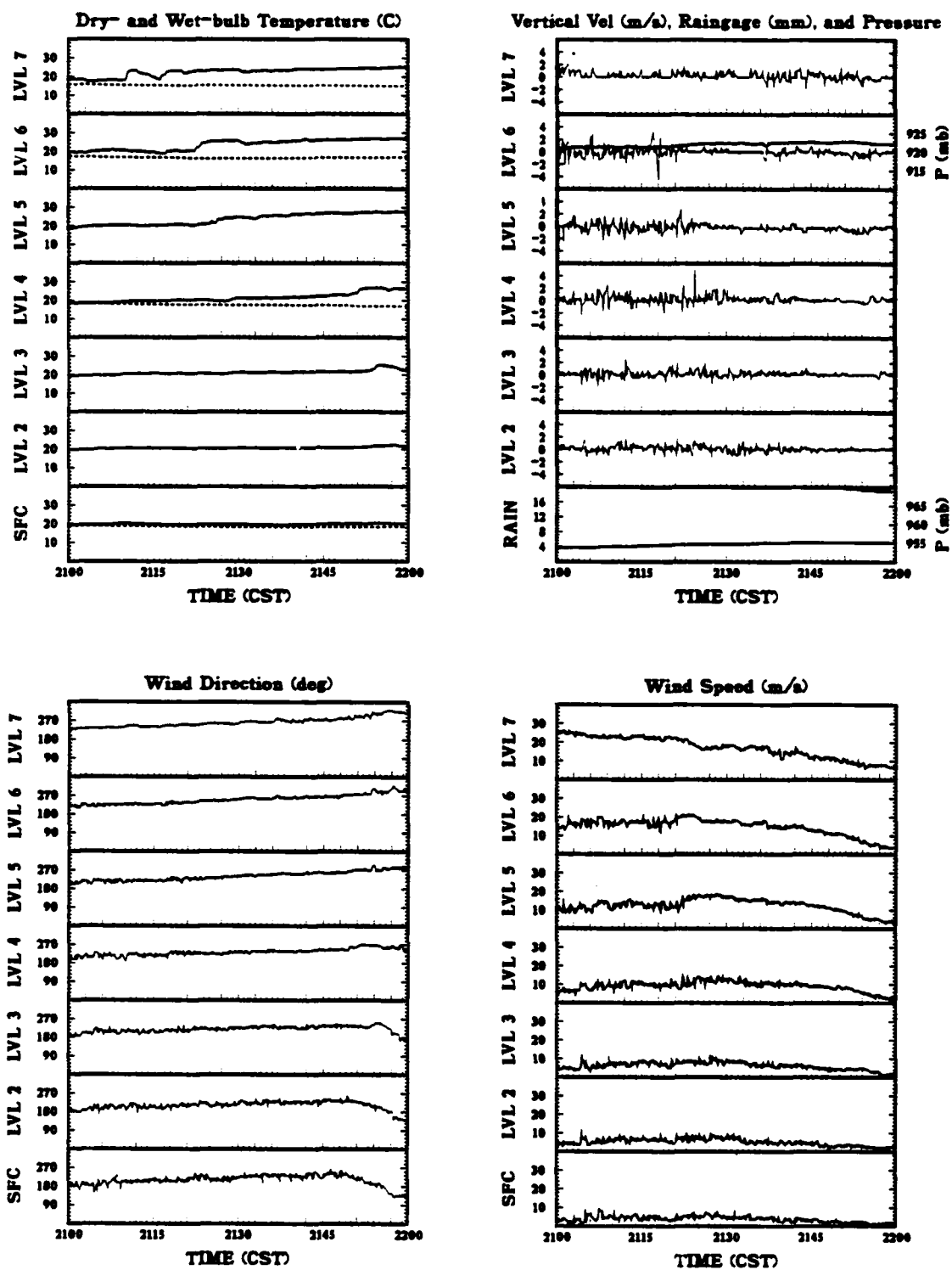
Fig. 4.12. NSSL-KTVY tower data for 27JUN83 case (2100 - 2200 CST).

Case 2:   June 28, 1983

This case occurred in the very early hours of June 28, 1983, and was first examined by Sickler, et al. (1985a). These storms began to develop in northern Texas as early as 1500 CST on 27JUN behind the strong cold air advection from the high plains. The storms entered northwestern Oklahoma by 2100 CST. The surface meso-analysis for 2200 CST, June 27, (Fig. 4.13) showed that the low was northeast of Lubbock (LBB) and southeast of Amarillo (AMA), Texas. The frontal system was moving very slowly to the east. The instability line in eastern Oklahoma continued to move rapidly to the east, and the meso-high behind
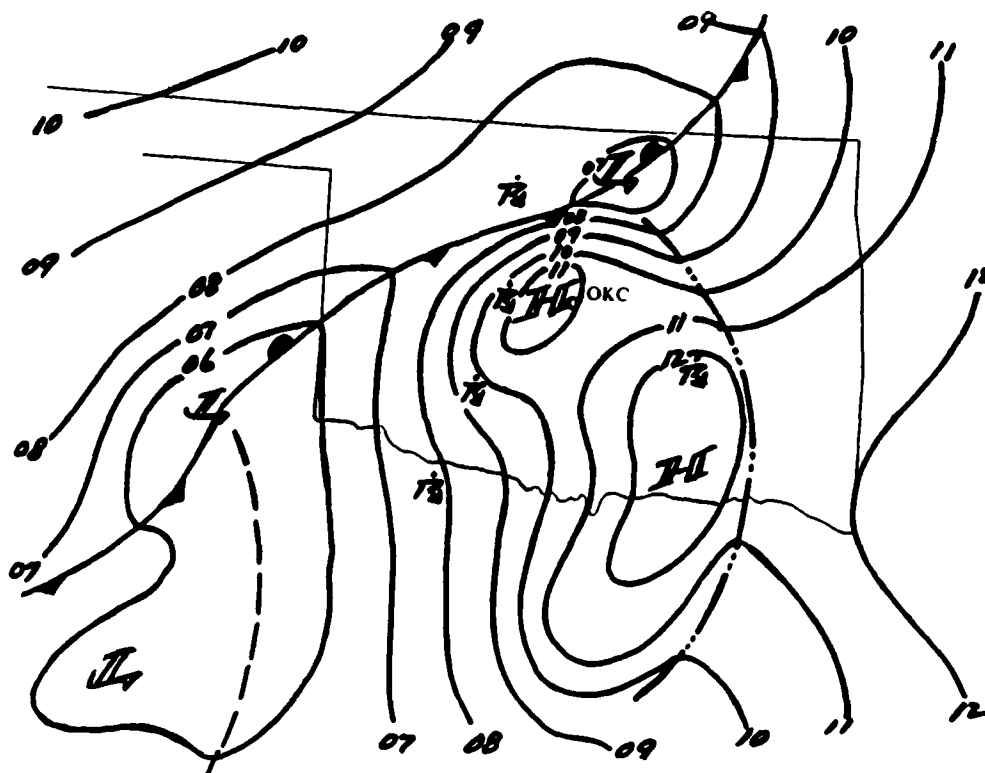
Fig. 4.13. Surface meso-analysis for 2200 CST on 27JUN83.

this line continued to persist. The 60-series SAM complex at 2200 CST (Fig. 4.14) showed that winds were southerly at 5 - 10 m s^{-1}. Pressure slowly rose, and dry- and wet-bulb temperatures remained fairly uniform. The 40-series SAM site at the same time (Fig. 4.15) showed winds veering to 180° by about 2233 CST. Wind speed had decreased, and the temperature had slowly increased, while the wet-bulb temperature remained constant. The pressure began to slowly increase from a minimum at approximately 2218 CST.

The surface meso-analysis for 2300 CST (Fig. 4.16) continued to track the instability line into extreme eastern Oklahoma. A small wave had formed on the frontal system north-northwest of OKC. At 2330 CST winds at the 60-series complex began to veer to 290°. At the same time, wind speed and average pressure increased, peaking around 2348 CST. At 2336 CST, radar reflectivity data indicated that the leading edge of a 10 dBZ area was immediately northwest of the 60-series SAM complex (Fig. 4.17) and moving from about 250° at 25 m s^{-1}. No 40 dBZ echoes passed over the complex, and no rain was observed. At 2351 CST, wind speeds, dry- and wet-bulb temperatures, and pressure began to decrease. Wind direction veered to 340°. The 40-series SAM complex registered similar conditions with the sequence beginning at about 2351 CST.
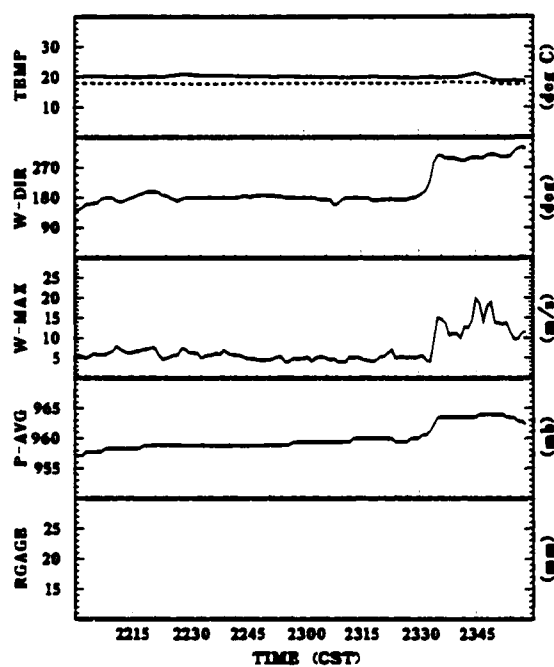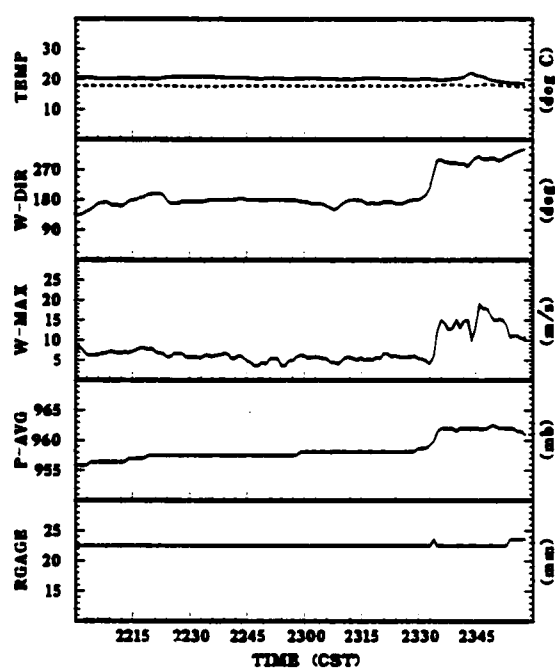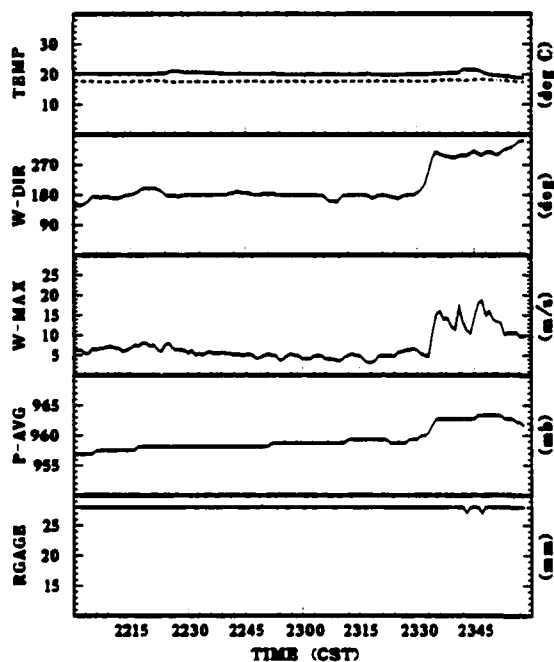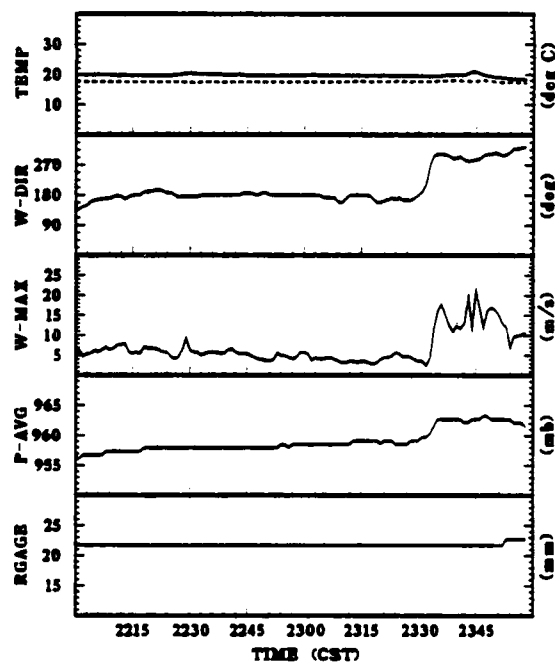
Fig. 4.14. SAM data (60-series) for 28JUN83 case (2200 - 2400 CST, 27JUN83).
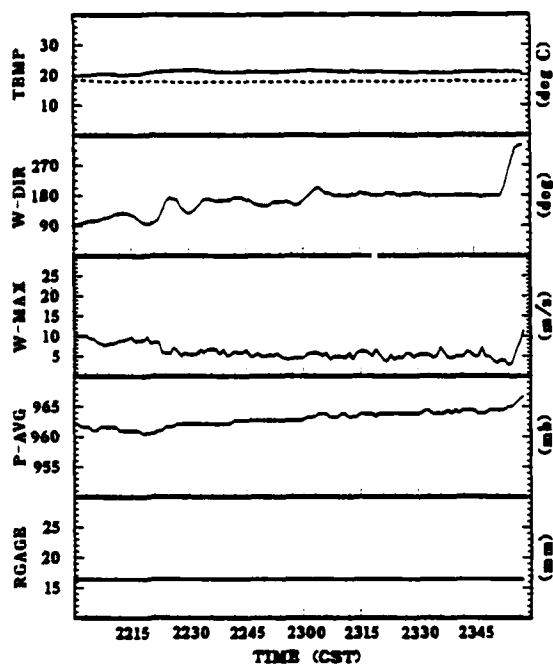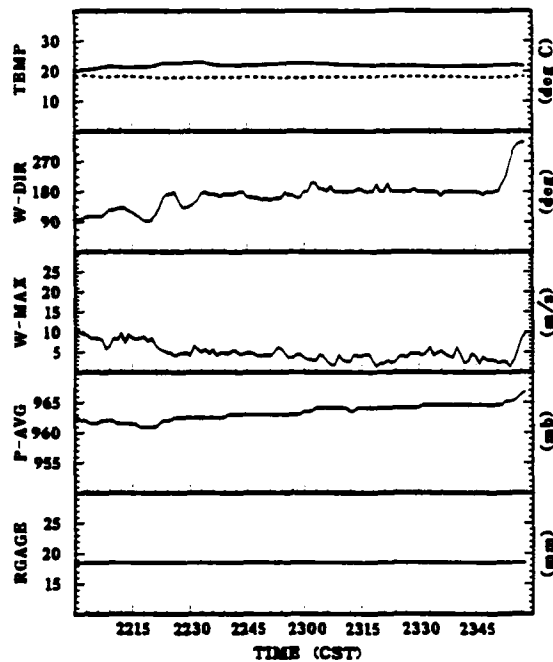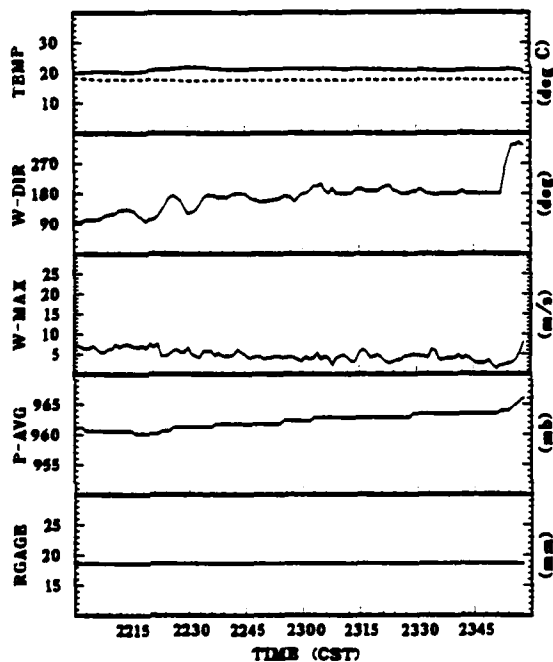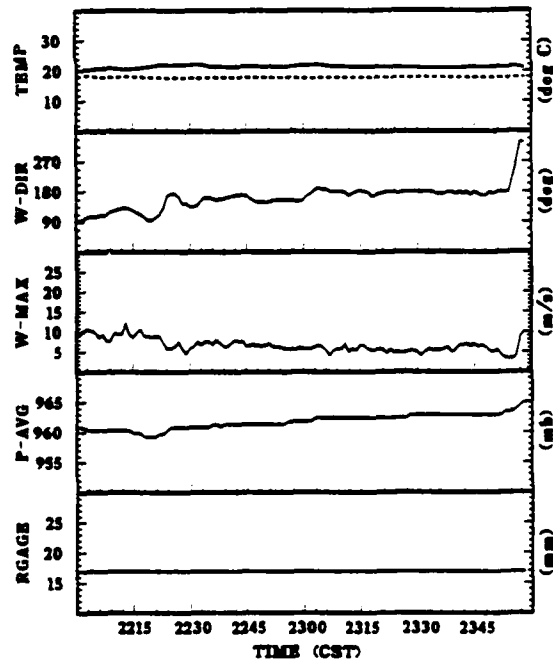
Fig. 4.15. SAM data (40-series) for 28JUN83 case (2200 - 2400 CST, 27JUN83).
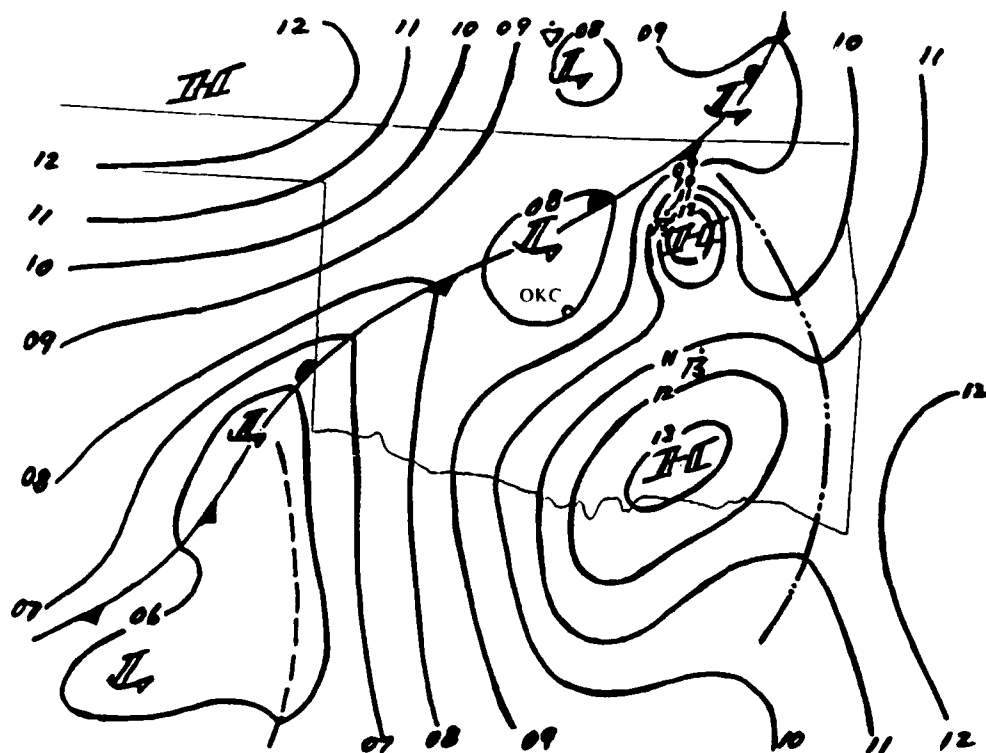
Fig. 4.16. Surface meso-analysis for 2300 CST on 27JUN83.

NORMAN DOPPLER   28JUN83   23:36:14   0.6   REFLECTIVITY
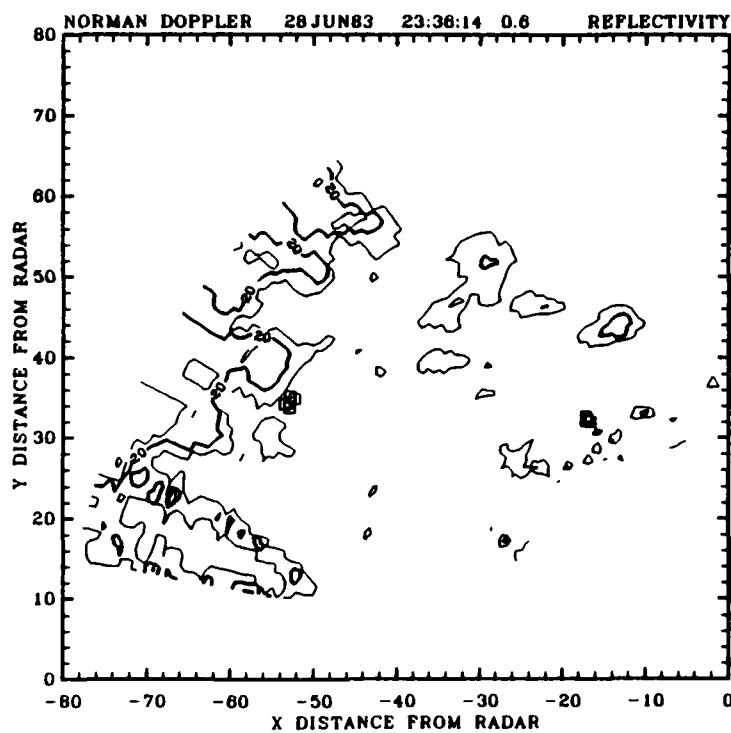
Fig. 4.17. Norman Doppler radar contoured reflectivity plot for
23:36:14 CST on 27JUN83.

The tower (Fig. 4.18) showed rather constant dry- and wet-bulb temperatures with the exception of a number of small "wet cool pulses" at the upper levels around 2318 CST. Wind direction began from the east at all levels and veered with time. At the top level, the veering was constant, but at the lower levels, there was a rapid wind shift beginning at about 2306 CST. Winds then remained generally southerly until about 2351 CST when they again veered sharply at the lower levels. At 2400 CST the winds were southerly at the tower top and northerly at the lower levels. This might have indicated an extremely strong wind shear except that the wind speeds were very low.

By the June 28, 1983, 0000 CST surface meso-analysis (Fig. 4.19), the frontal system continued to move slowly east. The original instability line and associated meso-high moved into Arkansas and Missouri. A new meso-high had developed, and an instability line had formed and was moving to the east. Radar reflectivity data at 0002 CST (Fig. 4.20) indicated that rather weak echoes had passed over the 60-series SAM complex and were approaching the 40-series complex. The 60-series SAM data (Fig. 4.21) showed winds generally from the northwest at 7 to 12 m s^{-1}. Pressure began a slow increase at approximately 0038 CST at which time the winds began to back to about 270°. Pressure peaked at 0045 CST and began to decrease at approximately 0052 CST. Concurrently, the winds began to veer reaching north at 0112 CST.
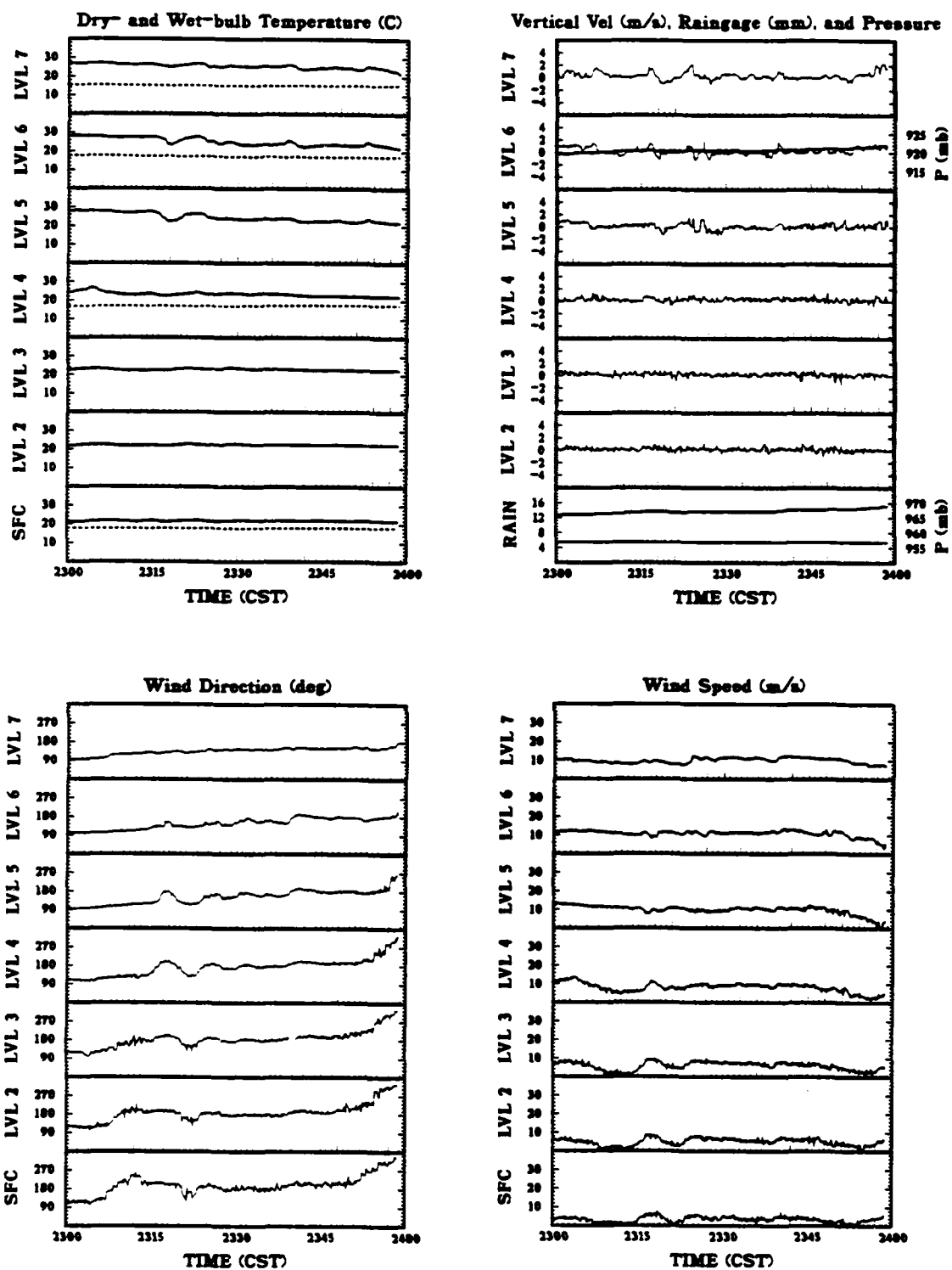
Fig. 4.18. NSSL-KTVY tower data for 28JUN83 case (2300 - 2400 CST, 27JUN83).
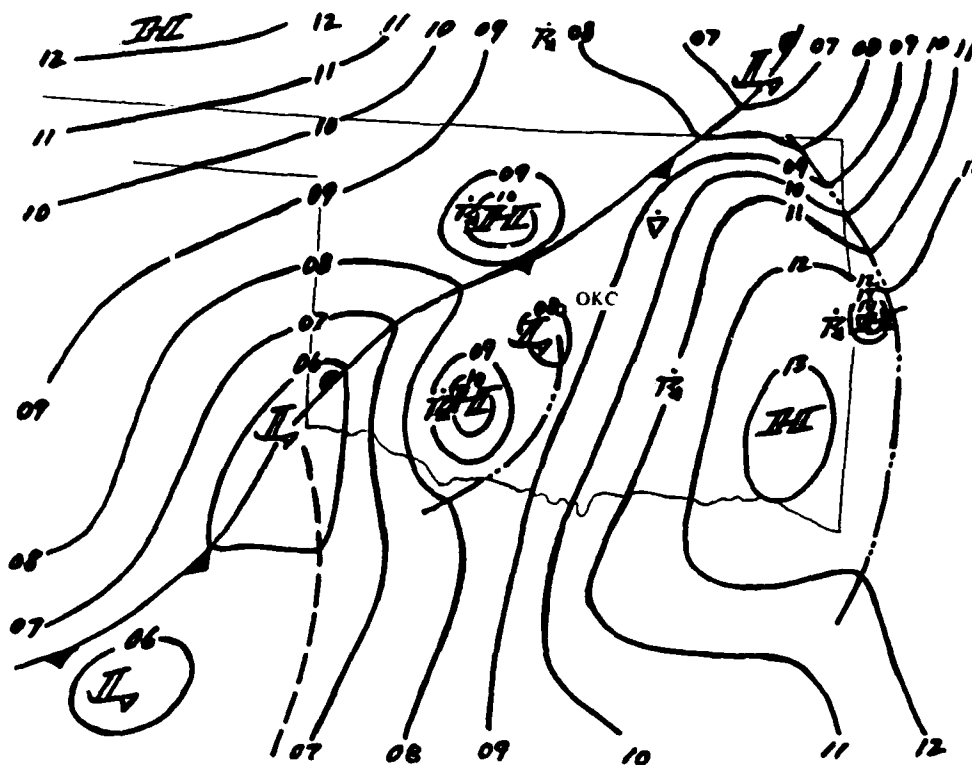
Fig. 4.19. Surface meso-analysis for 0000 CST on 28JUN83.
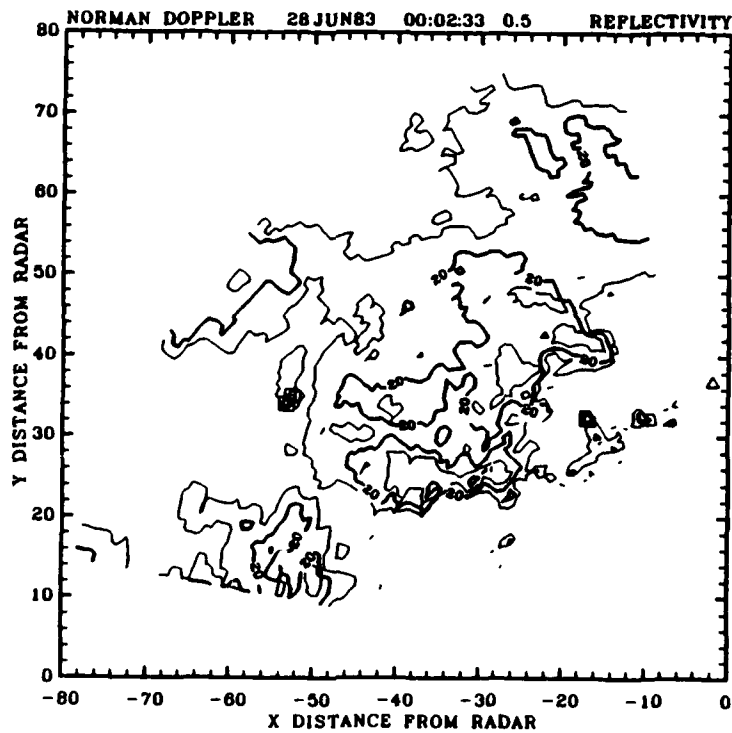
Fig. 4.20. Norman Doppler radar contoured reflectivity plot for 00:02:33 CST on 28JUN83.
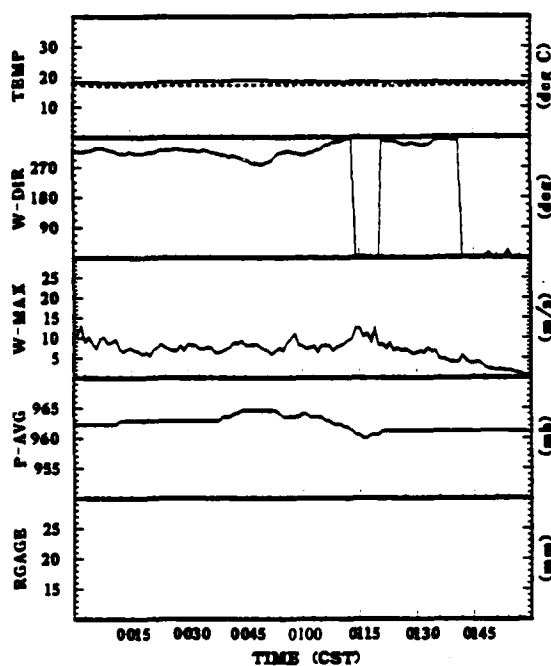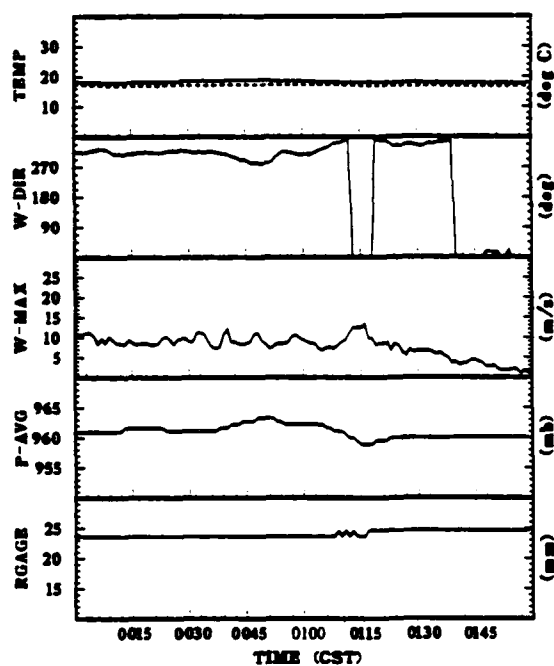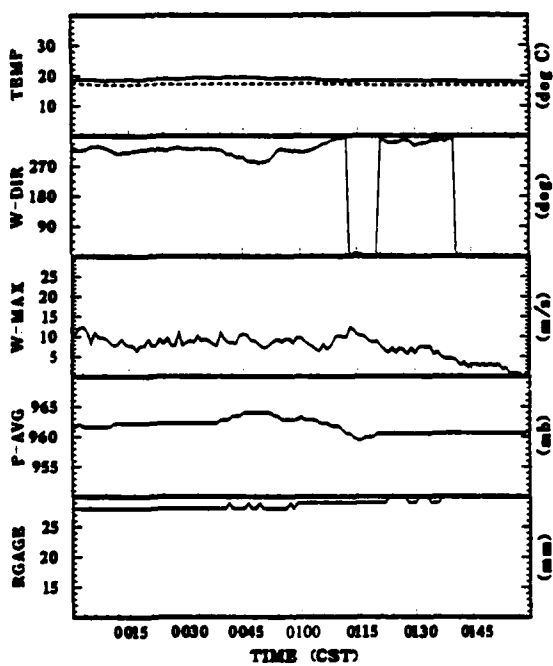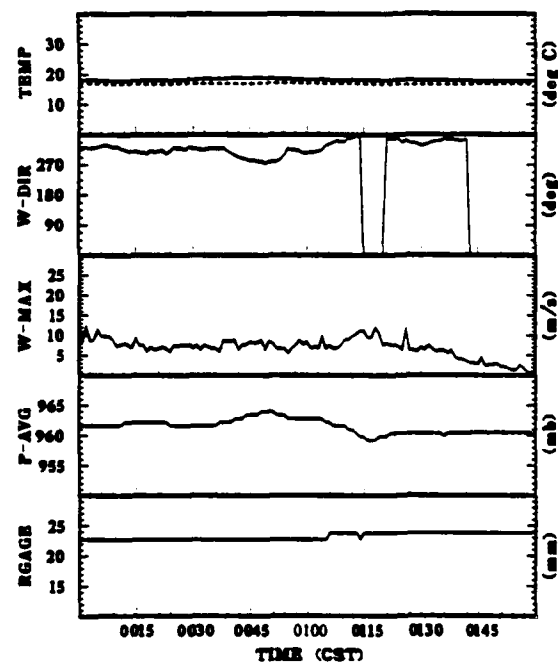
Fig. 4.21. SAM data (60-series) for 28JUN83 case (0000 - 0200 CST).

At approximately the same time wind speeds peaked at about 15 m s^{-1} and pressure reached a local minimum. These wind direction and pressure changes matched well with the period between the meso-analyses at 0000 CST (Fig. 4.19) and 0100 CST (Fig. 4.22). The radar data (Fig. 4.23) showed a 10 dBZ contour over the 60-series SAM cluster at 0041 CST. The 40-series SAM cluster (Fig. 4.24) showed similar features with a 10 to 30 minute lag behind the 60-series complex.
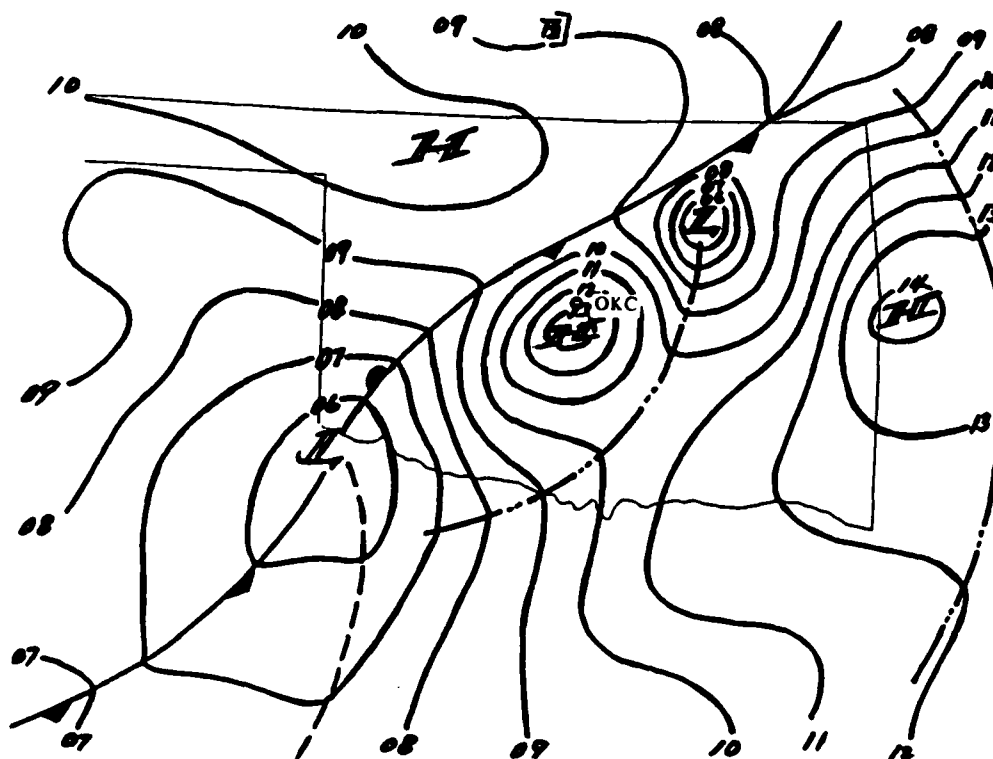
Fig. 4.22. Surface meso-analysis for 0100 CST on 28JUN83.

Temperature at all levels of the tower (Fig. 4.25) remained rather
uniform with a number of small "warm dry pulses" at the upper levels.
Wind direction at the top level veered rapidly, becoming northwest by
0002 CST. Winds at all levels then remained rather uniformly west-
northwest. Wind speeds at all levels picked up sharply just after 0000
CST. At the top level, winds peaked at 28 m s^{-1} at 00004 CST and,
except for two local minimums (0013 and 0027 CST), remained around 20
m s^{-1} at the upper levels. At the lower levels winds peaked near 20
m s^{-1} at about 0005 CST and then remained around 10 - 18 m s^{-1}.
Vertical velocity showed a period of up- and down-drafts from 0000 to
0030 CST, including a very strong convergence between levels 6 and 7.

By 0200 CST, the surface meso-analysis (Fig. 4.26) showed that this
latest instability line had moved well through central Oklahoma.
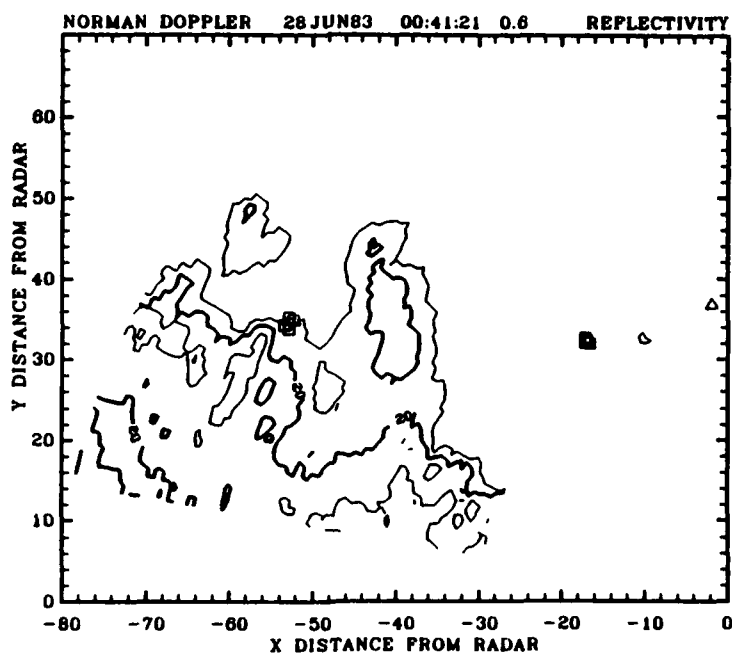
Fig. 4.23. Norman Doppler radar contoured reflectivity plot for
00:41:21 CST on 28JUN83.
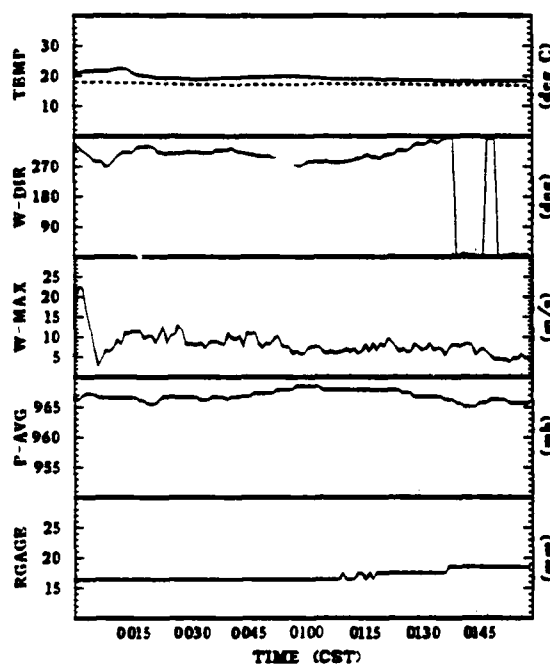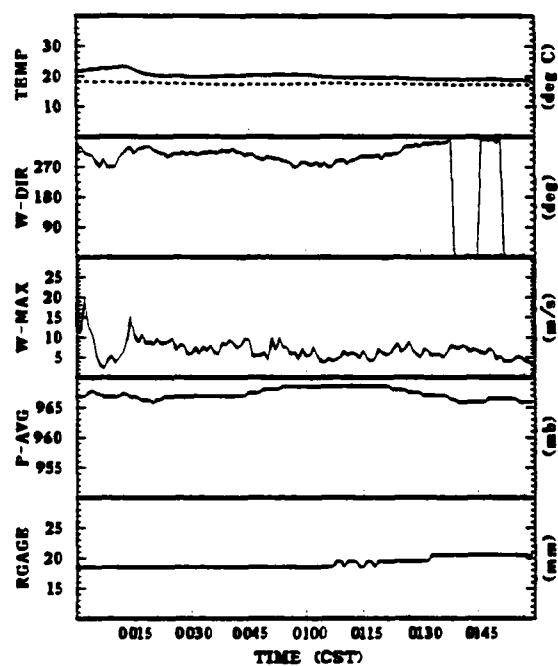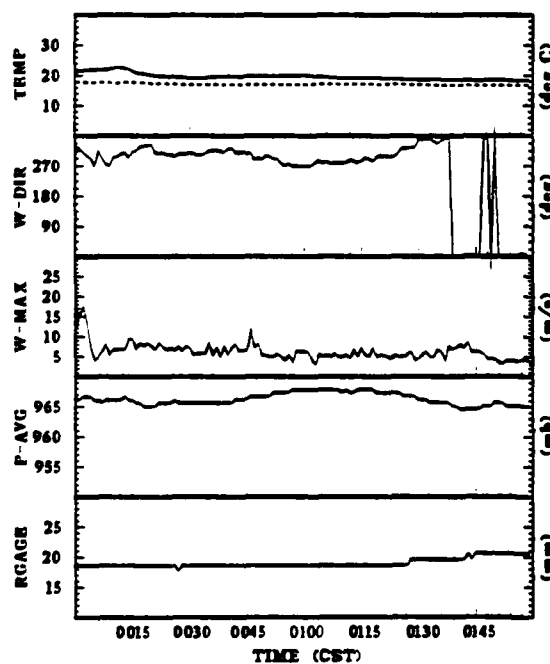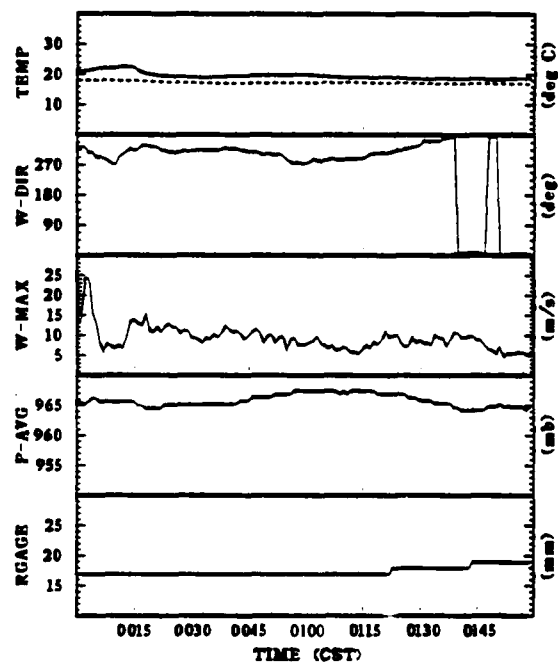
Fig. 4.24. SAM data (40-series) for 28JUN83 case (0000 - 0200 CST).
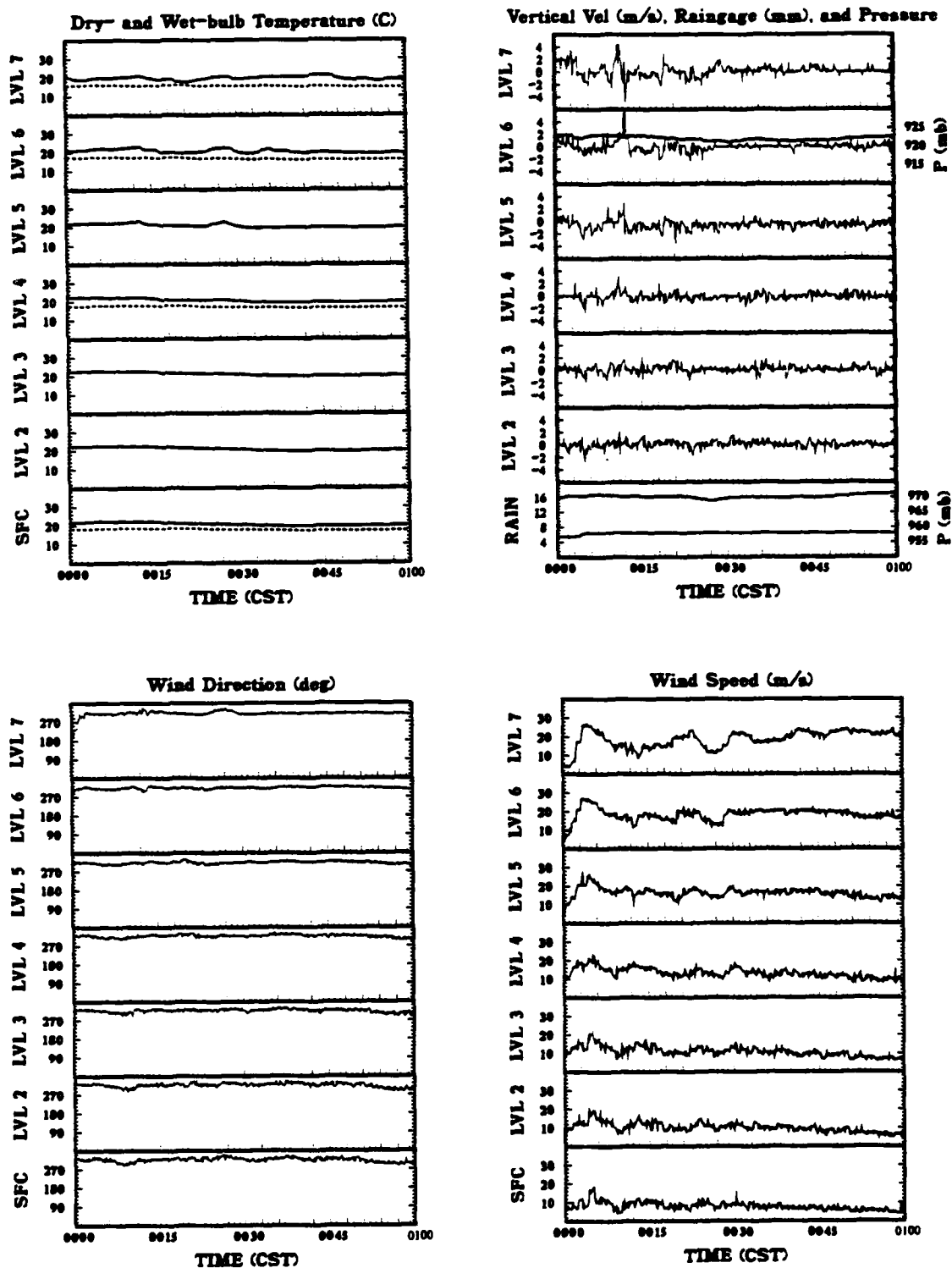
Fig. 4.25. NSSL-KTVY tower data for 28JUN83 case (0000 - 0100 CST).
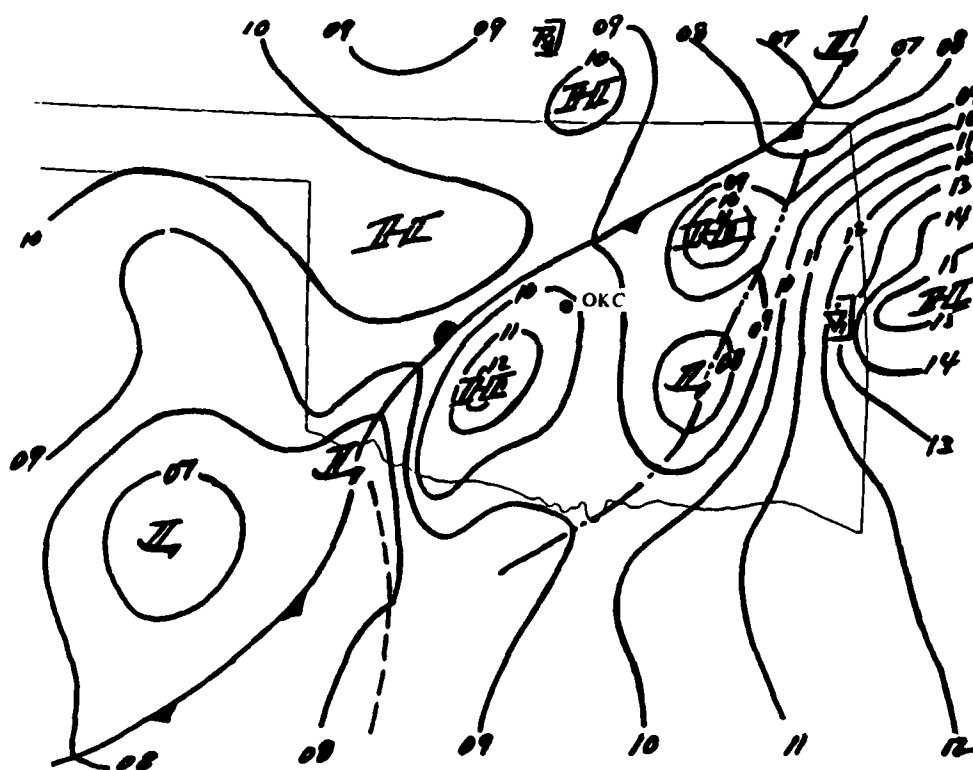
Fig. 4.26. Surface meso-analysis for 0200 CST on 28JUN83.

Case 3: April 22, 1983

This case was a frontal event, which occurred in the evening of April 22, 1983. This case was first discussed by Sickler, et al. (1985b). At 1800 CST, the surface low was located in the vicinity of Hobart (HBR), Oklahoma (Fig. 4.27) with an occluded front extending to a second low southwest of Ardmore (ADM), Oklahoma. A warm front extended east into Arkansas, and a cold front extended south between Stephenville (SEP) and Fort Worth (FTW), Texas. A line of showers and thunderstorms had formed along the cold front, and thunderstorms were reported at HBR and Altus (LTS), Oklahoma. As the system moved eastward, thunderstorms continued to be reported in central Oklahoma.
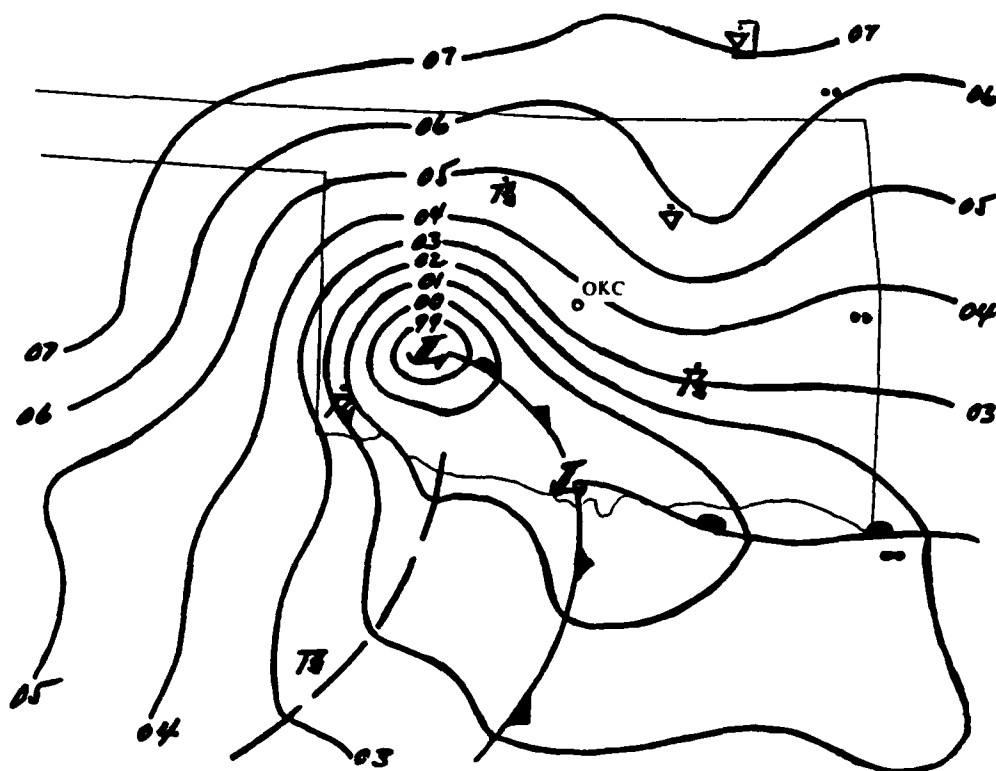
Fig. 4.27. Surface meso-analysis for 1800 CST on 22APR83.

The 18:38:29 CST radar reflectivity data (Fig. 4.28) were the first radar data available on this case and showed storms well over the 60-series SAM complex and moving toward the 40-series complex. The 60-series SAM complex (Fig. 4.29) indicated that at approximately 1813 CST winds began to veer, reaching west to west-northwest at 1827 CST. At 1819 CST pressure began to slowly increase. Winds speeds followed a rather steady increase, peaking at about 25 m s^{-1} around 1922 CST at which time rain began. In Fig. 4.29, note the sudden wind shift which occurred at all stations between 1830 and 1845 CST. This event is particularly intriguing due to its different appearance at each SAM site and the physical layout of the sites (Fig. 3.3a and 3.3b). Following
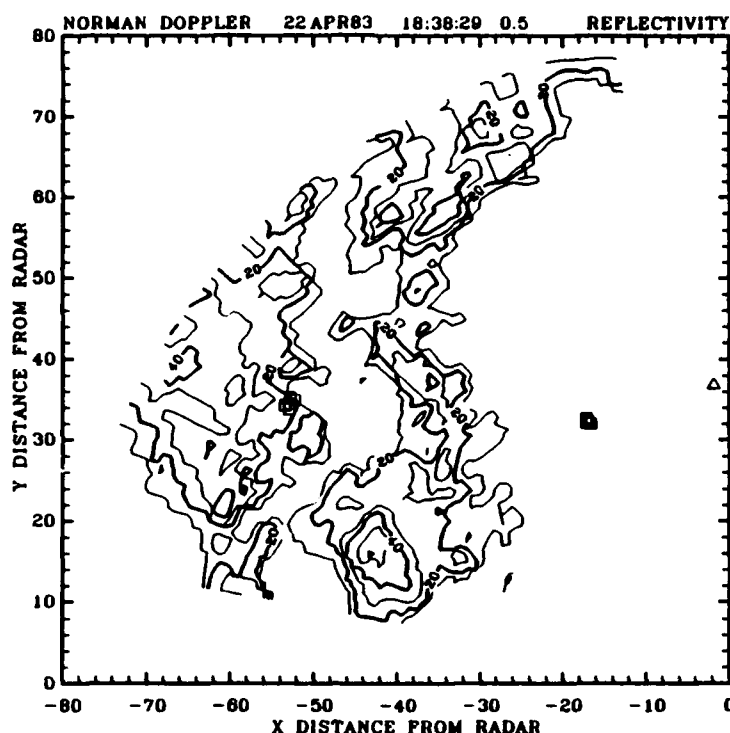
Fig. 4.28. Norman Doppler radar contoured reflectivity plot for
18:38:29 CST on 22APR83.

the perturbation, the wind direction returned to its previous veering

rate between 1845 and 1852 CST. Wind direction became north-

northeasterly around 1909 CST. Dry- and wet-bulb temperatures showed a

relatively constant decrease with an increase in humidity. At the

40-series complex (Fig. 4.30) the wind speeds peaked around 18 m s^{-1}

about 30 minutes after the 60-series. The unusual wind shift at the

60-series complex was not repeated here. Winds slowly backed until

about 1912 CST, when they rapidly veered, becoming northerly at 1924

CST.
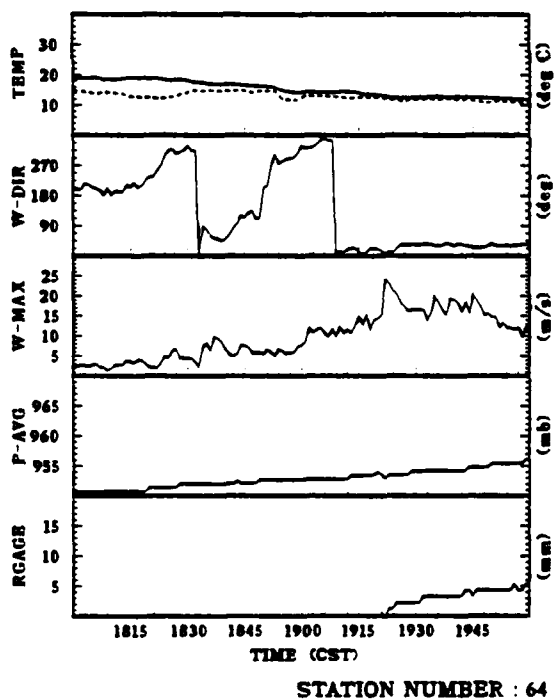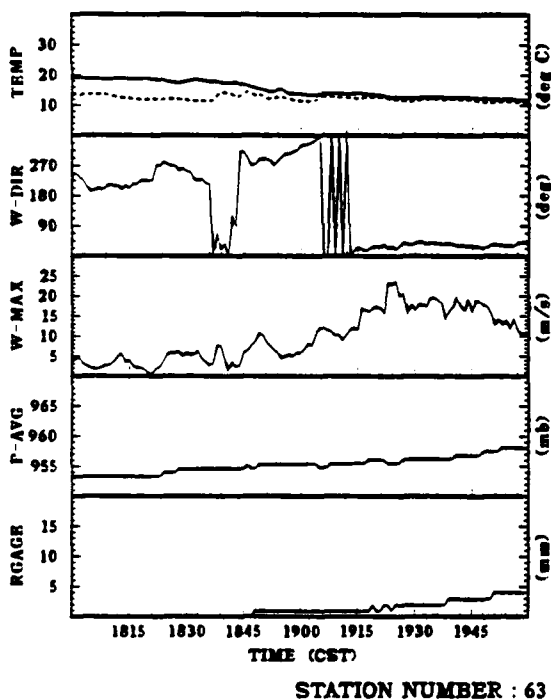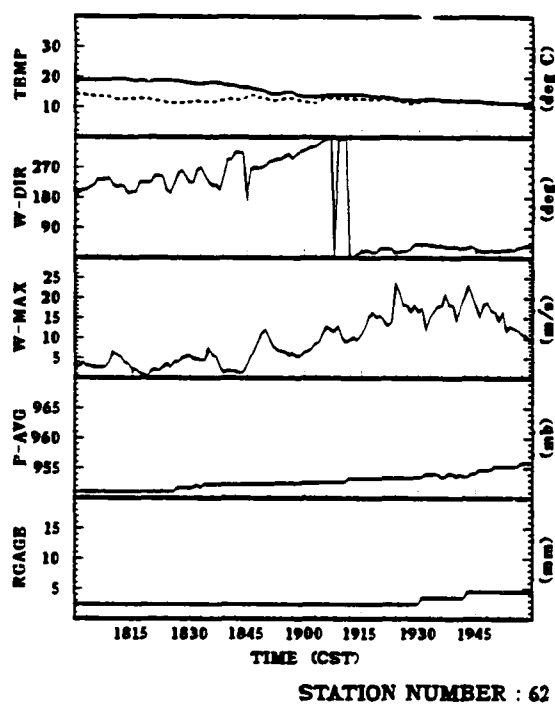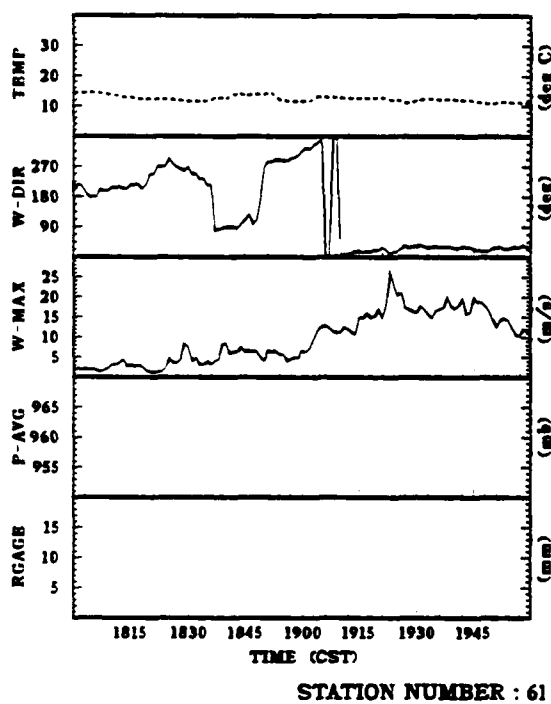
Fig. 4.29. SAM data (60-series) for 22APR83 case (1800 - 2000 CST).
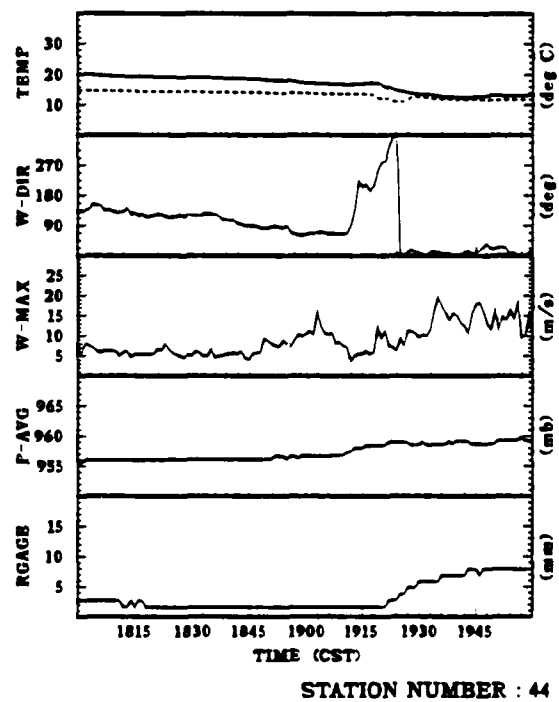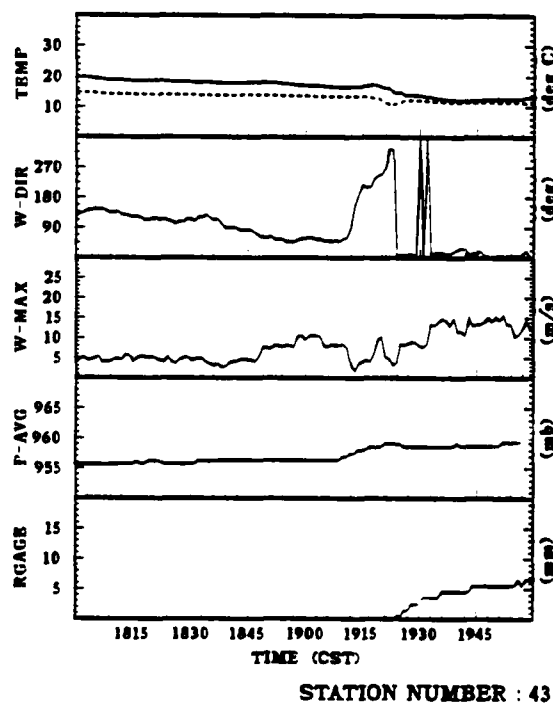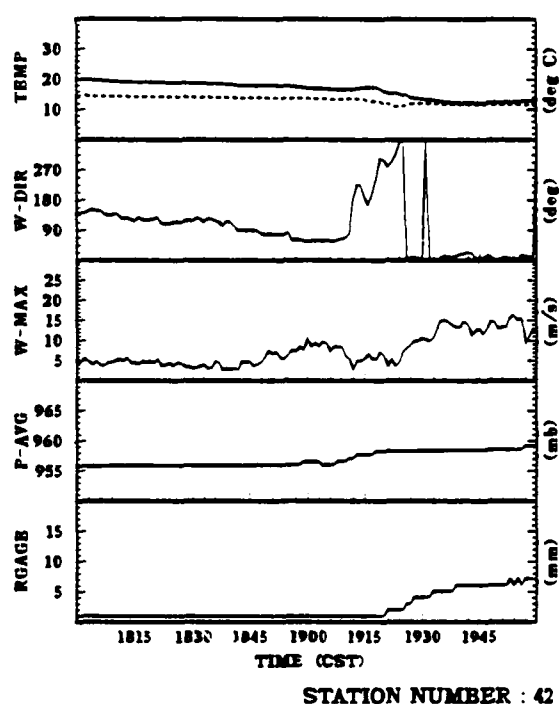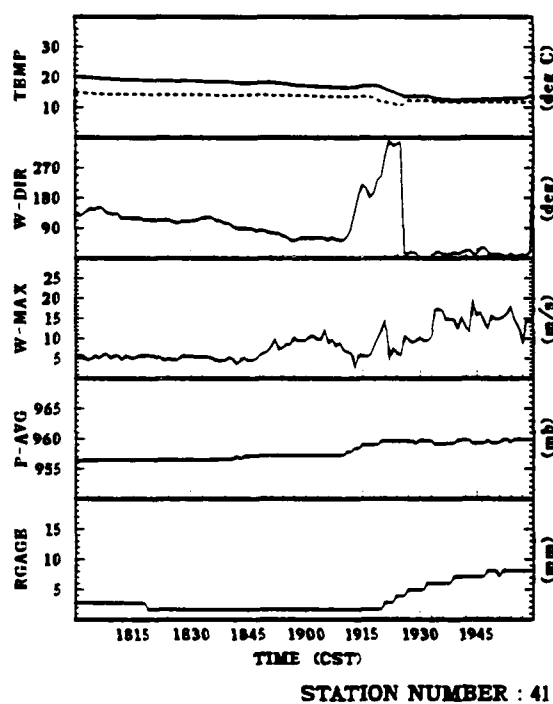
Fig. 4.30. SAM data (40-series) for 22APR83 case (1800 - 2000 CST).

The 1900 CST meso-analysis (Fig. 4.31) showed that the low
associated with the front had moved into the ADM area. The cold front
had moved east and was located over Fort Worth (FTW), Texas. The warm
front had moved slowly north. The 19:13:26 and 19:30:55 CST radar
reflectivity data (Fig. 4.32 and 4.33) indicated that the storms were
moving roughly west to east. At 1913 CST the leading edge of the 10 dBZ
echo had just reached the 40-series SAM cluster.
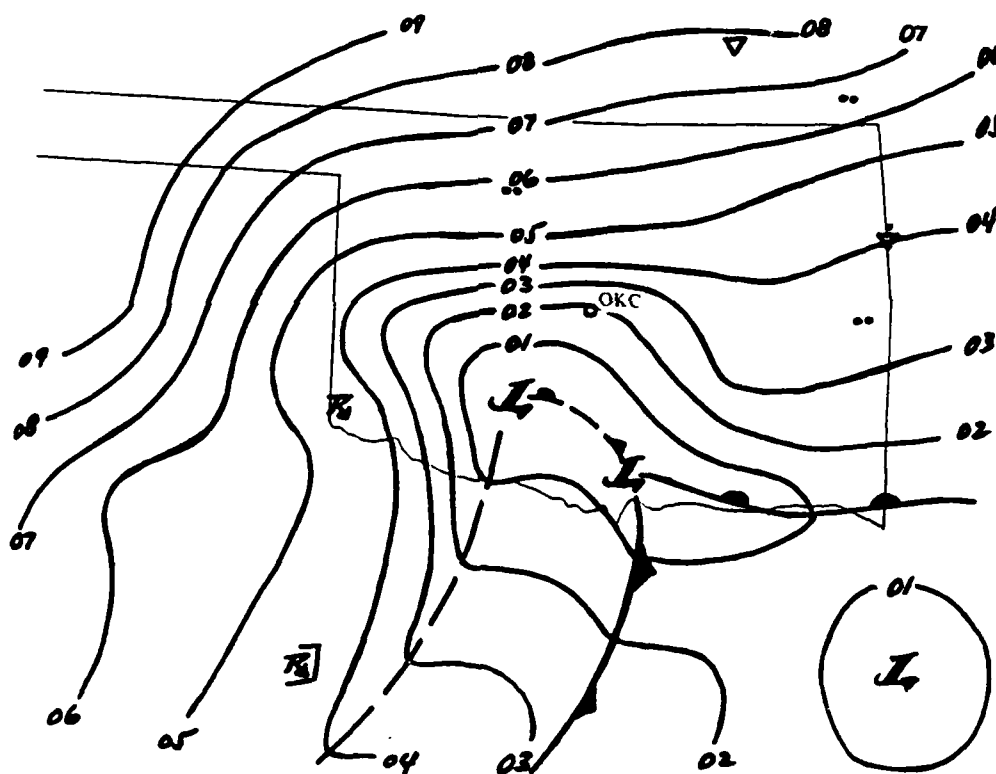
Fig. 4.31. Surface meso-analysis for 1900 CST on 22APR83.
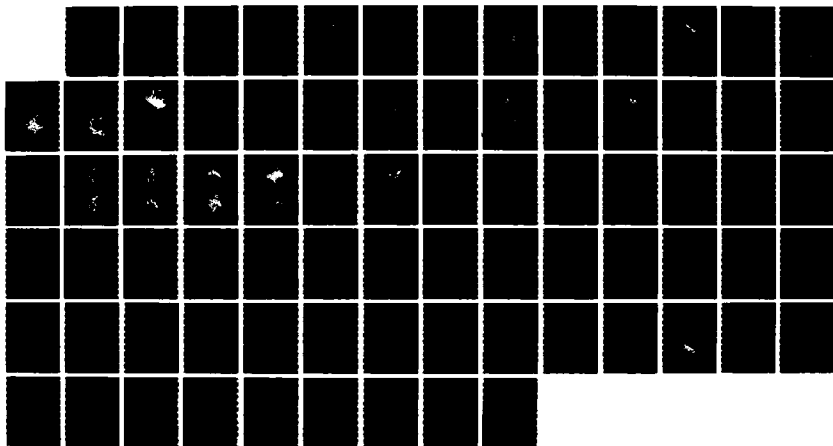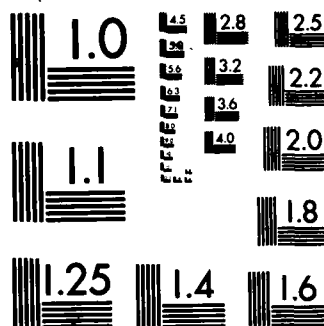
MICROCOPY RESOLUTION TEST CHART
NATIONAL BUREAU OF STANDARDS-1963-A
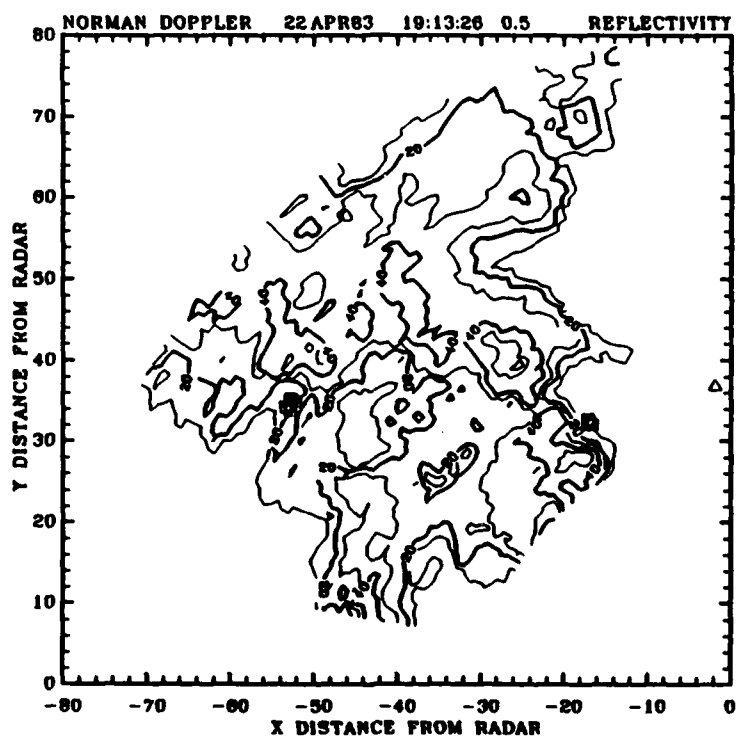
Fig. 4.32. Norman Doppler radar contoured reflectivity plot for
19:13:26 CST on 22APR83.
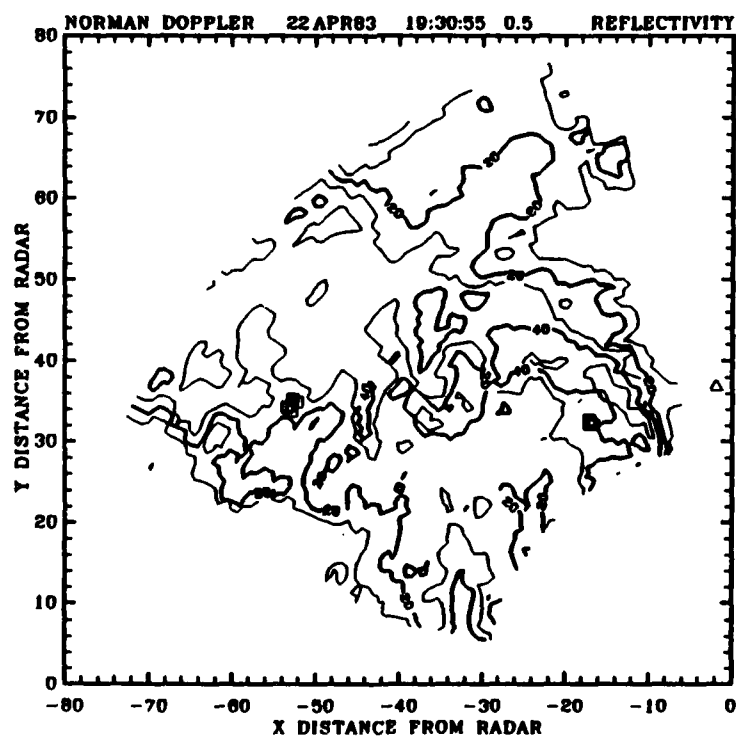
Fig. 4.33. Norman Doppler radar contoured reflectivity plot for
19:30:55 CST on 22APR83.

For the period 1900 - 2000 CST, only three features at the NSSL-KTVY tower (Fig. 4.34) seemed significant. The wind speeds never exceeded 12 m s^{-1} at any level. The wind direction did not veer as at the SAM complexes, but backed slowly to a northerly direction. The vertical velocity was more turbulent after 1930 CST, with distinct convergence between levels 6 and 7 after 1945 CST.

The 2000 CST meso-analysis (Fig. 4.35) showed that the low associated with the front continued to move slowly northeast, while the low with the trof moved east. The cold front continued to trace to the east having passed through FTW at approximately 1930 CST. Two meso-highs had formed, one near Oklahoma City (OKC), Oklahoma, and the other east of Fayetteville (FYN) and Fort Smith (FSM), Arkansas. The 60-series SAM cluster (Fig. 4.36) showed winds from the northeast, slowly decreasing wind speeds, and slowly increasing average pressure. The 40-series SAM cluster (Fig. 4.37) showed similar conditions with wind direction variable about 360°. Rain accumulation continued slowly at both sites, giving more of a stratiform precipitation appearance than that of convective activity.
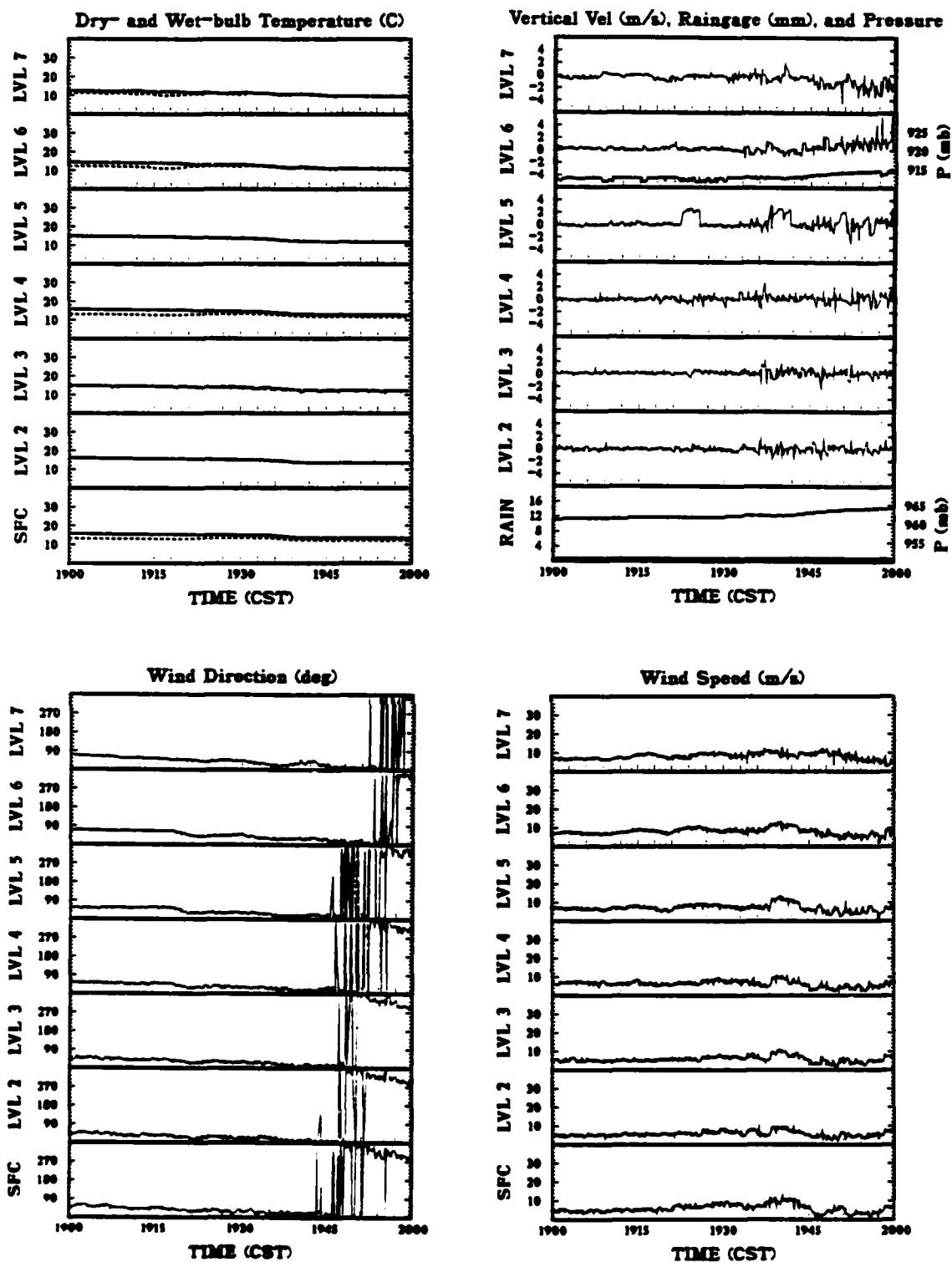
Fig. 4.34. NSSL-KTVY tower data for 22APR83 case (1900 - 2000 CST).
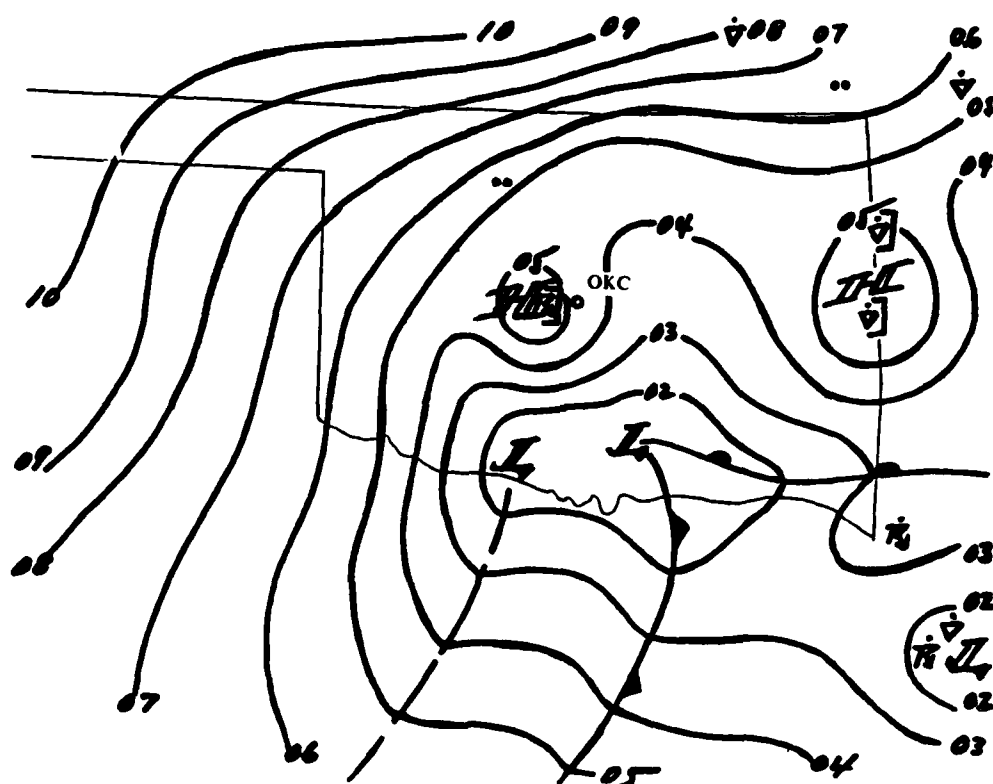
Fig. 4.35. Surface meso-analysis for 2000 CST on 22APR83.
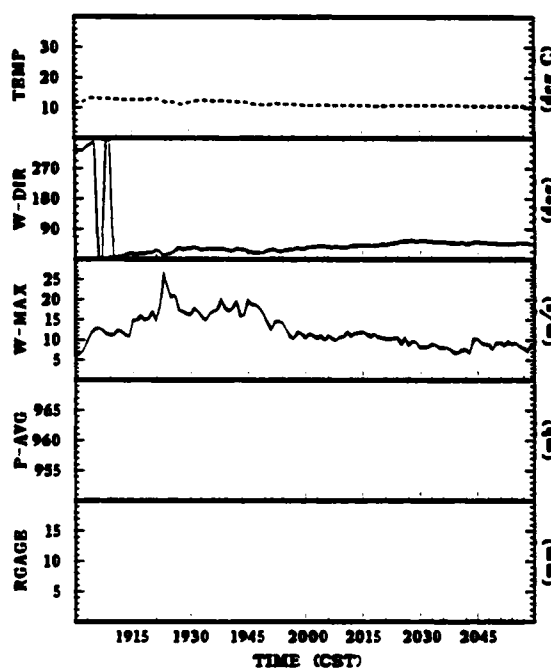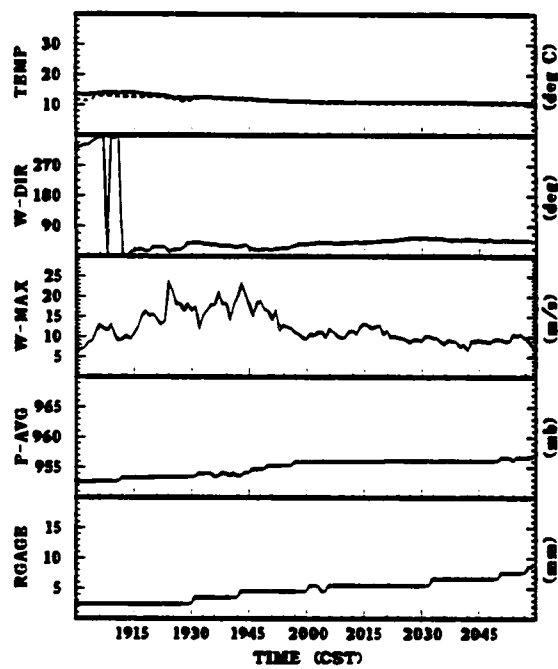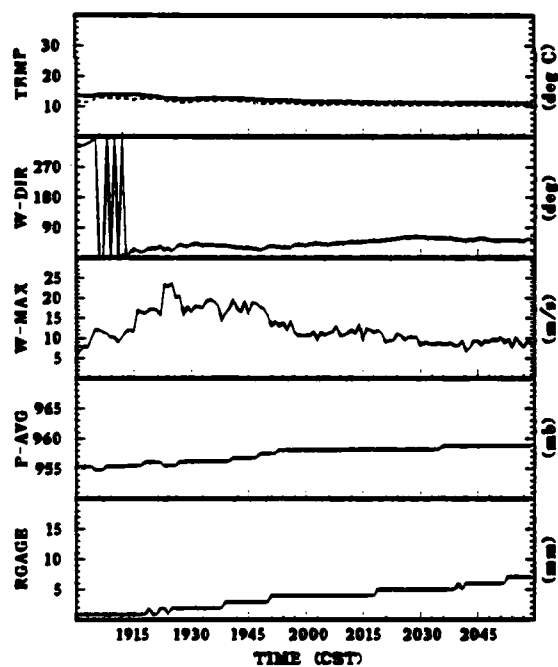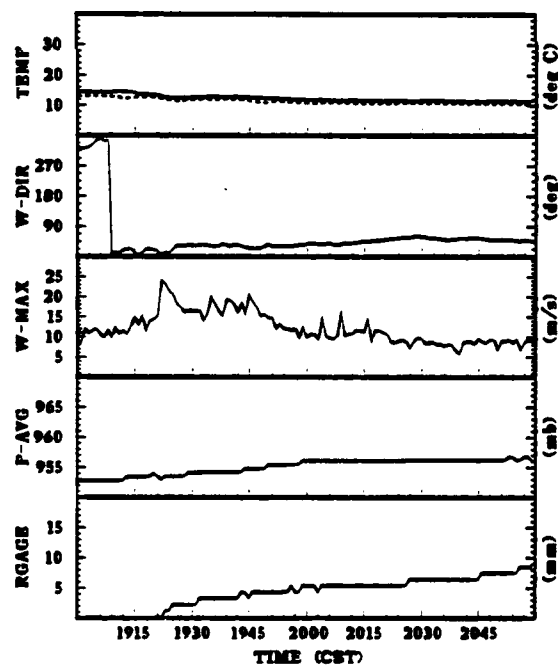
Fig. 4.36. SAM data (60-series) for 22APR83 case (1900 - 2100 CST).
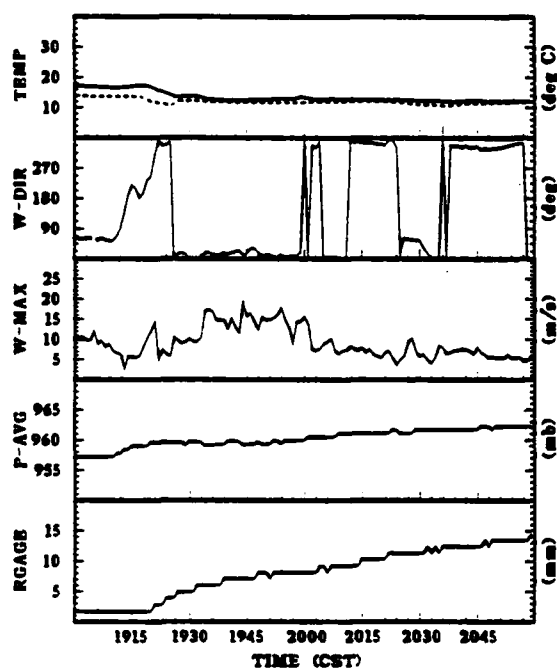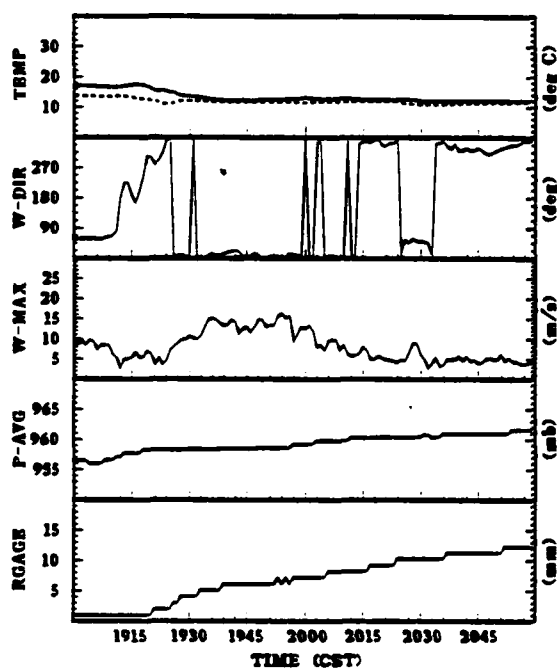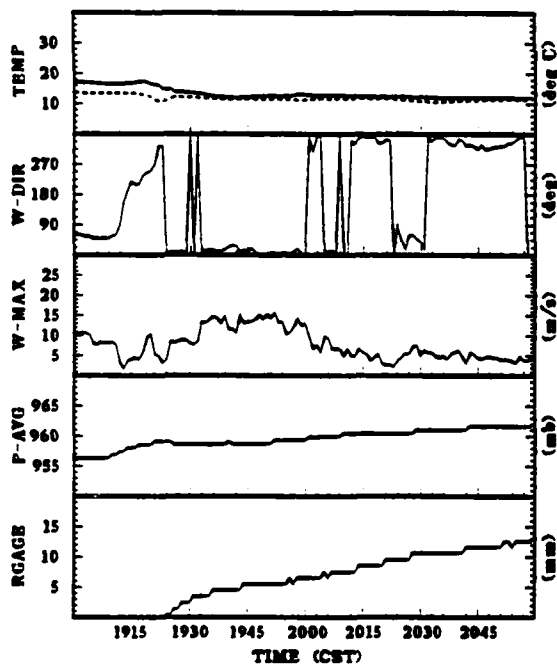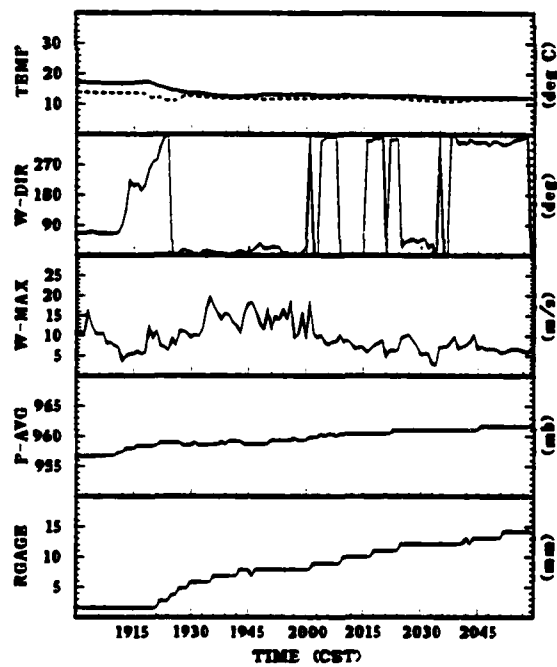
Fig. 4.37. SAM data (40-series) for 22APR83 case (1900 - 2100 CST).

The 2100 CST meso-analysis (Fig. 4.38) depicted the frontal low continuing to move slowly eastward and the trof low moving slowly eastward. The meso-high near OKC had slowly strengthened.
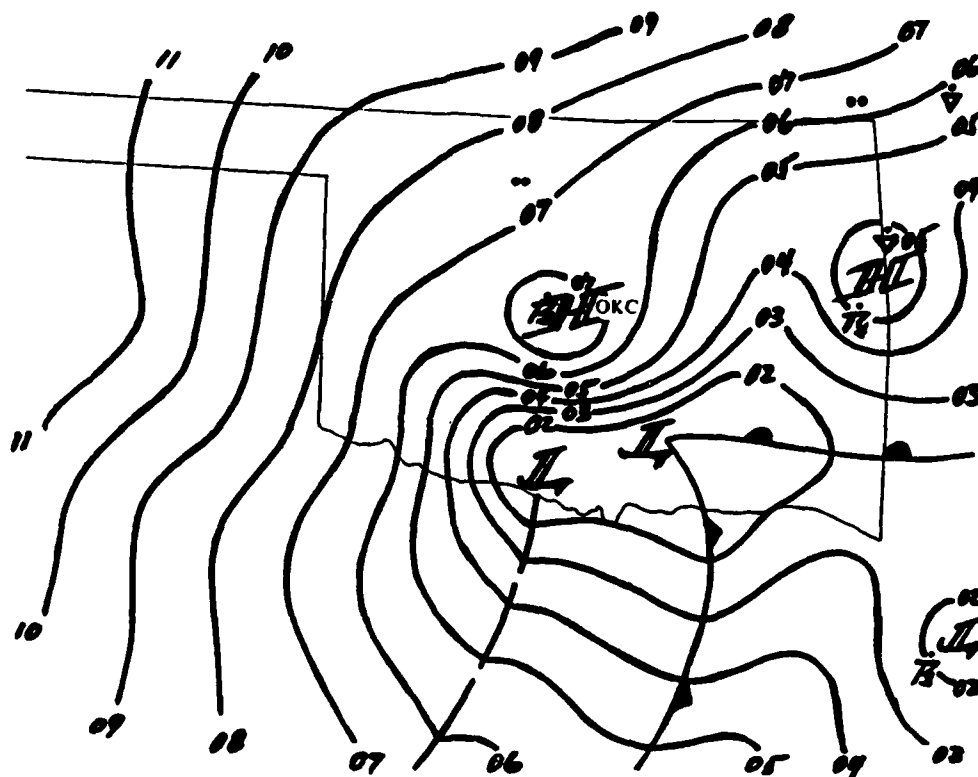
Fig. 4.38. Surface meso-analysis for 2100 CST on 22APR83.

CHAPTER V

RADAR-SURFACE RELATIONSHIPS

Introduction

This chapter serves to discuss the radar-surface relationships by examining the radar data products in light of the meso-scale environment as analyzed in Chapter IV.

Radar Observations

In this section each of the cases is examined in a time sequence, looking for features which can be identified by linking the radar data to the meso-scale features presented in Chapter IV. Much of the earlier work with the transverse wind technique (Rinehart, 1979; Smythe, 1981; Hamidi et al., 1983; Smythe and Harris, 1984) involved validation by "wind vector matching." In this research, the transverse wind technique has been used to identify meteorological features.

Case 1: June 27, 1983

The appearance of the 10 dBZ contour in the plot of data from the program (TWIND), which implements the NEXRAD Transverse Wind Algorithm, for the time period 19:45:42 to 19:46:40 (Fig. 5.1) indicated that the storms were just moving into the observation window. As discussed in Chapter IV, the surface winds at this time were in a southerly direction. Fig. 5.1 confirms that the winds derived by the transverse wind algorithm were predominantly southerly inside the 10 dBZ region.

(Fig. 5.1 can be compared with Fig. 2.9 to observe the effect of a 0.85 maximum correlation coefficient threshold.) The TWIND plot for the period 19:55:24 to 19:56:22 (Fig. 5.2) showed the 10 dBZ region further impinging on the window, and the wind field becoming more predominantly southerly as the 10 dBZ area moved into the test area.
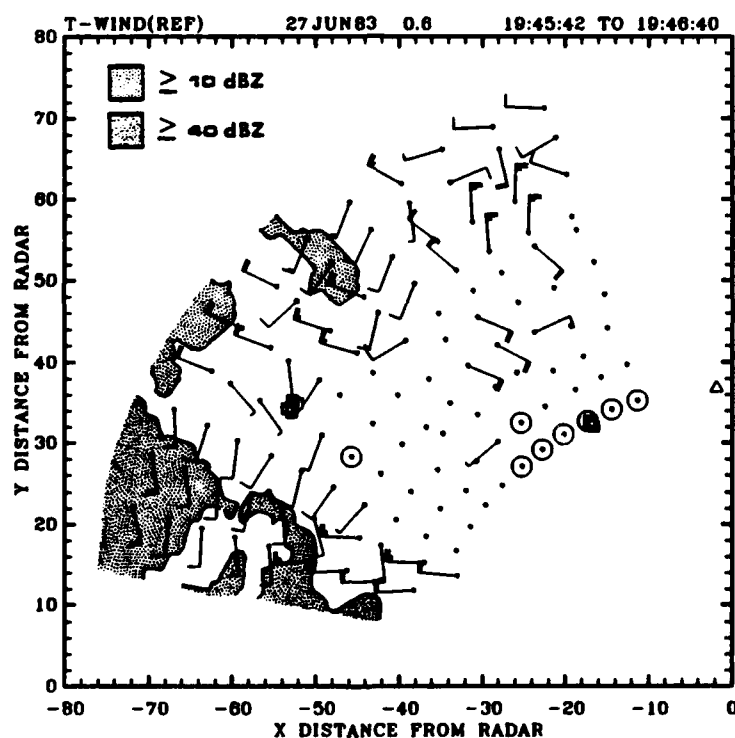
Fig. 5.1. TWIND plot for 27JUN83 case (19:45:42 to 19:46:40) with maximum correlation coefficient threshold set at 0.85.
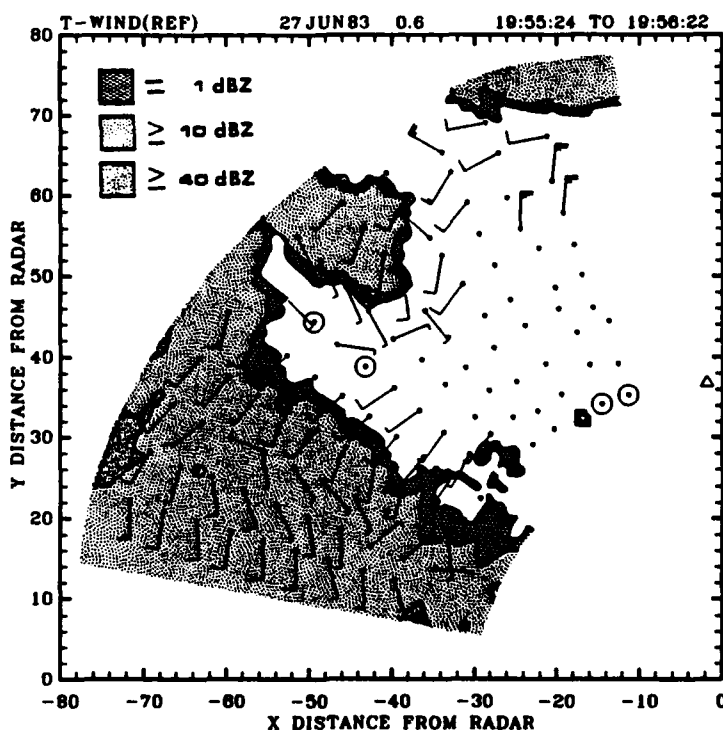
Fig. 5.2. As in Fig. 5.1, except for 19:55:24 to 19:56:22 and inclusion of a 1 dBZ contour.

A correlation can be drawn between the radar data at 0.6° elevation angle (i.e., 784 m above the surface) and the 60-series SAM complex winds when the 10 dBZ contour passed. From the transverse wind data (Fig. 5.2) the winds around the surface automated mesonet (SAM) complex were observed to be south-southwesterly at 5 - 10 m s^{-1}. In general, at around 1955 CST at each site in the 60-series SAM cluster (Fig. 4.3) winds were about 7 m s^{-1} from the south just prior to the arrival of the squall line. So, although the data derived by the TWIND program were 784 m above the SAM complex, under the meteorological conditions of a squall line there appeared to be a close correlation between observations at the SAM site and the TWIND derived wind field. However, even using just the data with higher correlation coefficients did not

mean that all of the vectors were going to agree. Some deviations, caused by the averaging process and local turbulence, were to be expected. Because of this and the spatial and temporal differences in the data, confirmation of a coupling between the low-level winds and the radar-derived low-level wind field could not rely on an exact one-to-one match between the SAM data and the TWIND data. Confirmation would come from matching general patterns --- a predominant wind field --- not an exact match with perfect timing.

Having examined the period prior to the squall line, the derived wind field needed to be examined as the squall line passed through the experimental area. The TWIND plot for the period 20:05:06 to 20:06:04 (Fig. 5.3) was the first time, based on the meso-analysis, that the squall line was in the general area of the 60-series SAM complex. According to the earlier analysis (Chapter IV), the squall line still was located to the southwest of OKC and consequently to the southwest of the 60-series SAM cluster. At this time (Fig. 5.3), the first 40 dBZ echo had moved over the 60-series complex, and the 10 dBZ contour was within about 5 km of the 40-series complex. Further, this figure verified that the higher value correlation coefficients were now dominating the whole field. At the 40-series SAM complex at 2009 CST (Fig. 4.9) the southerly to southwesterly wind suddenly accelerated to 20 m s^{-1}, which was much like the winds produced by TWIND just outside the 10 dBZ contour in this area (Fig. 5.3). This reinforced the observation that the SAM observed wind and the TWIND derived observations were linked.

At about 2005 CST (Fig. 5.3) westerly winds that had not appeared within the 10 dBZ contour of previous TWIND plots were observed. These

strong (20 - 25 m s⁻¹) westerlies were in a region where, from previous

observations, the winds had exhibited features similar to the

environmental winds. From the meso-analysis (Fig. 4.6) the meso-high

with associated squall line feature was entering the experimental area.

Therefore, this westerly wind direction must have been due to the

structure of the squall line. The meso-analysis indicated that winds in

advance of the northern end of the squall line were southerly and winds

behind the squall line were westerly. Looking along the beam to the

west, as the squall line approached the radar, first southerly winds

were found, then westerlies. The TWIND data appeared to be providing a

reasonable representation of the meso-scale flow within the observation

area.
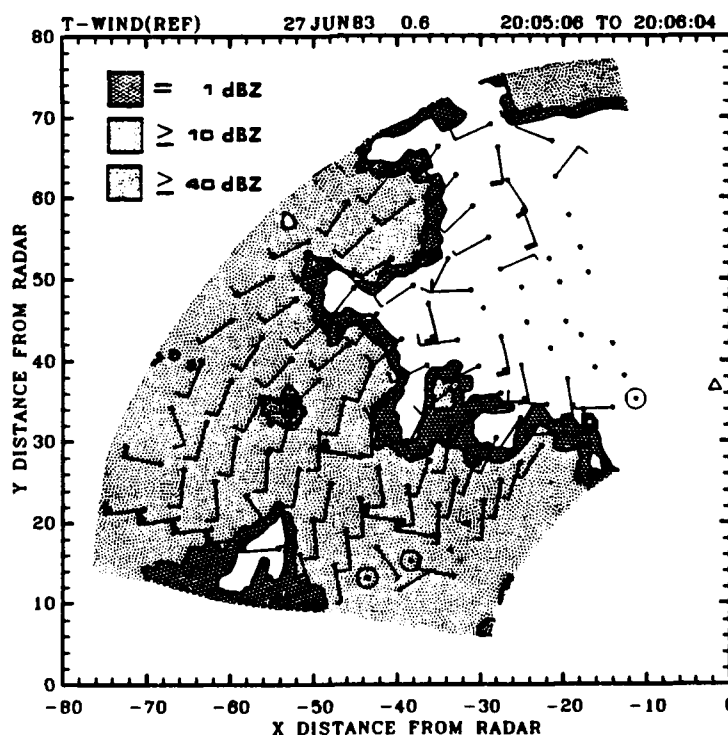
Fig. 5.3. As in Fig. 5.2, except for 20:05:06 to 20:06:04.

The TWIND plot for the period 20:14:48 to 20:15:46 (Fig. 5.4) had a
much larger region of westerly winds with some southerly winds. These
southerly winds reinforced the earlier observation that the averaging
process and the TWIND process itself did result in some apparent
"errors." It was recognized that the TWIND data could not be used by
itself, but had to be coupled with other information to filter out these
"errors" as much as possible. At this time the winds were predominantly
westerlies. This region might be the zone where the winds would veer
from southerly to westerly across a squall line (Tepper, 1950; Fujita,
1955).
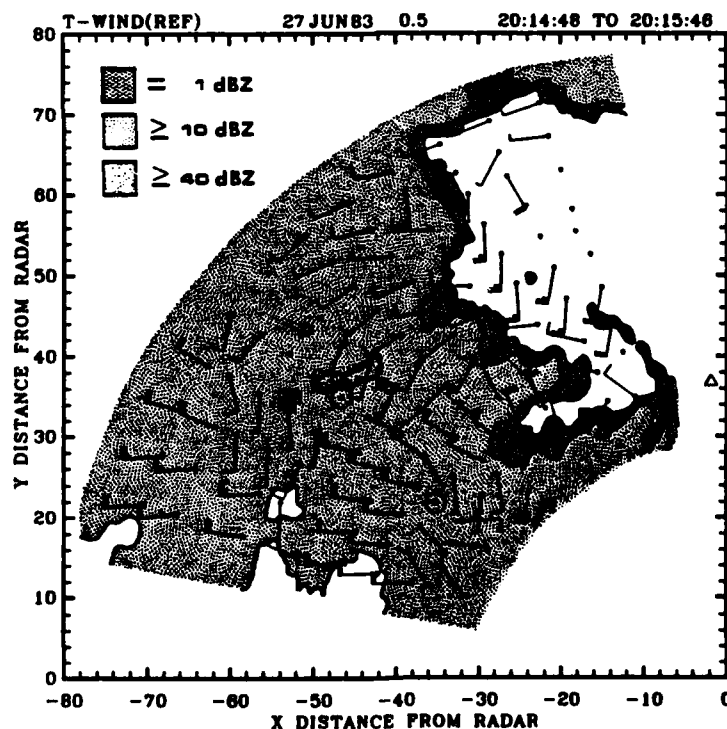
Fig. 5.4. As in Fig. 5.2, except for 20:14:48 to 20:15:46.

In Fig. 5.5, the 1 dBZ contour began to delineate a roll cloud. In the TWIND plot for the period 20:14:53 to 20:15:50 (Fig. 5.5), it was readily apparent that the higher values of velocity were associated with a gust front. This gust front might have been forming as early as 2005 CST as evidenced by the five high velocity wind vectors in Fig. 5.3 and the indications of "gust front passage" at the 40-series complex as discussed in chapter IV (Fig. 4.9). The TWIND plot for the period 20:24:35 to 20:35:32 (Fig. 5.6) showed an excellent view of the roll cloud and the associated derived wind vectors. From these two figures it appeared that the gust front passed the NSSL-KTVY tower between 20:15:50 and 20:25:32 CST. Tower data (Fig. 4.10) confirmed that gust front passage occurred at approximately 2017 CST.
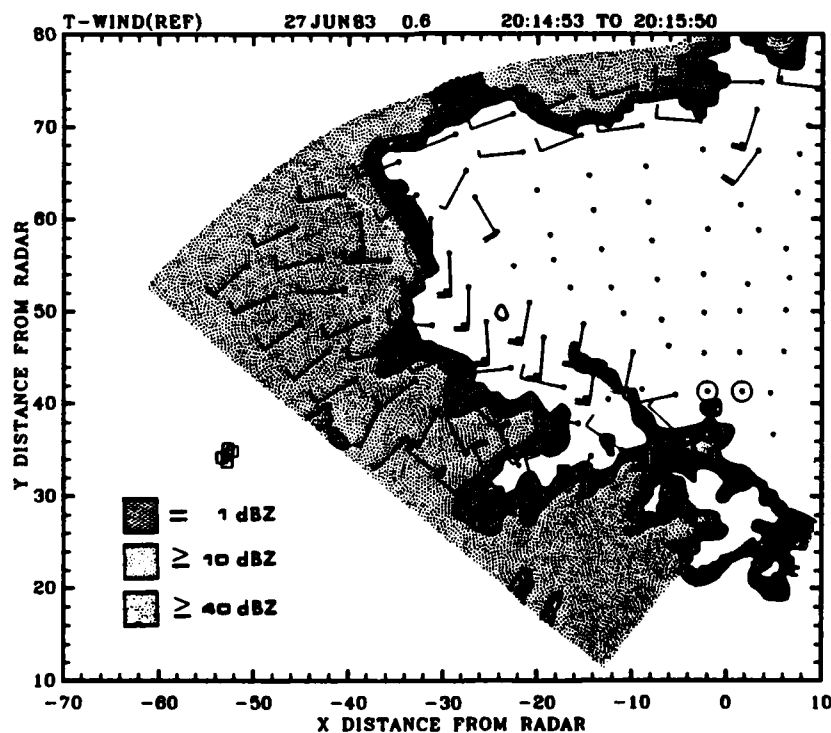
Fig. 5.5. TWIND plot for 27JUN83 case (20:14:53 to 20:15:50) with maximum correlation coefficient threshold set at 0.85.
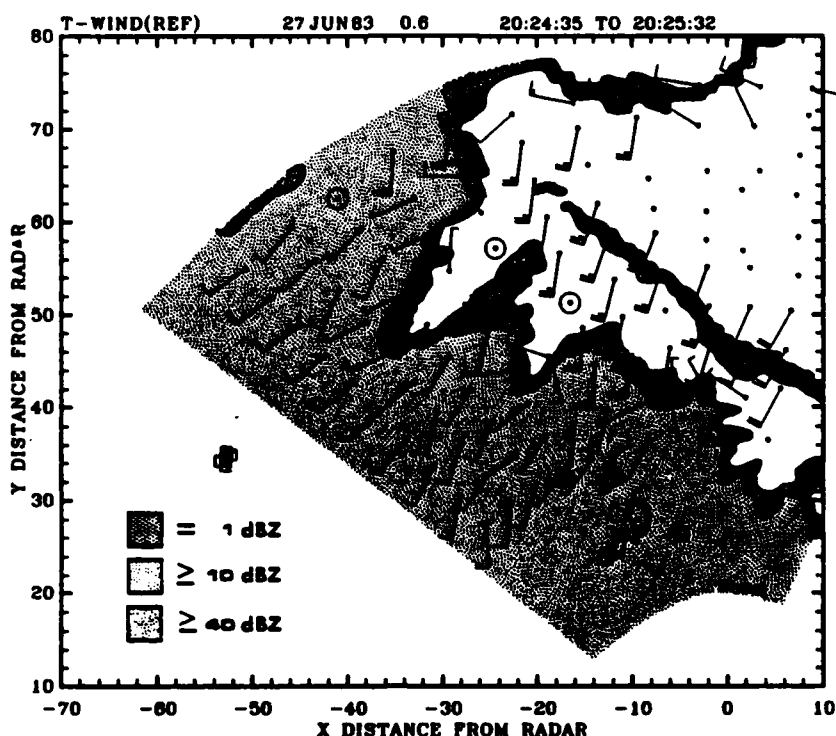
Fig. 5.6. As in Fig. 5.5, except for 20:24:35 to 20:35:32.

It appeared that the TWIND approach delineated the micro-scale (gust front) winds, as well as the meso-scale. However, what was particularly interesting was that the TWIND vectors associated with the gust front (Figs. 5.3, 5.4, 5.5, and 5.6) could not have been developed from generator level motions. The gust front and roll cloud are low-level phenomena. This was the first observation with the use of the TWIND approach where generator level motions could be definitely ruled out.

There is frequent discussion in the literature regarding horizontal momentum conservation from the mid-levels of a storm to the outflow region at the surface (Byers and Braham, 1949; Walters, 1975; Goff, 1976; Bonewitz, 1978). The conservative properties of equivalent potential temperature (θ_e) make it an excellent tracer. θ_e was computed

and plotted for all of the SAM sites. At the 60-series complex, a
sudden decrease in the value of Θ_e occurred around 2000 CST when Θ_e
decreased rapidly from 358 K (1958 CST) to a value of 339 K (2000 CST).
Θ_e continued to decrease at a slower rate reaching a minimum of
approximately 330 K at about 2123 CST. The Θ_e rebounded and stabilized
at about 334 K at approximately 2145 CST. At the 40-series complex at
2007 CST, Θ_e dropped from around 360 K to 336 K at 2009 CST. This
remained stable until a slow cooling began around 2200 CST dropping to
332 K at 2221 CST. A representative plot is given in Fig. 5.7. The
tower Θ_e computation showed a sudden decrease at both levels beginning
at about 2018 CST (360 K) and stabilizing at 2021 CST (335 K) (Fig.
5.8).

Equivalent Potential Temperature (K) vs. Time

STATION NUMBER : 43
DATE : 6/27/83
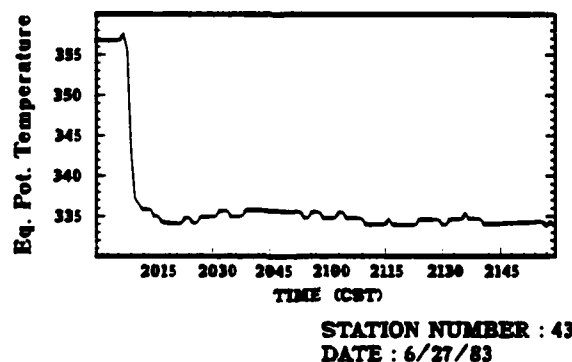
Fig. 5.7. Representative plot of equivalent potential temperature
(Θ_e) for a SAM site.

LVL 6 LVL 5 LVL 4 LVL 3 LVL 2 SFC

TIME (CST)

2000   2015   2030   2045   2100
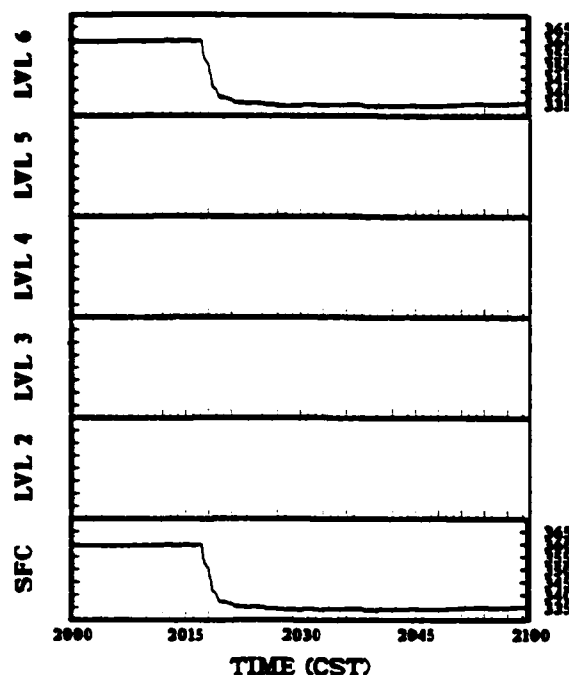
Fig. 5.8. Equivalent potential temperature (Θ_e) for the NSSL-KTVY tower.

If horizontal momentum conservation holds, then the horizontal winds
at the downdraft origin and the surface winds should show comparable
direction and speed. However, winds speeds may differ due to
gravitational acceleration, pressure differential effects, friction
effects, and other causes. Sounding winds (OKC, 0000 Z) demonstrated
classical veering with height, and from the minimum Θ_e layer the winds
exhibited a direction of approximately 270° at 23 m s^{-1}. The average
winds at the 60-series SAM cluster at 2014 CST were 208° at 15 m s^{-1}.
The TWIND plot had areas with westerly winds at 20 - 25 m s^{-1}, southerly
at 5 - 10 m s^{-1}, and others. The similarity of winds at the assumed
downflow origin and the region of westerly winds from TWIND, given the
theory of horizontal momentum conservation, was enough to suggest that

these winds might have represented a part of the downdraft, rather than representing the winds behind the squall line (meso-high). However, it appears more likely that these winds were associated with the meso-high, as this theory also explains the southerly winds. Also, the assumptions required to establish the origin of the downdraft air due to the difference in minimum Θ_e values put this wind direction in question. Finally, it is conceivable that these winds resulted from both the transfer of momentum from above and the meso-high. The conclusion of Greene et al. (1977) that "wind measurements near the ground often do not represent true gust-front intensity or movement" may account in part for the discrepancies between the SAM and TWIND data. Regardless of the error source, this analysis indicates that low-level TWIND data do give a good representation of winds from meso- and micro-scale features. Also, the TWIND data have shown themselves to be a good tool to identify the location, magnitude, and direction of the gust front. The general conclusion to this first case is that significant meteorological events are represented by the transverse wind derived wind field.

Case 2: June 28, 1983

From the TWIND plot for the time period 23:36:14 to 23:37:11 (Fig. 5.9) west-northwest winds were predominant within the 10 dBZ contour. Winds at the 60-series complex in this time frame were from the southwest. In front of the 10 dBZ contour, more than half of the wind flags indicated southwesterly winds. However, some strong winds were located in the north-central part of the window. The TWIND data at this time could have been a snapshot of the meso-low/high seen in the meso-analysis for 2300 CST (Fig. 4.16) and 0000 CST (Fig. 4.19). Winds close

to the radar were south to southwest and those farther away were west to northwest. This would correspond to the winds across a meso-low located to the west of the radar. Winds increased from 5 m s^{-1} to 15 - 20 m s^{-1} in the SAM data, and the TWIND plot also showed an increase from 5 m s^{-1} to 20 - 25 m s^{-1}.
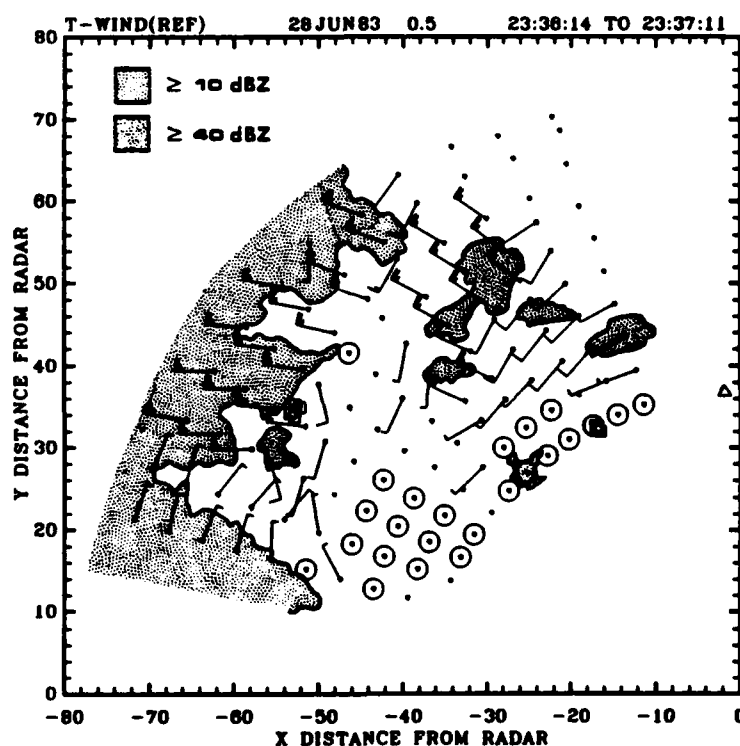
Fig. 5.9. TWIND plot for 28JUN83 case (27JUN83, 23:36:14 to 23:37:11) with maximum correlation coefficient threshold set at 0.85.

From the TWIND plot for the time period 23:42:05 to 23:43:03 (Fig.
5.10), more vectors had moved in and had veered to the northwest, with
the exception of some "marching vectors," which moved deeper and deeper
into the window with time. With the meso-low located northwest of OKC
before midnight (i.e., between Figs. 4.16 and 4.19), the TWIND plot for
the time period 23:47:57 to 23:48:55 (Fig. 5.11) properly indicated
winds from the west to northwest at 20 - 25 m s^{-1}. This wind pattern
moved closer to the radar, which matched the surface meso-analysis.
Even though a problem seemed to exist with "marching vectors," the TWIND
plot for the time period 23:53:49 to 23:54:46 (Fig. 5.12) revealed
southerly winds backing around to the west-northwest. It appeared that
the feature of the meso-low was well represented by the TWIND derived
field in a region of relatively low reflectivity returns (Fig. 4.20).
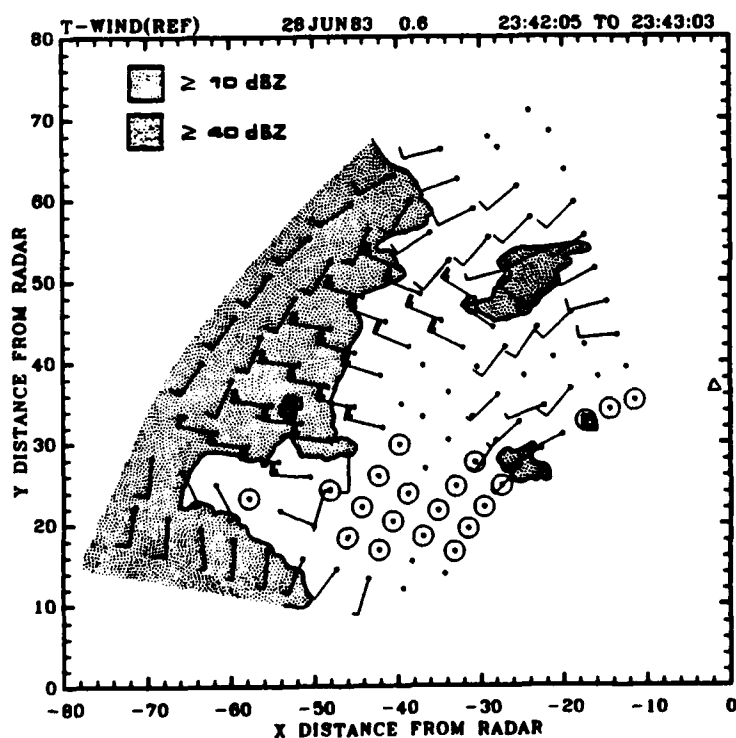
Fig. 5.10. As in Fig. 5.9, except for 23:42:05 to 23:43:03.
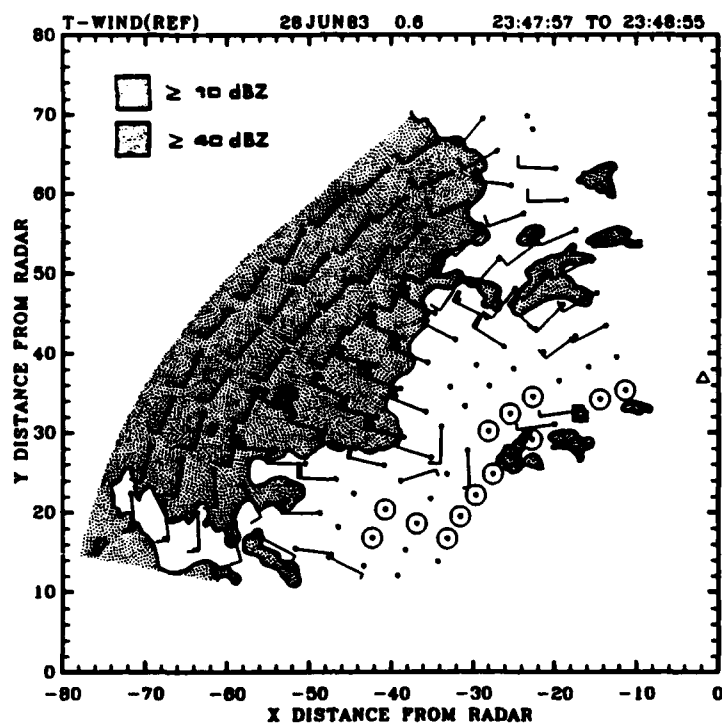
Fig. 5.11. As in Fig. 5.9, except for 23:47:57 to 23:48:55.
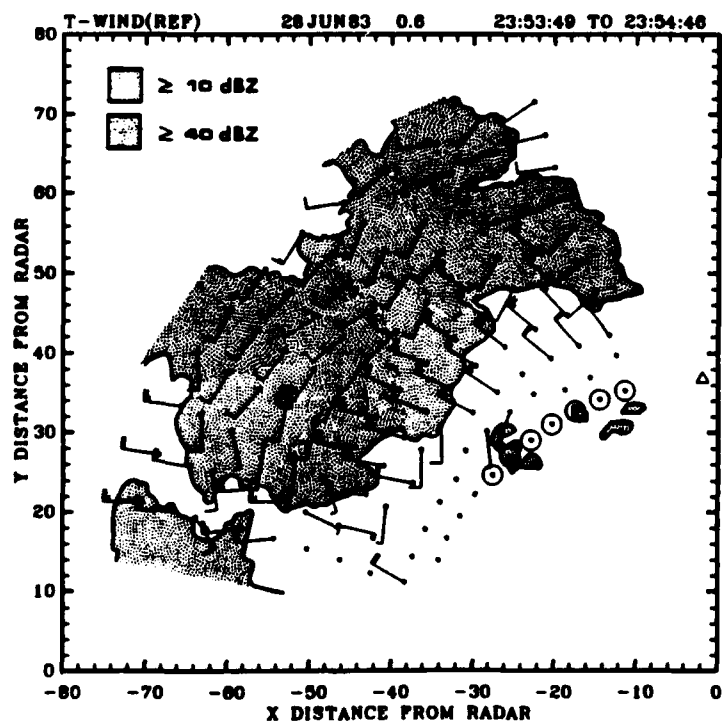
Fig. 5.12. As in Fig. 5.9, except for 23:53:49 to 23:48:56.

In case 1, "clear air data" were not highly correlated. In this case, the region behind the 10 dBZ reflectivity contour had highly correlated vectors (Fig. 5.13). It is most unlikely that these winds were associated with a thunderstorm downdraft, and the direction did agree with the meso-analysis (Fig. 5.14). Previously it was shown that derived winds outside the 10 dBZ contour were not reliable. That did not seem to be true in this case. The TWIND derived wind field (Fig. 5.14) did not seem to agree with the SAM observed surface winds, but continued to agree with the surface meso-analysis. Continuing in time with Figs. 5.15, 5.16, and 5.17, the winds became increasingly westerly. This agreed with the meso-analysis movement of the meso-low and meso-high during this period (i.e., Figs. 4.19 to 4.22).

No other significant features were observed in this case. The storms, with only one small 30 dBZ core within the observation window, had more of a stratiform, than convective appearance (Figs. 4.17, 4.20, and 4.23). The θ_e analysis confirmed the absence of downdraft air as the value of θ_e decreased only four degrees between 2300 CST and 0100 CST.
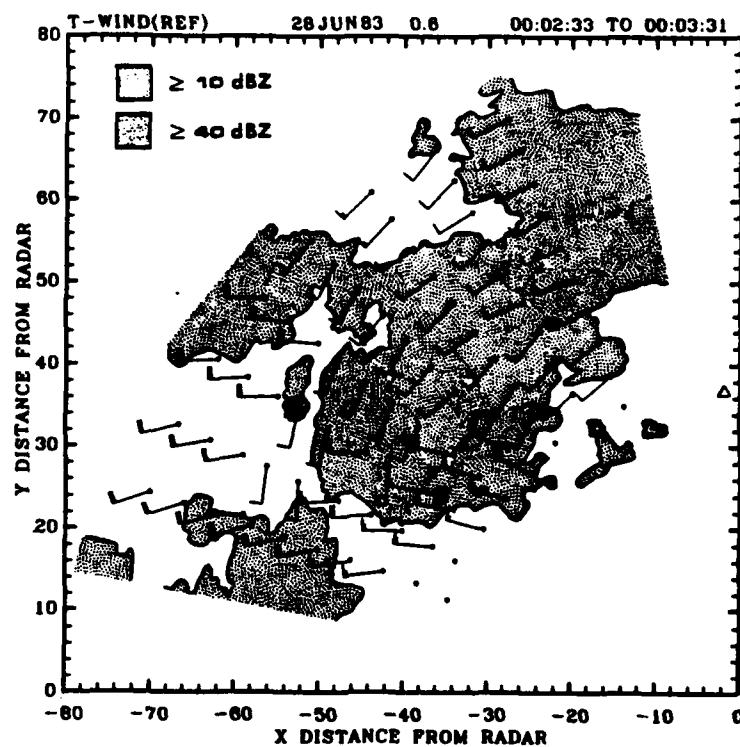
Fig. 5.13. As in Fig. 5.9, except for 00:02:33 to 00:03:31 (28JUN83).
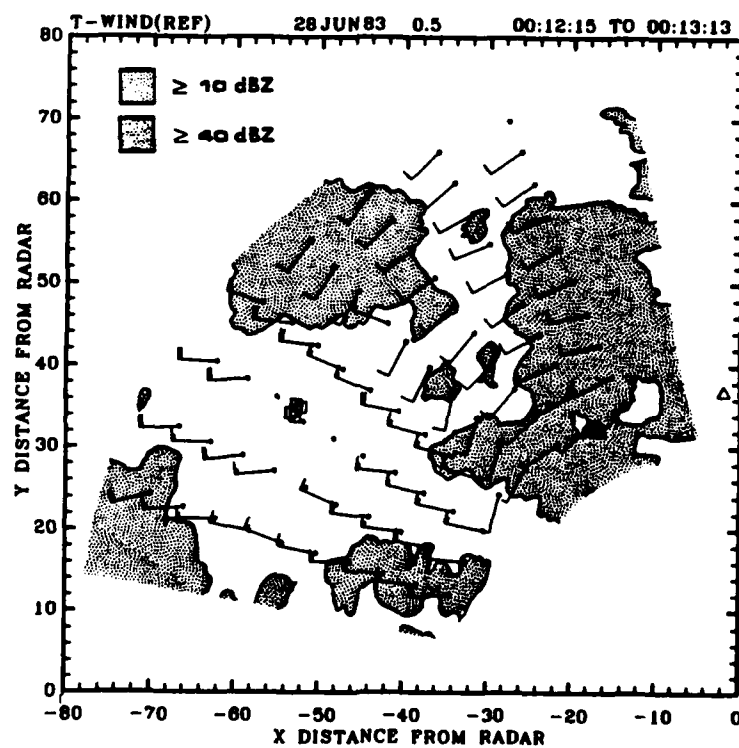
Fig. 5.14. As in Fig. 5.13, except for 00:12:15 to 00:13:13.
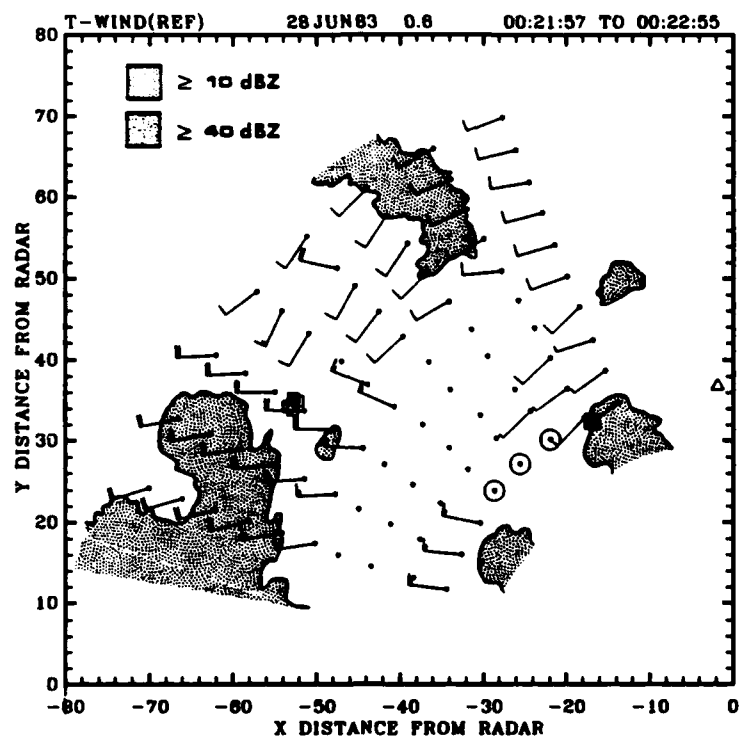
Fig. 5.15. As in Fig. 5.13, except for 00:21:57 to 00:22:55.
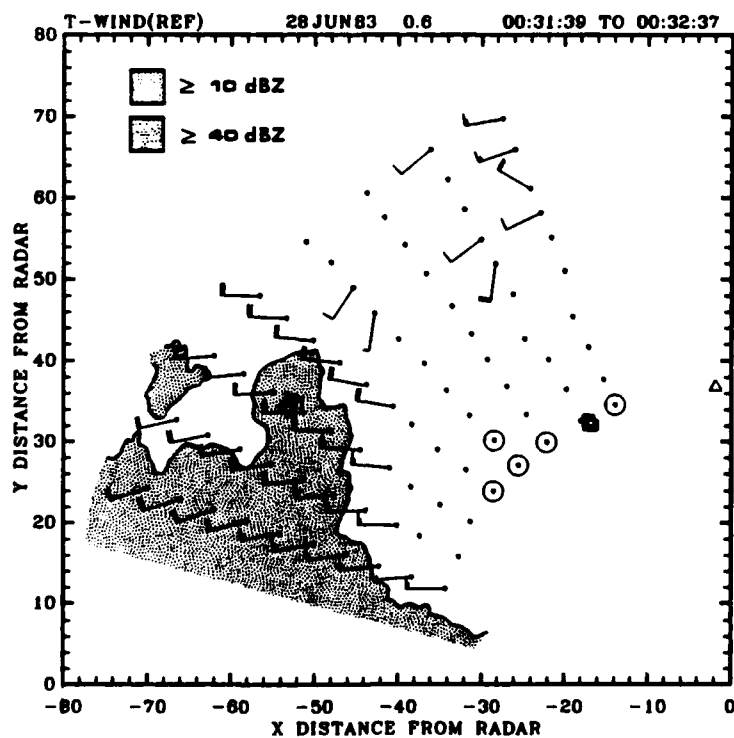
Fig. 5.16. As in Fig. 5.13, except for 00:31:39 to 00:32:37.
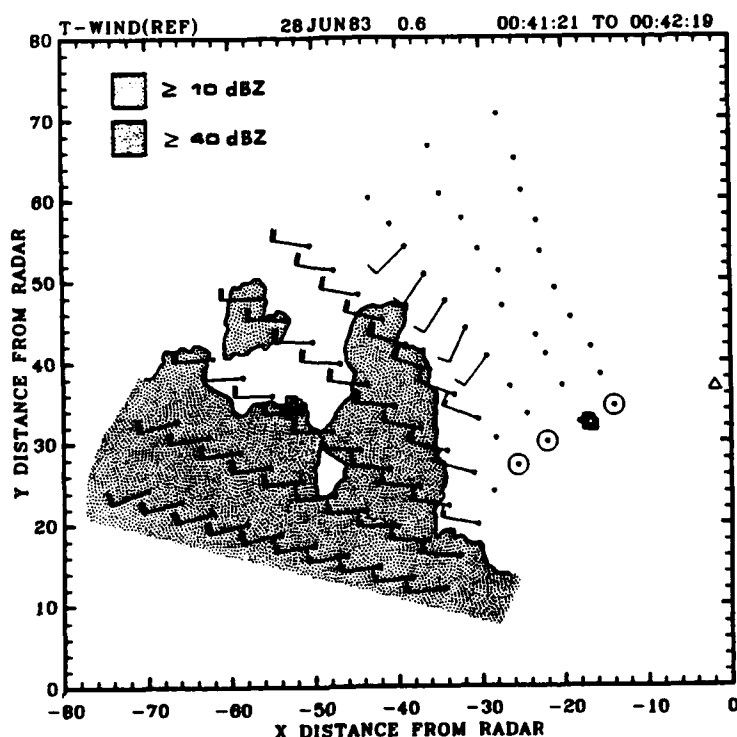
Fig. 5.17. As in Fig. 5.13, except for 00:41:21 to 00:42:19.

Several times in this case reference has been made to "marching vectors." These apparently anomalous vectors first appeared in this case in Fig. 5.10 behind the strong westerly winds. They might have gone unnoticed, except for two factors. First, these vectors were in an organized band and were roughly perpendicular to the radar beam, giving them the appearance of marching like a column of soldiers around the radar. Thus, the term "marching vectors" was adopted. Second, these vectors became more prevalent with each time period (Figs. 5.11, 5.12, and 5.13). Smythe (1983) observed 'radial vectors,' which were "produced because the radial motions are too small to allow detection with 1° data resolution and Δt = 66s." However, none of the previous researchers reported the "marching vector" phenomenon. The initial

reaction was that this might be a "boundary value" problem, but it does not occur all the time. Although it did not appear to be a boundary value problem, this was checked by shifting the observation window outward by 20 km. If this had been a boundary value problem, the "marching vectors" would have shifted out toward the new boundary and "good" data would have appeared in their place. This did not occur, confirming that this was not a boundary problem. Part of the cause of "marching vectors" might have been the 50% BOX1 overlap or the averaging process of TWIND itself. However, it appears more likely that this might have been a result of relative strength of meteorological features. In the current case, the reflectivity values were really rather weak, 10 to 20 dBZ. This suggests that the TWIND system may not have strong enough or sharp enough features to lock-on and track. The pressure gradient of the meso-high was a strong meteorological feature that began overriding the "marching vectors." By 0032 CST the field was uniform, as expected, and the 0.85 correlation coefficient threshold once again suppresses the "marching vectors" (Fig. 5.16).

Notice the difference between the TWIND plots at 0021 and 0031 CST (Figs. 5.15 and 5.16, respectively). The difference in meteorological conditions at these times fit the hypothesis as to why the "marching vectors" existed. This sequence of non-suppression to suppression fits with the concept of how the TWIND system really works---not from a mathematical standpoint, but from a meteorological standpoint. Whenever the field is governed by a significant event, as at 0031 CST when the winds were westerly, the suppression at the maximum correlation coefficient of 0.85 begins to work again.

In case 1, the lack of a large number of "marching vectors" might have been due to the strong storm features. Case 2 had relatively low reflectivity values throughout the event. However, high correlation matches had been made in the "clear air" in this case. Perhaps the winds in that region were so much stronger, even with the weaker pattern, that they obtained a good match anyway. This situation may be made to order for a multiple regression study. This might then allow culling the wind vectors on factors other than just the maximum correlation coefficient.

Case 3: April 22, 1983

The TWIND plot for the time period 18:38:29 to 18:39:26 (Fig. 5.18) indicated light westerly winds north and southerly winds south of the 60-series SAM complex. The southerlies appeared to coincide with the meso-analysis (Fig. 4.27) for this time period, and the westerlies were a reasonable match with the SAM data. A small number of "marching vectors" were evident in the ranks closest to the radar. The TWIND plot for the time period 18:47:13 to 18:48:11 CST (Fig. 5.19) showed little change. Note that in both of these time periods almost all of the TWIND wind speeds were reported as 5 m s^{-1}. Note also the large number of "calm" indications. These patterns continued (Figs. 5.20 and 5.21) until the time period 19:22:11 to 19:23:08 (Fig. 5.22) when a couple of northerly winds appeared in the northern portion of the plot. This trend continued (Figs. 5.23, 5.24, and 5.25) until the last period (Fig. 5.26), when almost every vector appeared to be 5 - 10 m s^{-1} from the east. In contrast, the SAM data indicated winds from the north to northwest throughout this period.
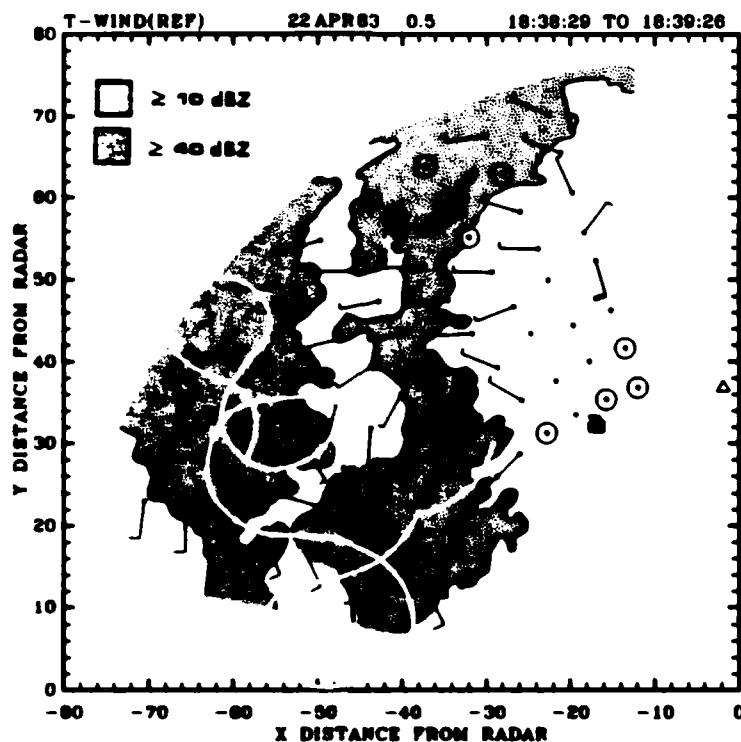
Fig. 5.18. TWIND plot for 22APR83 case (18:38:29 to 18:39:26) with maximum correlation coefficient threshold set at 0.85.
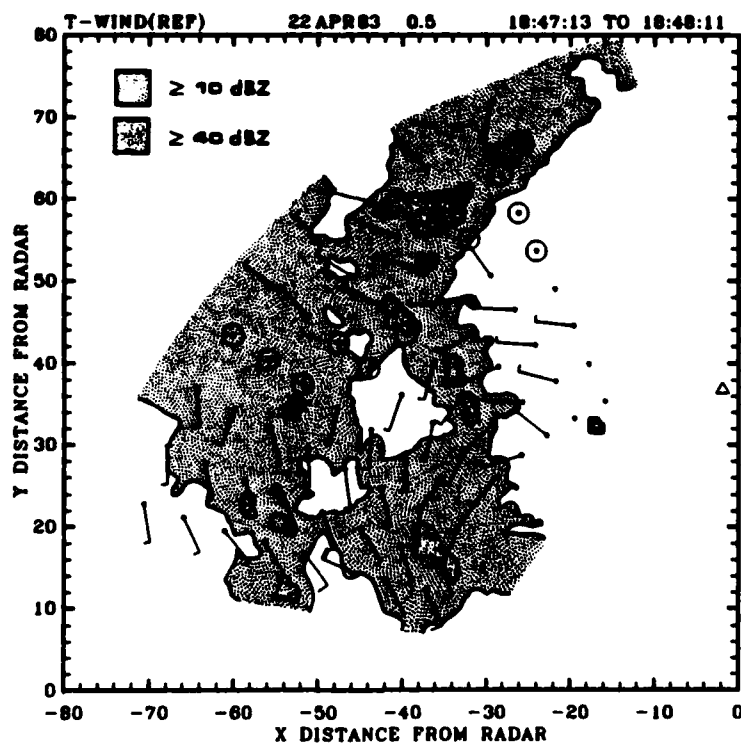
Fig. 5.19. As in Fig. 5.18, except for 18:47:13 to 18:48:11.
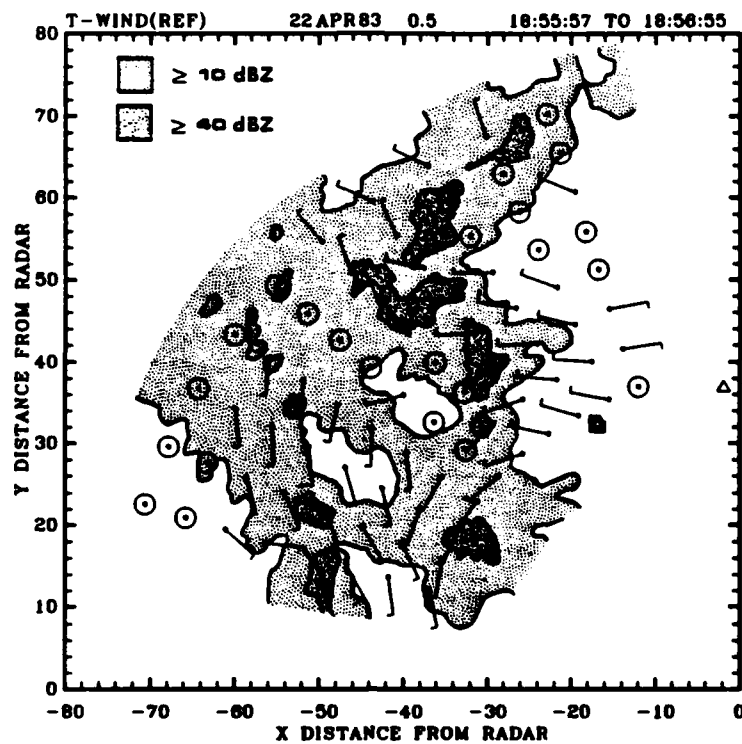
Fig. 5.20. As in Fig. 5.18, except for 18:55:57 to 18:56:55.
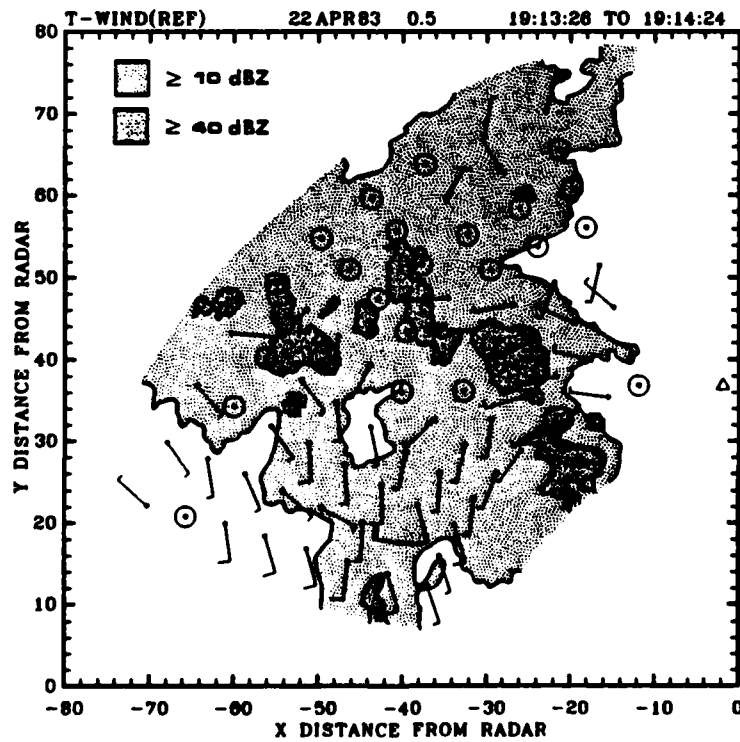
Fig. 5.21. As in Fig. 5.18, except for 19:13:26 to 19:14:24.
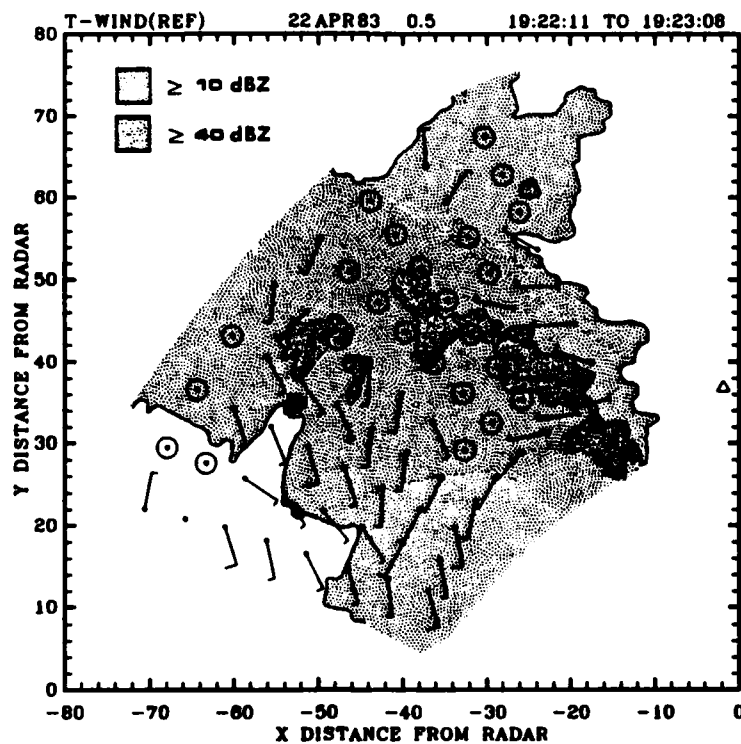
Fig. 5.22. As in Fig. 5.18, except for 19:22:11 to 19:23:08.
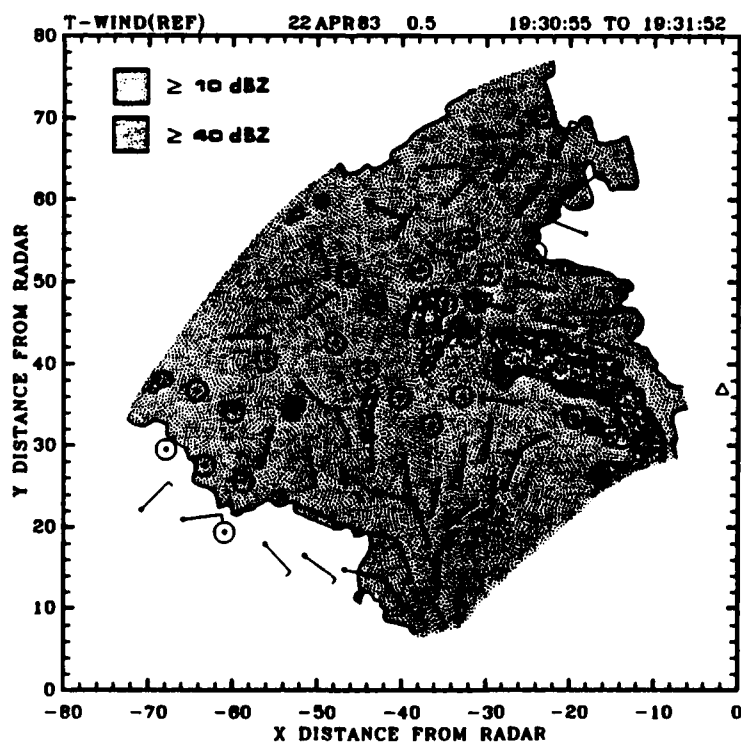
Fig. 5.23. As in Fig. 5.18, except for 19:30:55 to 19:31:52.
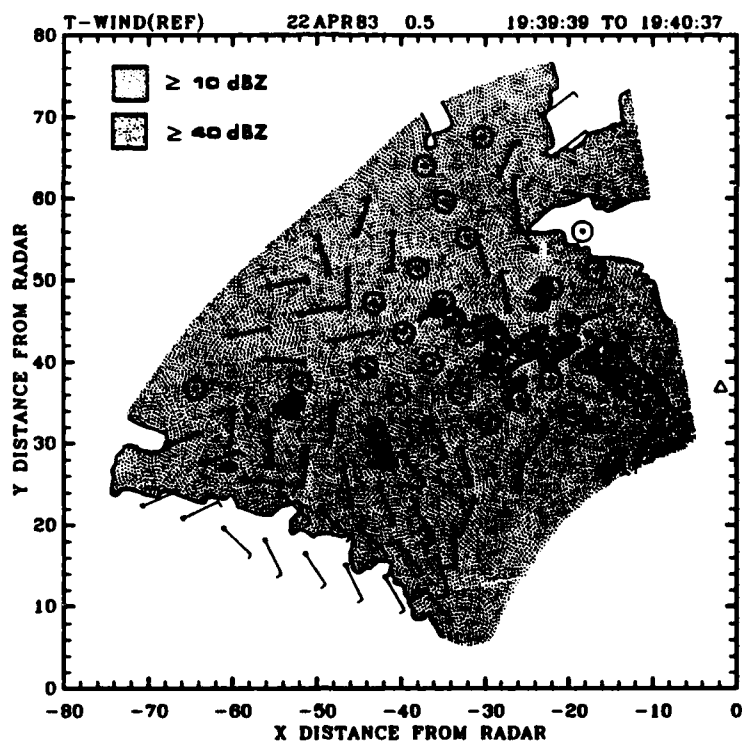
Fig. 5.24. As in Fig. 5.18, except for 19:39:39 to 19:40:37.
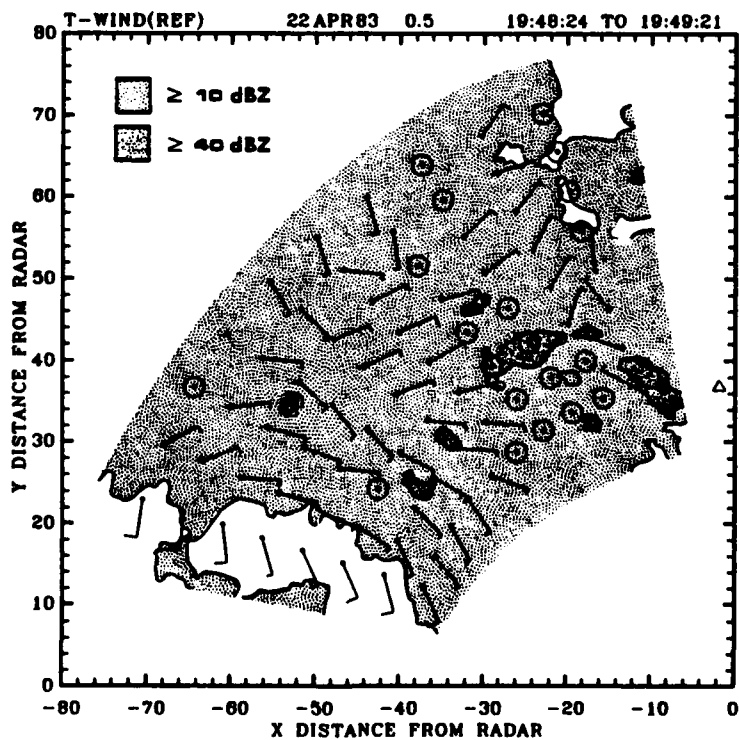
Fig. 5.25. As in Fig. 5.18, except for 19:48:24 to 19:49:21.

The surface meso-analyses (Figs. 4.27, 4.31, 4.35, and 4.38) indicated a sequence of wind directions (southeasterly [1800 CST], easterly [1900 CST], northerly [2000 CST], and westerly or easterly [2100 CST], depending on the exact position of the meso-high). The SAM sites indicated micro-scale features, which were not generally resolved by the TWIND data or the meso-scale analysis.

Figs. 5.27 through 5.30 are representative plots of the equivalent potential temperature (θ_e) for the 60- and 40-series SAM complexes. These plots display a general trend of decreasing θ_e, which corresponds to an airmass change or general cooling of the atmosphere. Spikes appear periodically in the θ_e data, which is interpreted to be thunderstorm outflow. Note how the original decreasing slope returns following a "thunderstorm spike," but at a slightly different rate. The upper level air is pulsed out in the thunderstorm outflow, which causes the spikes.
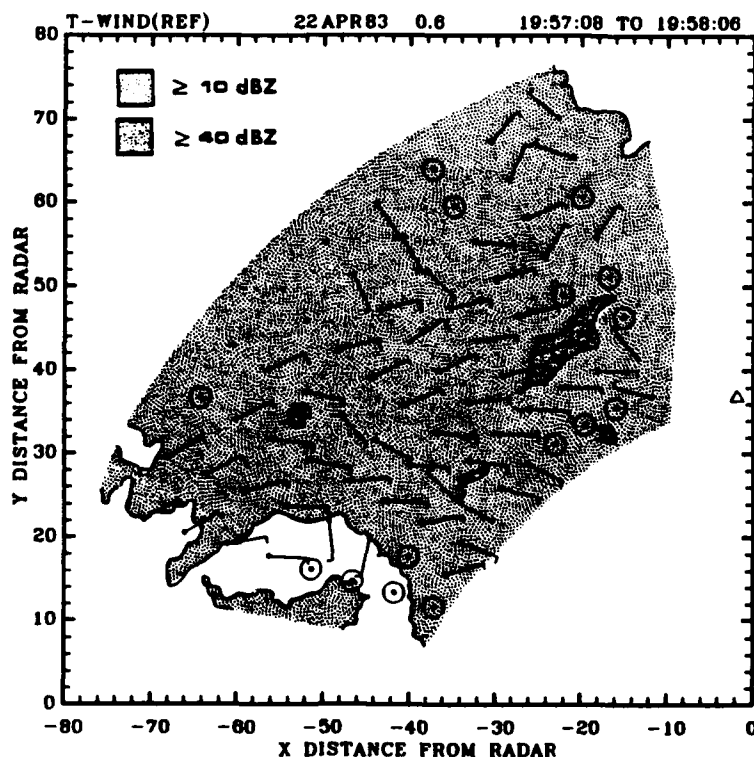
Fig. 5.26. As in Fig. 5.18, except for 19:57:08 to 19:58:06.

It is quite apparent from the meso-analysis (Figs. 4.27, 4.31, 4.35, and 4.38) that this case differed significantly from the previous two cases. This is further confirmed by the different pattern present in the Θ_e analysis for the SAM data collected during this period. The TWIND data began (Fig. 5.18) and ended (Fig. 5.26) in reasonable agreement to the meso-analysis. In between these two times there appeared to be a very slow transition. It is of interest that the TWIND data indicated almost all light winds over the observation window throughout the entire period.

It is of further interest that upon examining all the available data (radar reflectivity, TWIND plots, equivalent potential temperature analyses, and SAM observations) all of the fields seem to fit together, except for the SAM wind field. A possible explanation is that the SAM wind field is responding to micro-scale features, which are too small to be resolved by either the TWIND approach or the meso-analysis.

Equivalent Potential Temperature (K) vs. Time

STATION NUMBER : 61
DATE : 4/22/83
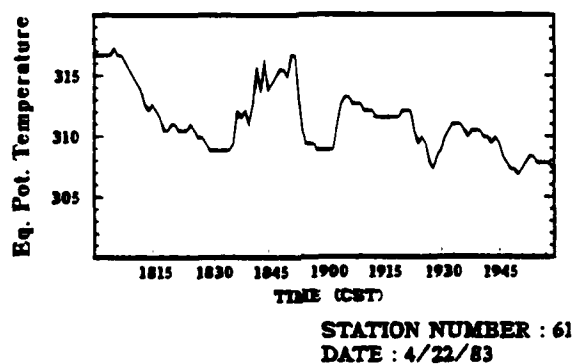
Fig. 5.27. Representative equivalent potential temperature (Θ_e) (60-series).

Equivalent Potential Temperature (K) vs. Time

STATION NUMBER : 61
DATE : 4/22/83
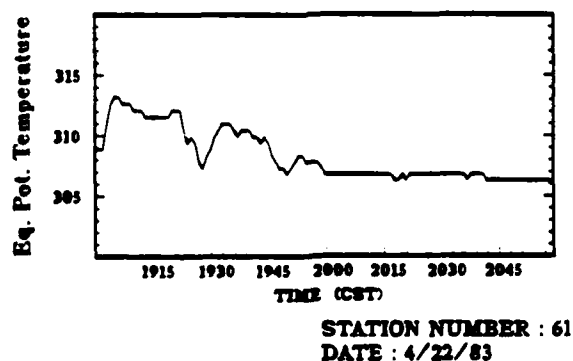
Fig. 5.28. As in Fig. 5.27, except for 1900 - 2100 CST.

Equivalent Potential Temperature (K) vs. Time
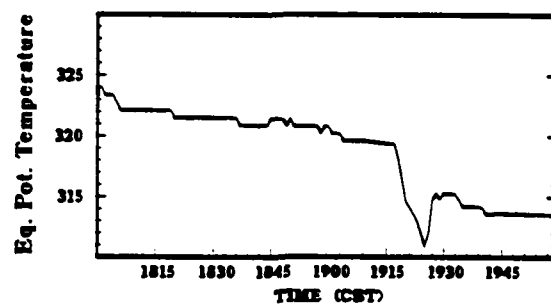
STATION NUMBER : 41
DATE : 4/22/83

Fig. 5.29. As in Fig. 5.27, except for 40-series.

Equivalent Potential Temperature (K) vs. Time
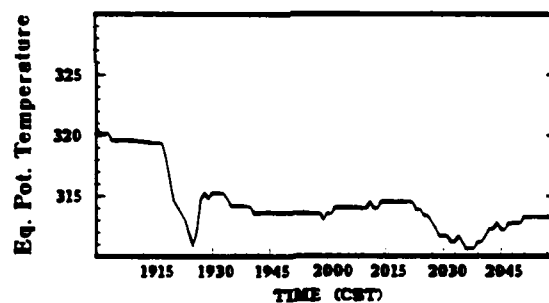
STATION NUMBER : 41
DATE : 4/22/83

Fig. 5.30. As in Fig. 5.29, except for 1900 - 2100 CST.

CHAPTER VI

CONCLUSIONS AND RECOMMENDATIONS

Conclusions

The objective of this investigation was to test the hypothesis that there is a determinable relationship between the true surface wind field and radar derived wind data. Since Doppler radar provides only the radial component of the wind field, an approach was taken to complement the Doppler data. The approach taken, known as the transverse wind technique, derives the wind field through pattern matching using a multiple correlation analysis. It uses temporally separated scans of radar reflectivity. This research went through two distinct phases. The first was to examine the data derived from the local implementation of the NEXRAD Transverse Wind algorithm (i.e., the TWIND program) to select desired TWIND parameters and assess the general usability of the data. The second was to examine the relationship of the TWIND data to other sources of surface wind data.

Data derived at low levels, using a long time period (ΔT) between consecutive radar scans, closely resemble upper level TWIND derived data at similar ΔT's. This could be due to the long ΔT's alone, or the long ΔT's may be a factor in allowing the "generator level winds" to dominate. It is possible that the long ΔT's allow for an apparent transfer of momentum from the upper to the lower levels. The short ΔT (55 - 57 seconds) TWIND data at low levels appear significantly

different from long ΔT data at both low and upper levels. The shorter ΔT's seem to model the winds at the observed level, not allowing the effects of a generator level to dominate the field.

The TWIND analysis for the three cases studied had higher maximum correlation coefficients than cases studied by previous researchers. Two factors that may have played a role are the nature of the storms and the range to the center of the observation window.

An additional measure of the "goodness" of the TWIND derived wind field is internal consistency. It was observed that the TWIND field was quite noisy outside the storm due to "weak reflectivity variability," which leads to random pattern matches. This is the result expected as the reflectivity field in the weak or no echo regions is effectively noise (i.e., random patterns). Attaining a noisy pattern in a region known to be noisy increases the confidence that the TWIND technique is operating as expected. Approximately 98% of the vectors within the 10 dBZ contour in the 27 and 28 June cases were judged to be internally consistent*. In addition, 97% of the consistent vectors in this group were found to have maximum correlation coefficients of 0.85 or greater. By using only the vectors within the 10 dBZ contour with maximum correlation coefficients ≥ 0.85, it was found that only 2% of the included vectors were classed as inconsistent. All but one of these inconsistent vectors appeared to be 5 m s^{-1} or less. There were fewer unexplained internally inconsistent vectors and almost no "radial" vectors as compared to previous studies.

---

*Internally consistent vectors are those vectors which seem in good agreement in magnitude and direction with the general trend of those vectors in close proximity.

The conclusion reached from the first phase of this investigation (based on pattern comparisons, maximum correlation coefficients, and internal consistency) was that data obtained at low elevation angles ($\cong 0.5°$) with short time lags between reflectivity passes ($\Delta T \cong 59$ seconds) represent the observed wind field. These data are most appropriate to study further with regard to the value and use of the TWIND approach. It was found that significant improvement could be made in the resulting wind field by using only data derived within the 10 dBZ contour, which have maximum correlation coefficients of 0.85 or greater.

The second phase of this investigation sought to test the hypothesis that there is a determinable relationship between the true surface wind field and the radar derived wind data. This phase was itself divided into two parts. The first part involved comparisons wherein a temporal or spatial scale difference in the data sets (Doppler radial velocity, TWIND derived data, and surface automated mesonet (SAM) data) might create interpretation difficulties. The second part involved a comparison of the TWIND data with the observed mesoscale environment.

Under part one, four comparisons were made. Winds from the SAM data were compared with the TWIND derived data. It was observed that only 57% of the TWIND winds were within 60° of the SAM wind direction (for all speed errors). It was further observed that only 41% of the TWIND winds were within 5 m s^{-1} of the SAM data (for all direction errors). Comparison was also made between the Doppler radial wind field and the radial component of the SAM data and the radial component of the derived TWIND data. It was observed that 92% of the SAM radial components fell within their appropriate Doppler radial wind field contour. Only 76% of the radial components of the TWIND data fell within their appropriate

Doppler contour. No other statistical analyses were conducted on these data due to the inherent problems in doing objective comparisons, including the very nature of the spatial and temporal differences in the data sets themselves, the mechanisms used to compare the data, the la.ge margin for error in the time-to-space conversion of the SAM data, and the larger number of vectors compared because of repeat comparisons among the vectors. However, even given these limitations on the analysis, two conclusions were reached. First, from the radial comparisons the Doppler data and SAM data seem reasonably well associated, especially since the Doppler data are above the surface. The TWIND data do not show as good an association with the Doppler data, which is probably due for the most part to the temporal and spatial averaging inherent in the technique. Coupling this averaging with possible contamination from outside the observation window and the 76% comparison should probably be viewed as a positive link between these two data fields.

The final comparison in this category was an attempt to modify the Doppler radial wind field with the TWIND derived wind direction to produce an improved wind field. This study confirmed the subjective observation by previous researchers that these fields were significantly dissimiliar. Unrealistically strong winds (100's to 1000's of m s^{-1}) were derived by this approach. The conclusion reached from this element of research is that the average wind direction derived by the TWIND approach does not reflect the instantaneous wind direction that produces the Doppler radial wind field. This finding does not mean that either data set is wrong---just that they are different.

The part two comparison was made between the TWIND derived wind fields and the observed meso-scale environment. Confirmation of a link between the TWIND data and the observed surface winds comes from matching general patterns (the predominant wind field), not an exact match with perfect timing.

In the first case, under the meteorological conditions of a squall line, close correlation was shown between observations at the SAM complex and the TWIND derived winds. The TWIND data appeared to provide a reasonable representation of the meso-scale flow within the observation area. The TWIND process resulted in some apparent "errors," but this was not unexpected. The TWIND data must be coupled with other information to filter out these "errors." These "errors" are actually inconsistencies and may not be in error at all, but just are smaller scale motions, which are not explained by this analysis. While most of the analyses held to the use of the 10 dBZ contour as the dividing line between presumed valid data and unacceptably noisy data, one notable exception was found. The observation of a gust front in the 27JUN case was the first use of the TWIND approach where the generator level motions could definitely be ruled out as the source for the low-level derived TWIND field. The conclusion from this first case is that the low-level TWIND data give a good representation of winds from both meso-and micro-scale features.

The second case had a more stratiform than convective appearance. In this case, the winds outside the 10 dBZ contour, but behind the echoes, appeared much more consistent than anticipated and matched up well with the winds within the 10 dBZ contour. While the TWIND data did not appear to agree with the SAM data, they continued to agree well with

the meso-analysis. It appeared that the nature of the storms under observation was highly significant in both the regions of valid derived winds and in the connection between the TWIND and surface data. This case presented a new feature, "marching vectors," not previously identified in TWIND studies. These "marching vectors" occurred in areas of relatively weak, uniform reflectivity. This suggested that they are an artifact of the processing technique, which appears only when not over-powered by the presence of a significant meteorological feature. The 0.85 maximum correlation coefficient threshold begins to suppress "bad" data, such as the "marching vectors," when a significant meteorological feature is present.

Based on the meso-scale and θ_e analyses, the third case appeared to present significantly different meteorological conditions than the first two cases. The TWIND analysis indicated almost nothing but light winds over the observation window throughout the entire period. The TWIND data and the meso-analysis seemed in reasonable agreement. However, the SAM wind field appeared to be out of agreement with all the other available data (TWIND derived, meso-analysis, and even the other levels of the SAM observation). The conclusion is that under these meteorological conditions the features, some micro-scale, observed by the SAM complex were not resolvable by TWIND approach.

In summary, this investigation has established the validity of TWIND data from low elevation angles with short ΔT's. The use of maximum correlation coefficient and reflectivity thresholds have been shown to improve the derived wind field. Doppler radial velocity, TWIND derived data, and SAM data have been compared with the results tempered by the temporal and spatial differences among these data sets. The attempt to

produce an improved wind field by modifying the Doppler radial wind field confirmed the dissimiliar natures of the Doppler and TWIND data. The TWIND derived wind field was shown to be closely related to the surface wind field as represented by surface meso-analysis. Although not defined, an apparent difference in storm structure results in a different response in the TWIND, yielding different degrees of comparison with the actual point observations (SAM data). A new feature, "marching vectors," which appears in areas of relatively weak, uniform reflectivity, was identified. Finally, the TWIND approach was successfully used in an area (gust front) where there is confidence that the TWIND vectors are derived from motions at their own level and not from some generator level.

Recommendations

Based on the results of this research effort, research involving the Transverse Wind algorithm should continue. This is obviously not a replacement for Doppler radar data, but could augment it. Since the ΔT must be short, data should be gathered with repeat scans at differing levels to further explore the generator level contribution to, or contamination of, the level of interest. Multiple regression studies should be conducted to better define the parameters used to select "good" vectors. Possible variables might include reflectivity, spectrum width, some measure of the uniformity of the reflectivity field, maximum correlation coefficients, storm type, and storm speed. At a minimum, efforts should be made to fine tune the 10 dBZ reflectivity and 0.85 maximum correlation coefficient thresholds used in this study. Research should be done to extend the study done by Hamidi et al. (1983) on

objective determination of box sizes. This work might also be best approached through some form of multiple regression study.

The data sets used in this study are quite interesting in their own right and should be examined further. These cases could be used to examine other fields (e.g., velocity) in the TWIND approach and compare with the current results. Further work is needed to determine why TWIND reacts differently to the different cases, particularly the 22 April case. The "marching vectors" warrant further examination to determine what causes them and how to suppress them when appropriate.

REFERENCES

Armstrong, G. M., and R. J. Donaldson, 1969: Plan shear indicator for real-time Doppler radar identification of hazardous storm winds. J. Appl. Meteor., 8, 376-383.

Atlas, D., 1963: Radar analysis of severe storms. Meteor. Monogr.,5, No. 27, 177-220.

Barnes, S. L., 1980: Report on a meeting to establish a common Doppler radar data exchange format. Bull. Amer. Meteor. Soc., 61, 1401-1404.

Battan, L. J., 1973: Radar Observations of the Atmosphere, Univ. of Chicago Press, Chicago, IL, 324 pp.

Bensinger, R., 1986: Personal communication.

Bjerkaas, C. L. and D. E. Forsyth, 1980: Operational test of a three-dimensional echo tracking program. Preprints, 19th Conf. on Radar Meteor., Miami Beach, Amer. Meteor. Soc., 244-247.

Bonesteele, R. G. and Y. J. Lin, 1978: A study of updraft-downdraft interaction based on perturbation pressure and single Doppler radar data. Mon. Wea. Rev., 106, 62-68.

Bonewitz, J. D., 1978: Development of Doppler radar techniques for severe thunderstorm wind advisories. M.S. Thesis, University of Oklahoma, unpublished, 69 pp.

------ , 1981: The NEXRAD program--an overview. Preprints, 20th Conf. on Radar Meteor., Boston, Amer. Meteor. Soc., 757-761.

Brandes, E. A., 1975: Severe thunderstorm flow characteristics revealed by dual-Doppler observations: 6 June 1974. Preprints, 9th Conf. on Severe Local Storms, Boston, Amer. Meteor. Soc., 85-90.

------, 1976: Gust front evolution in severe thunderstorms: Preliminary investigation with Doppler radar. Preprints, 7th Conf. on Aerospace and Aeronautical Meteor., Melbourne, Amer. Meteor. Soc., 56-61.

------, 1977: Gust front evolution and tornado genesis as viewed by Doppler radar. J. Appl. Meteor., 16, 333-338.

Brown, R. A., and L. R. Lemon, 1976: Single Doppler radar vortex recognition: Part II - tornadic vortex signatures. Preprints, 17th Conf. on Radar Meteor., Boston, Amer. Meteor. Soc., 104-109.

------, L. R. Lemon and D. W. Burgess, 1978: Tornado detection by pulsed Doppler radar. Mon. Wea. Rev., 106, 29-38.

Bumgardner, B., 1985: Personal communication.

Burgess, D. W., 1976: Single Doppler radar vortex recognition: Part I - Mesocyclone signatures. Preprints, 17th Conf. on Radar Meteor., Boston, Amer. Meteor. Soc., 97-103.

------, 1977: Personal communication.

------, J. D. Bonewitz and D. R. Devore, 1978: Joint Doppler operational project: Results year 1. Preprints, 18th Conf. on Radar Meteor., Atlanta, Amer. Meteor. Soc., 442-448.

Byers, H. R., and R. R. Braham, Jr., 1949: The Thunderstorm. U. S. Govt. Printing Office, Washington, D. C., 287 pp.

Carter, J. K., 1970: The meteorologically instrumented WKY-TV tower facility. NOAA Tech. Memo., ERLTM-NSSL 50, Norman, OK, 18 pp.

Cox, R., 1986: Personal communication.

Donaldson, R. J., Jr., 1970: Vortex signature recognition by a Doppler radar. J. Appl. Meteor., 9, 661-670.

Doviak, R. J., and D. S. Zrnic, 1984: Doppler Radar and Weather Observations, Academic Press, New York, NY, 458 pp.

Fujita, T. T., 1955: Results of detailed synoptic studies of squall lines. Tellus, 7, 405-436.

------, 1963: Analytical mesometeorology: A review. Meteor. Monog., 5, No. 27, 77-125.

Gal-Chen, T., and R. A. Kropfli, 1983: Deduction of thermodynamic properties from dual-Doppler radar observations of the PBL. Preprints, 21st Conf. on Radar Meteor., Edmonton, Amer. Meteor. Soc., 33-38.

Goff, R. C., and Zittel, W. D., 1974: The NSSL/WKY-TV tower data collection program, April-July 1972. NOAA Tech. Memo., ERL NSSL-68, Norman, OK, 45 pp.

------, 1976: Vertical structure of thunderstorm outflows. Mon. Wea. Rev., 104, 1430-1440.

Greene, G. E., H. W. Frank, A. J. Bedard, Jr., J. A. Korrell, M. M. Cairns, and P. A. Mandies, 1977: Wind shear characterization. FAA Report, FAA-RD-77-33, 120 pp.

Gunn, K. L. S., and J. S. Marshall, 1955: The effect of wind shear on falling precipitation. J. of Meteor, 12, 339-349.

Hamidi, S., R. E. Rinehart and J. D. Tuttle, 1983: Test of a transverse-wind algorithm for NEXRAD in real-time. Preprints, 21st Conf. on Radar Meteor., Edmonton, Amer. Meteor. Soc., 409-412.

------, 1984: Personal communication.

JDOP Staff, 1979: Final report on the Joint Doppler Operational Project (JDOP) 1976-1978. NOAA Tech. Memo., ERL-NSSL-86, Norman, OK, 84 pp.

Kraus, M. J., 1973: Doppler radar observations of the Brookline, Massachusetts tornado of 9 August 1972. Bull. Amer. Meteor. Soc., 54, 519-524.

Langleben, M. P., 1956: The plan pattern of snow echoes at the generating level. J. of Meteor., 13, 554-560.

Lemon, L. R., D. W. Burgess, and R. A. Brown, 1978: Tornadic storm airflow and morphology derived from single Doppler radar measurements. Mon. Wea. Rev., 106, 48-61.

Lhermitte, R. M., and D. Atlas, 1961: Precipitation motion by pulse Doppler. Proc. Ninth Weather Radar Conf., Boston, Amer. Meteor. Soc., 218-223.

------, 1964: Doppler radar as severe storm sensors. Bull. Amer. Meteor. Soc., 45, 587-596.

------, 1969: Doppler radar observations of a convective stor. Preprints, 6th Conf. Severe Local Storms, Boston, Amer. Meteor. Soc., 139-145.

Marshall, J. S., 1953: Precipitation trajectories and patterns. J. of Meteor., 10, 25-29.

NEXRAD JSPO Staff, 1983a: NEXRAD research and development plan. NEXRAD Report, Silver Spring, MD, 48 pp.

------, 1983b: Plan for Spring 1983 demonstration of prototype NEXRAD products in an operational environment. NEXRAD Report, Silver Spring, MD, pg 6-5.

------, 1984: Next generation weather radar algorithm report. NEXRAD Report R400A-AR202, Silver Spring, MD, 284 pp.

NSSL Staff, 1971: The NSSL surface network and observations of hazardous wind gusts. NOAA Tech. Memo. ERLTM-NSSL No. 55, 19 pp.

Peace, R. L., Jr., R. A. Brown, and H. G. Camnitz, 1969: Horizontal motion field observations with a single pulse Doppler radar. J. Atmos. Sci., 26, 1096-1103.

Pophin, D., 1986: Personal communication.

Rabin, R. M., and D. Zrnic, 1980: Subsynoptic-scale vertical wind revealed by dual Doppler-radar and VAD analysis. J. Atmos. Sci., 37, 644-654.

Reid, T., 1981: Computer graphics software for the Amdahl. Data Processing Center Report, Texas A&M University, College Station, TX, 136 pp.

Rinehart, R. E., and E. T. Garvey, 1978: Three-dimensional storm motion detection by conventional weather radar. Nature, 273, 287-289.

------, 1979: Internal storm motions from a single non-Doppler weather radar. NCAR Tech. Note NCAR/TN-146+STR, Boulder, CO, 262 pp.

Sanders, L. E., and A. H. Weber, 1970: Evaluation of roughness lengths at the NSSL-WKY Meteorological tower. NOAA Tech. Memo., ERLTM-NSSL47, Norman, OK, 24 pp.

Sickler, G. L., 1984: Personal communication.

------, J. D. Bonewitz, and G. L. Huebner, Jr., 1985a: A study of non-tornadic thunderstorm fields detected during the NEXRAD operational test facility's spring 1983 demonstration. Preprints, 14th Conf. on Severe Local Storms, Indianapolis, Amer. Meteor. Soc., 236-239.

------, ------, and ------, 1985b: Horizontal and vertical structure of non-tornadic meso-beta scale convective complexes. 2d Conf. on Mesoscale Processes, Univ. Park, PA. Amer. Meteor. Soc.

Smith, R. L., and D. W. Holmes, 1961: Use of Doppler radar in meteorological observations. Mon. Wea. Rev., 89, 1-7.

Smythe, G. R., 1981: Correlation of Doppler-radar velocities and reflectivities with application to retrieving the transverse wind. CIMMS Report No. 4, Norman, OK, 72 pp.

------, 1983: Sub-storm scale motions as determined by single-Doppler and non-Doppler radar data. Preprints, 13th Conf. on Severe Local Storms, Tulsa, Amer. Meteor. Soc., 109-112.

------ and F. I. Harris, 1984: Sub-cloud layer motions from radar data using correlation techniques. AFGL Tech. Report AFGL-TR-84-0272, Hanscom AFB, MA, 24 pp.

Snell, R., 1985: Personal communication.

Tepper, M., 1950: A proposed mechanism of squall line: The pressure jump line. J. Meteor., 7, 21-29.

Waldteufel, P., and H. Corbin, 1979: On the analysis of single-Doppler radar data. J. Appl. Meteor., 18, 532-542.

Walters, G. W., 1975: Severe thunderstorm wind gusts. M.S. Thesis, Colorado State University, unpublished, 81 pp.

Wardius, J., 1986: Personal communication.

Wexler, R., and D. Atlas, 1959: Precipitation generating cells. J. of Meteor., 16, 327-332.

Zrnic, D., 1985: Personal communication.

APPENDIX A

ACRONYMS AND ABBREVIATIONS

BSCAN	B-Scan computer program
DISKW	Disk Write computer program
DRWF	Doppler Radial Wind Field
IOTF	Interim Operational Test Facility
JDOP	Joint Doppler Operational Project
JSPO	Joint System Program Office
NCAR	National Center for Atmospheric Research
NEXRAD	Next Generation Weather Radar
NSSL	National Severe Storms Laboratory
NWS	National Weather Service
RADPLOT	Radar Plot computer program
UFT	Universal Format Tape
UTF	Universal Tape Format
SAM	Surface Automated Mesonet
SAMPLOT	SAM Plot computer program
SAMWRITE	SAM Write data transfer computer program
TWIND	NEXRAD Transverse Wind algorithm computer program
TWRITE	Tower Write data transfer computer program
VAD	Velocity-Azimuth Display
VCS	Vertical Cross-Section computer program
VCSPLOT	Vertical Cross-Section Plot computer program
VVP	Velocity Volume Processing
WPLOT	Wind Plot computer program
ΔT	Time period between consecutive radar scans
Θ_e	Equivalent potential temperature

APPENDIX B

BASIC PRINCIPLES OF DOPPLER WEATHER RADAR

The Doppler measurement of the radial component of the velocity of
the scatterers within the sampled volume results from the measurement of
the change in phase over time of the wave emitted by the coherent radar.
This sample volume is defined by the characteristics of the radar beam
and the discrete gate spacing along the beam. As the main lobe is
assumed to be of constant dimensions, the radar measurements are
considered to be valid at the center of this "pulse volume." The
average radial velocity of the scatters in the pulse volume is given by

$$f = \frac{2V}{\lambda} , \qquad (B.1)$$

where f = Doppler shift frequency and λ = radar wavelength.

With a given pulse repetition frequency (PRF), the maximum Doppler
shift frequency that can be detected is

$$f_{max} = \frac{PRF}{2} , \qquad (B.2)$$

so that the maximum unambiguous Doppler velocity is

$$V_{max} = PRF\left(\frac{\lambda}{4}\right). \qquad (B.3)$$

On the other hand, unambiguous range is

$$r_{max} = \frac{C}{2PRF} , \qquad (B.4)$$

where c ≡ speed of light. The term PRF, common to both equations, results in what is often called the "Doppler dilemma"

$$V_{max} r_{max} = \frac{\lambda c}{8} \ . \tag{B.5}$$

The radar output is effectively a spatial average over each pulse volume. Variations within a pulse volume are not detectable. However, spectrum width is a measure of the variation of the radial velocity within the pulse volume.

Most of the observed winds will be less than the true-mean wind speed due to the radar perspective (i.e., only the radial component is measured). The radial component can be computed as shown in Fig. B.2.

$$\beta = AZ - DIR \tag{B.6}$$

$$\vec{V}_r = \vec{V}_{true} \cos \alpha \cos \beta + \vec{V}_{true} \sin \alpha \tag{B.7}$$
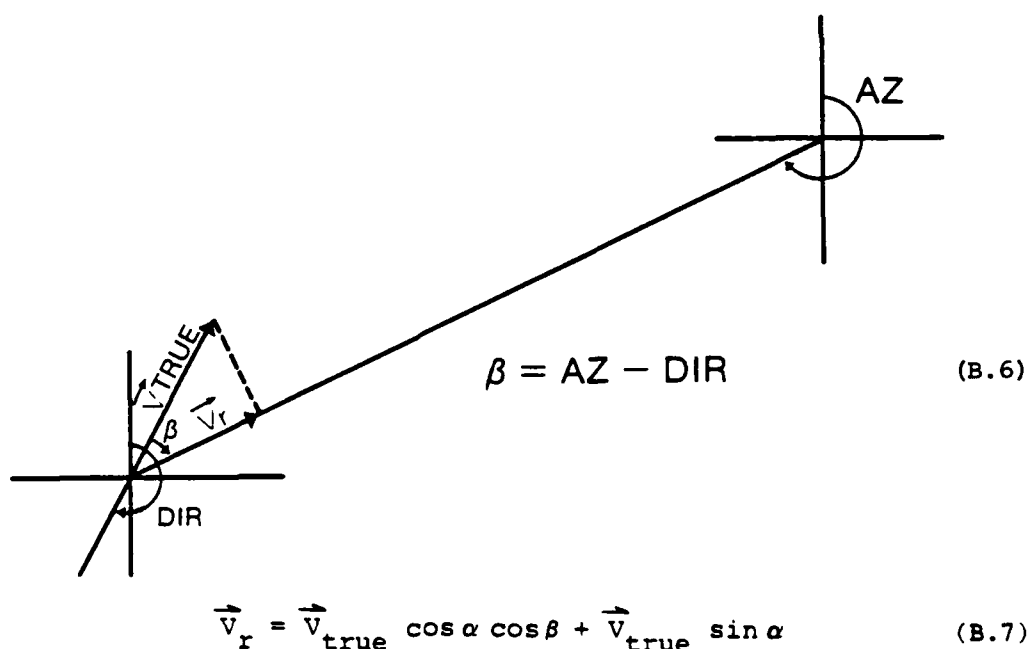
Fig. B.1. Radar azimuth/wind direction geometry. AZ is azimuth of the radar. DIR is horizontal wind direction. $\vec{V}_r$ is the Doppler horizontal radial wind, and $\vec{V}_{true}$ is true horizontal wind. α is the radar elevation angle.

At low elevation angles, (B.7) can be simplified as the cosine of α $\cong$ 1, and the sine of $\alpha \cong 0$. The error induced by this assumption is less than 0.0039 for the cosine term and 0.013 for the sine term at an elevation angle less than or equal to 5.0 degrees. Dropping the sin α term might also be justified due to the very small additive component of the vertical fall velocity. A 40 m s^{-1} downdraft (directly vertical) would only have about 6 m s^{-1} projected in the radial direction if the elevation angle was as large as 10 degrees. Thus, it is common practice in Doppler research to neglect this contribution to the Doppler velocity (horizontal motion) by vertical motions if the elevation angles are small (see Donaldson, 1970). This presumes the absence of any significant downdraft (downburst, microburst, etc.), and, thus, may not be a valid assumption in all cases.

Therefore, (B.7) can be reduced to

$$\vec{V}_r = \vec{V}_{true} \, \cos \beta \, , \tag{B.8}$$

or by rearranging and considering magnitude alone (i.e., without regard to the sign of the radial component), (B.8) becomes

$$\left| \vec{V}_{true} \right| = \frac{\left| \vec{V}_r \right|}{\left| \cos \beta \right|} \, . \tag{B.9}$$

Since β = AZ − DIR, it is apparent that the only missing element is the actual direction of the horizontal wind.

APPENDIX C

UNIVERSAL TAPE FORMAT

An agreement was reached among the principal Doppler weather radar research groups establishing a common format to be used to facilitate the exchange of Doppler radar data (Barnes, 1980). This "common Doppler radar exchange format" is frequently referred to as a universal tape format (UTF) and the result as a universal format tape (UFT). This appendix provides some of the details about this format.

Doppler radar data in UTF are exchanged on 1600 bpi, 9-track tapes. Data are stored in a mix of ASCII and binary using 16-bit words (signed integers; 2's complement). ASCII words are left justified and blank filled. Each tape contains one or more radar volume scans separated by end-of-file marks. Each volume scan is composed of a sequence of radials of Doppler radar data. As physical records are ≤ 4095 16-bit words, a radial may require one or more records. Each radial is composed of header blocks and data in a sequence as follows.

	MANDATORY HEADER BLOCK

Word	Description
1	UF (ASCII)
2	Number of 16-bit words (i.e., record length)
3	Pointer to first word of the first header block following the mandatory header block
4	Pointer to first word of local use header block, if present, or to the start of the data header block
5	Pointer to first word of data header block
6	Number of physical record from start of file
7	Number of: volume from start of tape
8	radial within volume scan
9	the physical record for this radial
10	the elevation scan within this volume scan
11-14	Radar name (ASCII)
15-18	Site location name (ASCII)
19	Latitude (degrees) [Positive ≡ North; Negative ≡ South]
20	(minutes)
21	(seconds X 64)
22	Longitude (degrees) [Positive ≡ East; Negative ≡ West]
23	(minutes)
24	(seconds X 64)
25	Height of antenna above sea level (meters)
26	Date of data (Year) [Last two digits]
27	(Month)
28	(Day)
29	Time of data (Hour)
30	(Minute)
31	(Second)
32	Time Zone (ASCII) [e.g., UT ≡ Universal Time; CS ≡ Central Standard; etc.]
33	Azimuth (degrees X 64) [Measured to midpoint of sample]
34	Elevation angle (degrees X 64)
35	Sweep mode [e.g., 1 ≡ PPI; 3 ≡ RHI; etc.]
36	Fixed angle (degrees X 64) [e.g., PPI elevation; RHI azimuth; etc.]
37	Instantaneous sweep rate ((degrees/second) X 64)
38	UFT generation date (Year) [Last two digits]
39	(Month)
40	(Day)
41-44	Name of UFT generator (ASCII)
45	Deleted or missing data flag (100000 octal recommended)

	OPTIONAL HEADER BLOCK
Word	**Description**
1-4	Project name (ASCII)
5	Baseline azimuth (degrees X 64)
6	elevation (degrees X 64)
7	Time of start of current volume scan (Hour)
8	(Minute)
9	(Second)
10-13	Field tape name (ASCII)
14	Flag [Number of range gates, minimum range, and gate spacing same for all data within: this volume scan ≝ 0 each elevation scan ≝ 1 each radial ≝ 2

LOCAL USE HEADER BLOCK
If present, may be any length and contain any information desired

	DATA HEADER
Word	**Description**
1	Number of: fields in this radial
2	records used for this radial
3	fields in this record
4	Field name (ASCII) [e.g., DM ≝ reflected power (dBm) VE ≝ radial velocity (m s^{-1}) SW ≝ spectrum width (m s^{-1})]
5	Pointer to 1st word of this field header
	WORDS 4-5 ARE REPEATED TO COVER ALL INCLUDED FIELDS

	FIELD HEADER FOR DM

Word	Description
1	Pointer to 1st data word
2	Scale factor (divide value on tape by scale factor to obtain meteorological values)
3	Range to first gate (kilometers)
4	Adjustment to center of first gate (meters)
5	Sample volume spacing (meters)
6	Number of sample volumes
7	Sample volume depth (meters)
8	Beam width: Horizontal (degrees X 64)
9	Vertical (degrees X 64)
10	Receiver bandwidth (MHz)
11	Polarization transmitted (0 = horizontal, 1 = vertical, 2 = circular, 2 ≥ eliptical)
12	Wavelength (cm X 64)
13	Number of samples used in field estimate
14	Threshold field (ASCII) [e.g., DM]
15	Threshold value
16	Scale factor
17	Edit code (ASCII)
18	Pulse repetition time (microseconds)
19	Bits (16) per sample volume
20	Radar constant (RC) [dBZ = ((RC + DATA)/SCALE) + 20 log (range in kilometers)]
21	Noise power (dBm X SCALE)
22	Receiver gain (dB X SCALE)
23	Peak power (dBm X SCALE)
24	Antenna gain (dB X SCALE)
25	Pulse duration (μs X 64)

DATA FOR THIS FIELD FOLLOWS TO END OF RADIAL

FIELD HEADER FOR VE	
Word	Description
1-19	Same as for DM
20	Nyquist velocity (m s^{-1} X SCALE)
21	FL (ASCII) [NCAR bad velocity flag with least significant bit set = 1 (good velocity) or = 0 (bad velocity)]

DATA FOR THIS FIELD FOLLOWS TO END OF RADIAL

FIELD HEADER FOR SW	
Word	Description
1-19	Same as for DM

DATA FOR THIS FIELD FOLLOWS TO END OF RADIAL

FIELD HEADER-DATA PAIRS CONTINUE UNTIL ALL FIELDS COVERED

APPENDIX D

MICRO-SCALE FEATURES

As discussed in Chapter II, one level of comparisons made in this study was that which compared wind fields at a common time as derived through several approaches. This became much like the vector matching done by earlier researchers. Table 2.4 provided the comparisons and the procedure used for each comparison. Two computer programs, composite plot (COMPLOT) and modified wind plot (MODPLOT), provided the capability to do these comparisons. This chapter discusses these programs and the analysis conducted.

Composite Plot

The computer program COMPLOT (Composite Plot) provided the mechanism to compare SAM data with the TWIND derived winds. In addition, the Doppler radial wind field (DRWF) could be compared with (1) the radial component of the SAM winds and (2) the radial component of the TWIND derived winds. Since comparisons were made with the SAM data, the composite plot program (COMPLOT) expanded the data within an indicated expansion radius around a selected SAM site to a full size figure. COMPLOT adjusted the grid boundary outward as necessary to ensure convenient grid values. Fig. D.1 shows the data in the region of the 60-series SAM site with an expansion factor of 10 km.

In order to increase the area of the surface field available for comparison with the radar data, a time-to-space conversion was done on

the SAM data. The mid-point time (MPT) was computed from the times of scan 1 and scan 2 in TWIND. Using the estimated storm speed and direction as obtained from consecutive low-level radar scans, each one-minute interval between SAM observations was converted to a distance traveled. Data were plotted in their respective positions along the line of storm movement. Fig. D.1 shows an example of the time-to-space conversion. SAM data recorded at the MPT were plotted at the physical location of the SAM site. Data from observations recorded at a time (T) before (after) MPT were assumed to have moved downstream (upstream) with the storm from the physical SAM location by a distance given as

$$\text{distance} = \text{storm speed} * (\text{MPT} - \text{T}).$$

The program computed an average u and average v for all sites in one cluster. This averaging process provided some smoothing of the data over the surface area, which was approximately the size of a pulse volume (see Fig. 3.1). With the assumption that an observation at some time could be plotted at a distance from the SAM location based on the speed of the storm, steady-state conditions were also assumed for the time period covered. Possible errors included incorrect storm motion (speed and/or direction), surface features not moving with storm motion, vertical influences, failure of steady-state assumption, attempt to extrapolate too far, and radar data obtained from higher in the storm at longer range.
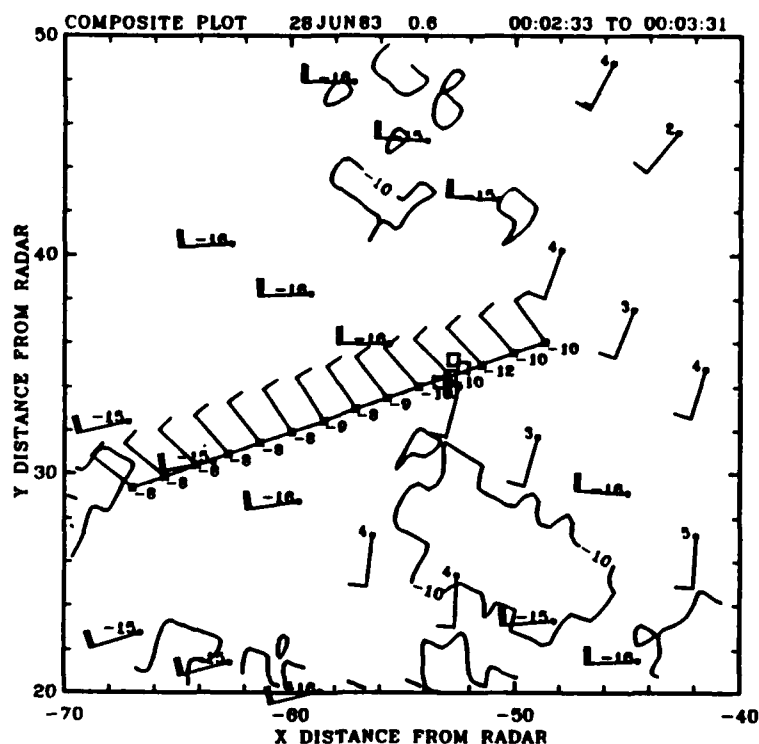
Fig. D.1. Example of expanded data field. Distances are in kilometers. 60-series SAM complex identified as open squares. Site averaged time-to-space converted data plotted (filled squares) along line of estimated storm motion. Doppler radial velocity data contoured with an interval of 10 m s^{-1}. Numbers to left of TWIND derived wind flags are the radial component of the TWIND data. Numbers to the right of the SAM wind flags are their radial components. Wind flags are plotted as in Fig. 2.9.

The approach taken in each of the comparisons using the COMPLOT product was very similar. (Representative composite plots are shown in Figs. D.2 and D.3.) The comparison of the DRWF with the radial component of the SAM or the TWIND derived winds was direct. Based on their plotted radial components, the individual wind vectors within their DRWF contour were counted. For those wind vectors which fell outside their appropriate DRWF contour the nature of the direction of
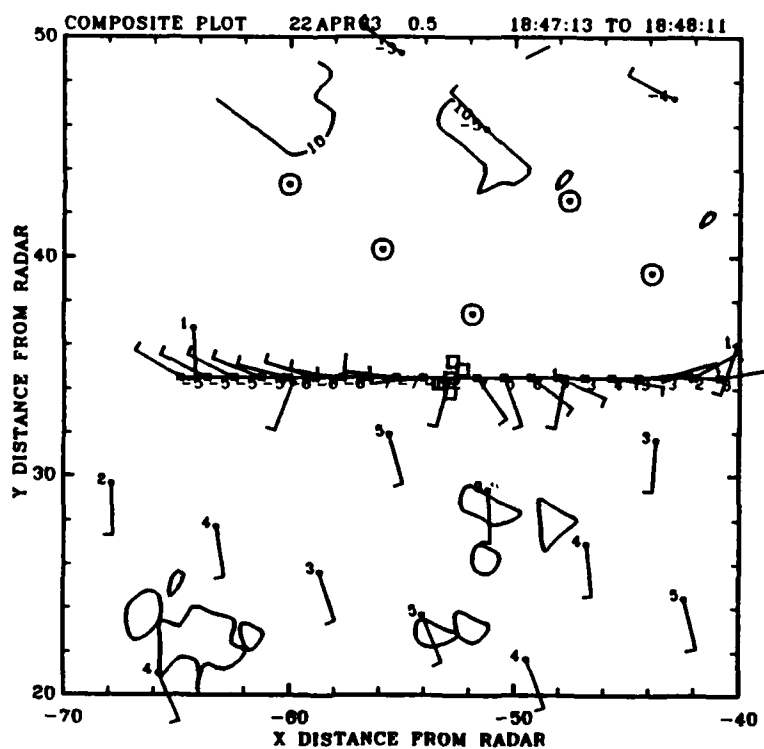
Fig. D.2. Representative composite plot for 22APR83 case.
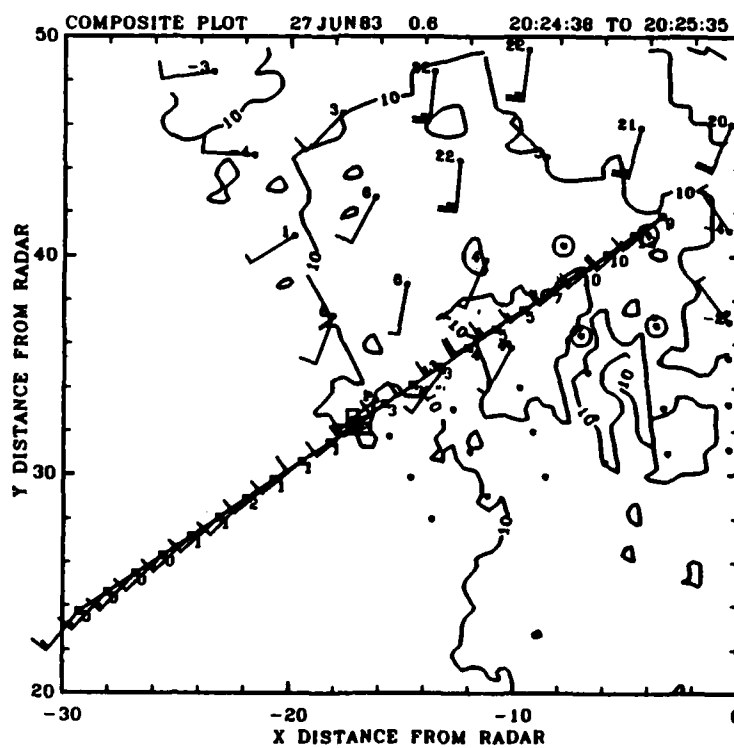
Fig. D.3. Representative composite plot for 27JUN83 case.

the error (i.e., the sign) was recorded. The results were tabulated in Table D.1. The comparison of the TWIND derived winds with the SAM observed winds was done using the time-to-space extension to the SAM data. At each derived SAM position along the line of assumed storm movement a radius of 5 km was drawn. All of the TWIND derived winds within the circle were compared to the SAM wind. The actual comparison was of direction and magnitude. The results were grouped and tabulated in Table D.2.

While this approach puts an element of objectivity into the analysis, there is a risk that too much meaning might be attached to any statistical analysis conducted on these data. The way that these data were compared, the large margin for error in the time-to-space conversion, and the multiple comparisons among the vectors made it apparent that these data should only be used for a broad scale comparison. The radial component comparison (Table D.1) indicated that 92% of the SAM data fell within its proper contour. Only 76% of the radial components of the TWIND derived winds were within their proper contour. The TWIND to SAM wind comparison (Table D.2) indicated that 57% of the TWIND winds were within 60° of the SAM wind direction (for all speed errors). From the other perspective, 41% of the TWIND derived winds, without regard to direction error, were within 5 m s^{-1} of the SAM wind speed.

Table D.1. Radial component comparisons.

Field	Vectors	Inside Contour	Outside Contour		
			Levels	Sign	
			Off	Correct	Wrong
SAM	535	494	1	41	0
			2	0	0
			≥3	0	0
TWIND	542	414	1	78	5
			2	37	4
			≥3	1	3

Table D.2. TWIND derived to SAM observed wind comparison.

Δ Speed	Δ DIRECTION					
	0-15	16-30	31-45	46-60	61-75	> 75
0-5	93	75	63	39	18	146
6-10	27	61	104	77	39	153
11-15	2	10	5	13	3	92
16-20	3	0	14	17	2	3
>20	0	0	0	1	0	0

Modified Wind Plots

A procedure (computer program) was developed to compare the SAM winds with a modified Doppler radial wind field (DRWF). The computer program modified wind plot (MODPLCT) was used to adjust the DRWF by the wind direction from the TWIND program. Recall (B.8) states that

$$\vec{V}_r = \vec{V}_{true} \cos \beta ,$$

then from (B.9)

$$\left|\vec{V}_{true}\right| = \frac{\left|\vec{V}_r\right|}{\left|\cos \beta\right|} .$$

Recall that since β = AZ − DIR, only the true wind direction is required to derive the magnitude of the "true wind" ($\left|\vec{V}_{true}\right|$). The $\left|\vec{V}_r\right|$ and AZ are available from the Doppler radial velocity field, and with the assumption that the TWIND wind direction is correct, DIR is available from the transverse wind program. This wind direction was applied to all the radial velocity values within a radius of influence of the x,y location of the TWIND wind. Note in Fig. D.4, the extensive overlap with a radius of influence of 5 km. To simplify processing, the assumption was made that wind directions associated with a BOX1 with a larger maximum correlation coefficient were more reliable. The BOX1's were sorted by correlation coefficients from low to high, and in this way the values in the array were over-written as the program stepped through the field from BOX1 location to BOX1 location from the lowest to the highest correlation coefficients. Fig. D.5 is an example of this output.
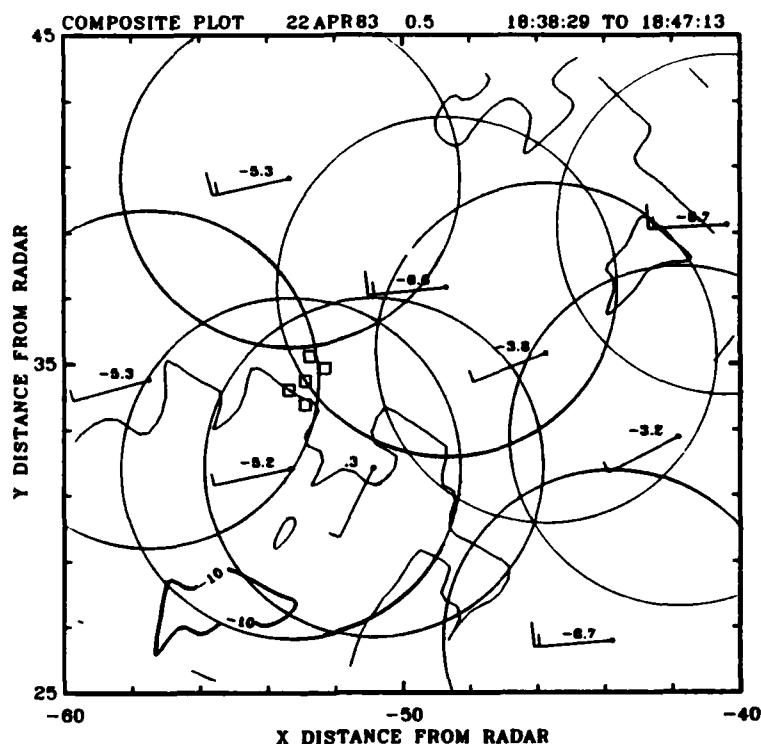
Fig. D.4. Example of data expansion (5 km expansion factor and 5 km radius of influence).

As can be seen in the stippled region of Fig. D.5, a problem results. This is a region where $|\cos \beta|$ approaches 0.0, resulting in the $|\vec{V}_{true}|$ approaching infinity.

After examining a minimum of data, it became apparent that the problem resulting when the TWIND derived wind direction was close to orthogonal to the radar beam, any benefit of this approach would be negated. When the TWIND direction was close to orthogonal to the radar azimuth, the "true" wind computed was completely unrealistic (values on the order of 100's to 1000's of meters per second). Although data in an "orthogonal region" could have been suppressed, the occurrence of such data cast significant doubt on the accuracy of all of the data within

the observation window derived through MODPLOT, even when the TWIND

direction might parallel the radar beam. Indeed, this strongly

confirmed the "apples and oranges" nature of TWIND and Doppler radial

data (Hamidi et al., 1983). It was readily apparent that nothing was to

be gained along this path of research.
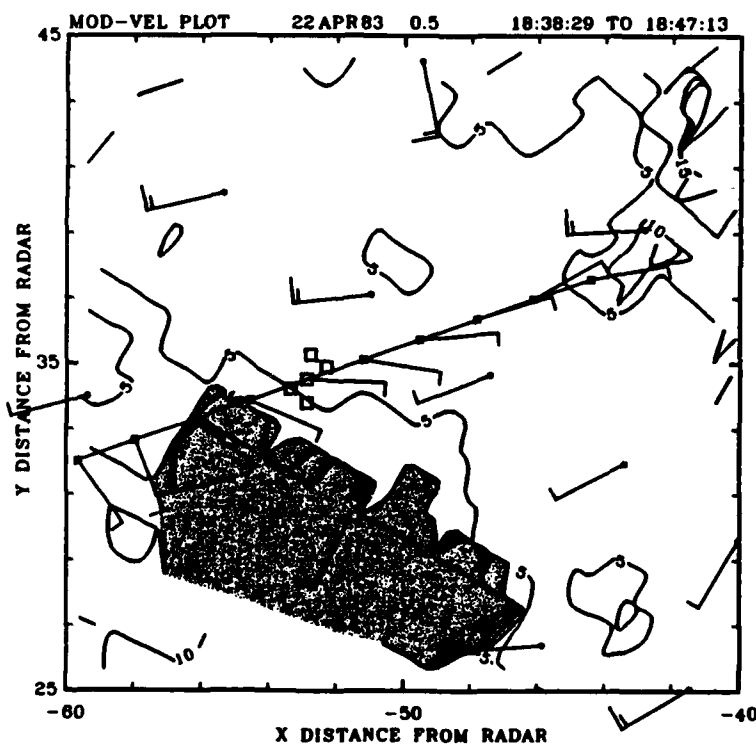
Fig. D.5. Example of modified velocity plot. SAM data and TWIND data plotted same as in Fig. D.1. Contours are of magnitude of the wind field derived from the radial velocity and the direction of TWIND vectors (increment of 5 m s^{-1}).

APPENDIX E

SELECTED SURFACE OBSERVATIONS

This appendix contains selected hourly surface observations used in the surface meso-analyses for 22 APR, 27 JUN, and 28 JUN 83.

SELECTED HOURLY OBSERVATIONS (SA)
JUNE 27-28, 1983

STATION	OBS TIME (CST)	PRES (mb)	T (°F)	Td (°F)	WIND DIR (°)	WIND SPEED (kt)	CURR WX	REMARKS
ABI	1800	033	100	51	200	21G29	–	CB N MOVG NE / TCU NW
	1900	043	98	51	190	17G27	–	CB NNE MOVG NE
	2000	046	95	53	170	17	–	CB NE MOVG NE
	2100	050	91	64	160	19G25	–	
	2200	061	88	64	160	19	–	
	2300	064	86	64	160	16G21	–	CB SW MOVG NE
	0000	068	85	65	180	16G21	–	T B 12 SE-S MOVG NE
	0100	068	83	54	200	24G33	T	T E 34 MOVD NE PKWND 2038/44
	0200	079	79	54	200	26G38	–	
AMA	1800	041	89	57	110	08	–	CB 40 NW MOVG E / CB DSNT SE
	1900	039	85	57	110	12	–	CB 40 N MOVG E
	2000	054	71	55	320	25G35	T	T E B15 MOVG SE PKWND 3340/37
	2100	087	64	58	050	13	T	T E MOVG SE
	2200	084	65	56	010	06	–	T E 30 MOVE SE
	2300	090	63	56	010	10	–	
	0000	085	60	56	100	13	–	
	0100	090	59	56	310	12	–	WSHFT 47
	0200	093	58	55	320	07	–	

SELECTED HOURLY OBSERVATIONS (SA)
JUNE 27-28, 1983

STATION	OBS TIME (CST)	PRES (mb)	T (°F)	Td (°F)	WIND DIR (°)	WIND SPEED (kt)	CURR WX	REMARKS
DFW	1800	075	92	70	170	15	—	
	1900	090	89	71	170	11	—	
	2000	086	88	71	160	11	—	
	2100	100	87	71	160	07	—	
	2200	117	80	64	030	13	—	WSHFT 42
	2300	115	75	66	050	07	—	
	0000	114	77	67	050	05	—	
	0100	108	77	67	110	04	—	
	0200	103	80	73	150	08	—	
END(WDG)	1800	(974)	86	68	140	04	—	CB SW MOVG NE
(WDG)	1900	(976)	85	70	160	05	—	(LAST)
(WDG)	2000	(979)	82	73	140	05	—	
	2100	M	M	M	M	M	T	T OVHD-W MOVG NE
	2200	068	69	63	070	05		
	2300	M	M	M	M	M	TRW	CB MOVD NE
	0000	099	67	65	280	30G38		
	0100	M	M	M	M	M	—	
	0200	099	65	63	310	08		

SELECTED HOURLY OBSERVATIONS (SA)
JUNE 27-28, 1983

STATION	OBS TIME (CST)	PRES (mb)	T (°F)	Td (°F)	WIND DIR (°)	WIND SPEED (kt)	CURR WX	REMARKS
ICT	1800	066	79	69	090	09	T	OCNL LTGICCG IN TRWU NW AND NE
	1900	075	70	66	030	08	−	T E 49 MOVD E / OCNL LTGICCG IN CB NE-SE MOVG E
	2000	081	69	66	110	06	−	CB NE-S MOVG E
	2100	094	72	66	080	06	TRW−	T B38 T OVHD AND W-SE MOVG SE
	2200	083	70	67	E130	07	TRW−	T OVHD AND NE-SE
	2300	077	70	68	140	05	RW−	T E 20 MOVD E
	0000	080	67	66	160	06	TRW−	T B 04 57 S MOVG SE
	0100	090	66	62	240	05	TRW−	T S MOVG E
	0200	096	66	64	220	07	T	T SE-SW MOVG E R E 46
LTS	1800	078	76	64	180	25G35	TRW-BD	T SE MOVG NNE
	1900	067	73	63	160	17G25	TRW−	T NE MOVG NNE
	2000	M	M	M	M	M		
	2100	067	71	64	140	17G23	TRW−	T S-SE MOVG ENE PRESRR
	2200	M	M	M	M	M		
	2300	M	M	M	M	M		
	0000	M	M	M	M	M		
	0100	M	M	M	M	M		
	0200	088	69	61	040	10	−	CBS ENE AND SE MOVG ESE

SELECTED HOURLY OBSERVATIONS (SA)
JUNE 27-28, 1983

STATION	OBS TIME (CST)	PRES (mb)	T (°F)	Td (°F)	WIND DIR (°)	WIND SPEED (kt)	CURR WX	REMARKS
OKC	1800	064	87	73	170	10	–	CB SW AND N MOVG NE
	1900	068	84	73	140	08	–	CB NW-N MOVG NE TRB 02 OVHD MOVG NE PKWND 2238/01 PRESRR
	2000	083	82	73	150	06	–	
	2100	114	70	65	190	15G23	TRW–	T NE MOVG NE TRE 05 MOVD NE
	2200	110	69	64	040	08	TRW–	CB SE MOVG NE
	2300	078	73	61	160	14	–	CB SE-W MOVG E PRESRR
	0000	082	70	60	120	06	–	
	0100	129	69	60	260	10	–	
	0200	106	66	61	350	13	TRW–	PKWND 3345/15 PRESFR TB 25 SE-S MOVG E RB0652
SPS	1800	059	87	73	130	11	–	CB SW MOVG E
	1900	125	74	63	190	17	TRW–	TB07 FQT LTGICCCCG ALQDS MOVG E PKWND 2569/31 PRESRR
	2000	091	71	63	110	17	TRW–	T FQT LTGICCCCG NW-SW MOVG E PRESFR
	2100	069	72	63	090	17	T	T FQT LTGICCCCG ALQDS MOVG E PRESFR

SELECTED HOURLY OBSERVATIONS (SA)
JUNE 27-28, 1983

STATION	OBS TIME (CST)	PRES (mb)	T (°F)	Td (°F)	WIND DIR (°)	WIND SPEED (kt)	CURR WX	REMARKS
SPS	2200	083	71	63	050	10	T	T NW CONTS LTGICCCCG FQT LTGIC ALQDS
	2300	093	70	63	130	18	–	
	0000	080	72	62	120	20	–	CB NW–N MOVG SE
	0100	072	74	61	120	10	–	CB NW–N MOVG SE
	0200	096	74	61	020	18	–	PRESRR WSHFT04
TUL	1800	077	85	75	170	11	–	
	1900	077	84	77	170	12	–	
	2000	081	82	76	150	08	–	
	2100	084	82	77	160	10	–	
	2200	084	82	77	160	12	–	
	2300	124	72	70	350	10	TRW–	T B 13 E MOVG NE R B 15 PKWND 2357/13 PRESRR
	0000	107	70	69	180	07	RW–	R B 49 PRESFR R E 25
	0100	055	72	67	170	26G33	–	PRESRR
	0200	109	74	64	210	07	–	

SELECTED HOURLY OBSERVATIONS (SA)
April 22, 1983

STATION	OBS TIME (CST)	PRES (mb)	T (°F)	Td (°F)	WIND DIR (°)	WIND SPEED (kt)	CURR WX	REMARKS
ABI	1800	025	73	34	300	14	T	TB48 SW MOVG SE / CB RWU SW NW
	1900	042	65	44	020	11	–	TE28 MOVD SE CB / ESE RB04E25
	2000	055	62	45	320	07	–	
	2100	069	59	44	320	06	–	
AMA	1800	068	54	45	360	14G25	–	
	1900	086	52	43	350	21G27	–	
	2000	093	50	44	350	18G27	–	
	2100	112	49	44	350	20G26	–	
DFW	1800	009	73	58	270	12	–	CB W N
	1900	016	67	56	010	06	–	CB NE D W
	2000	027	65	54	310	11	–	
	2100	034	68	46	280	08	–	
END(WDG)	1800	(968)	58	53	340	20	RW	T W-E
(WDG)	1900	(971)	55	53	020	20	R	CB E
(WDG)	2000	(974)	M	M	360	20	R	
	2000	049	55	51	030	24G33	–	
(WDG)	2100	M	M	M	360	10	R	(LAST)
ICT	1800	068	52	49	040	15	–	
	1900	081	51	49	040	14	–	
	2000	095	51	49	040	10	–	
	2100	091	51	49	020	08	RW	RB15

SELECTED HOURLY OBSERVATIONS (SA)
April 22, 1983

STATION	OBS TIME (CST)	PRES (mb)	T (°F)	Td (°F)	WIND DIR (°)	WIND SPEED (kt)	CURR WX	REMARKS
LTS	1800	007	61	49	320	18	TRW	LN CB E OVHD W MOVG E OCNL LTGCCCGCA PRESRR PKWND 2828/35
	1900	043	59	50	320	09	T	CB WNW MOVG E LN CB N-S-E MOVD E OCNL LTGIC W PKWND 31030/10
	2000	054	59	51	330	15	–	
	2100	069	58	51	340	15G22	–	
OKC	1800	041	70	53	120	10	–	CB ALQDS MOVG ENE
	1900	018	63	53	090	12	–	CB SE-SW-NW MOVG E RWU WNW OCNL LTGIC W
	2000	047	55	50	350	16	TRW	T B 15 OVHD MOVG E R B 25 FQT LTGICCCCG ALQDS PRESRR
	2100	073	55	52	310	14	TRW	T E MOVG E OCNL LTGIC E PRESRR
SPS	1800	010	66	47	250	17	–	PKWND 2348/12
	1900	013	65	50	280	14G20	–	VIRGA DSNT W
	2000	022	63	47	330	19	–	
	2100	039	59	48	320	13	–	PRESRR

SELECTED HOURLY OBSERVATIONS (SA)
April 22, 1983

STATION	OBS TIME (CST)	PRES (mb)	T (°F)	Td (°F)	WIND DIR (°)	WIND SPEED (kt)	CURR WX	REMARKS
TUL	1800	063	57	55	010	17	RWF	TE30 T MOVD E
	1900	049	58	55	040	16G23	—	
	2000	049	57	53	030	10	—	
	2100	049	56	52	010	05	—	

VITA

Joel David Bonewitz was born in Gulfport, Mississippi, on August 31, 1949, to Emmett B. and Martha L. Bonewitz. He graduated from Gulfport High School in May, 1967. In June he began studies at the Georgia Institute of Technology and earned a Bachelor of Aerospace Engineering degree on the co-operative plan, working alternate quarters for General Dynamics. A participant in Air Force ROTC, upon graduation in 1972, he was commissioned in the U.S. Air Force. After a year of meteorology training at North Carolina State University, he served as a forecaster at Langley AFB, Virginia. In 1975, he was assigned as an Aerial Reconnaissance Weather Officer in the 54th Weather Reconnaissance Squadron, Andersen AFB, Guam. Returning to school via the Air Force Institute of Technology (AFIT), he earned a Masters of Science in Meteorology degree from the University of Oklahoma, and represented the Air Force during the first operational test of Doppler weather radar, the Joint Doppler Operational Project (1977). This led to an assignment as Radar Operations Officer, and later Assistant Chief, Science and Technology Division, Headquarters Air Weather Service, Scott AFB, Illinois. In 1980, he was assigned as one of two Department of Defense representatives on the Next Generation Weather Radar (NEXRAD) Joint System Program Office as Chief, Operations and Requirements Branch, and later Chief, Research and Development Branch. During this time, he earned a Masters of Science degree in computer science from Johns Hopkins University. In August, 1983, he entered Texas A&M University to seek the degree of Doctor of Philosophy under AFIT sponsorship. His permanent mailing address is 1000 Wanda Place, Gulfport, MS 39501.

END

11-86

DTIC